AD-A195 399 STRUCTURE AND DYNAMICS OF SOLUTIONS OF LITHIUM SALTS RELEVANT TO BATTERY CONSTRUCTION(U) POLYTECHNIC UNIV FARMINGDALE NY DEPT OF CHEMISTRY 1988 ARO-21750.12-CH 1/1

UNCLASSIFIED DAAG29-85-K-0051 F/G 7/4 NL

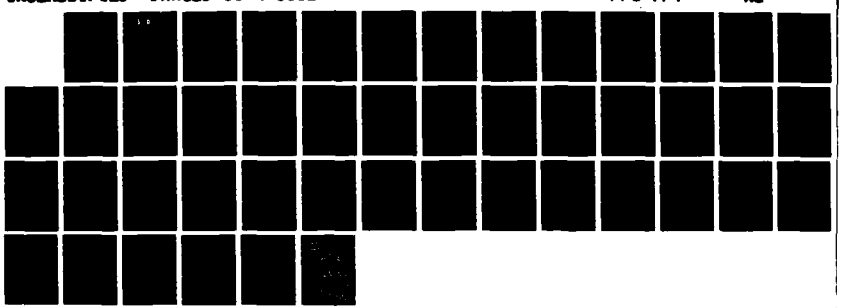

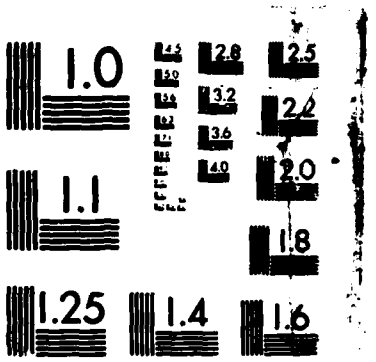

REPORT DOCUMENTATION PAGE

1a. REPORT SECURITY CLASSIFICATION: Unclassified	1b. RESTRICTIVE MARKINGS
2a. SECURITY CLASSIFICATION AUTHORITY	3. DISTRIBUTION/AVAILABILITY OF REPORT: Approved for public release; distribution unlimited.
2b. DECLASSIFICATION/DOWNGRADING SCHEDULE	
4. PERFORMING ORGANIZATION REPORT NUMBER(S)	5. MONITORING ORGANIZATION REPORT NUMBER(S): ARO 21758.12-CH
6a. NAME OF PERFORMING ORGANIZATION: Polytechnic University, Chemistry Department	6b. OFFICE SYMBOL (If applicable)
6c. ADDRESS (City, State, and ZIP Code): Route 110, Farmingdale, New York 11735	7a. NAME OF MONITORING ORGANIZATION: U. S. Army Research Office
	7b. ADDRESS (City, State, and ZIP Code): P. O. Box 12211, Research Triangle Park, NC 27709-2211
8a. NAME OF FUNDING/SPONSORING ORGANIZATION: U. S. Army Research Office	8b. OFFICE SYMBOL (If applicable)
8c. ADDRESS (City, State, and ZIP Code): P. O. Box 12211, Research Triangle Park, NC 27709-2211	9. PROCUREMENT INSTRUMENT IDENTIFICATION NUMBER: DAAG29-85-K-0051
	10. SOURCE OF FUNDING NUMBERS: PROGRAM ELEMENT NO. / PROJECT NO. / TASK NO. / WORK UNIT ACCESSION NO.

11. TITLE (Include Security Classification)
"Structure and Dynamics of Solutions of Lithium Salts Relevant to Battery Construction"

12. PERSONAL AUTHOR(S)

13a. TYPE OF REPORT	13b. TIME COVERED	14. DATE OF REPORT (Year, Month, Day)	15. PAGE COUNT
Final	FROM 3/85 TO 3/88		

16. SUPPLEMENTARY NOTATION
The view, opinions and/or findings contained in this report are those of the author(s) and should not be construed as an official Department of the Army position, policy, or decision, unless so designated by other documentation.

17. COSATI CODES			18. SUBJECT TERMS (Continue on reverse if necessary and identify by block number)
FIELD	GROUP	SUB-GROUP	

19. ABSTRACT (Continue on reverse if necessary and identify by block number)

Solutions of lithium salts in media of low permittivity without or with addition of macrocycles have been characterized in their structural and dynamical behavior using various methods as infrared spectra, audio frequency electrical conductivity, microwave dielectric relaxation and ultrasonic relaxation techniques.

The above electrolyte solutions and the criteria of their choice are highly relevant topics for the construction of secondary lithium batteries, the optimization of their use and of their recycling.

20. DISTRIBUTION/AVAILABILITY OF ABSTRACT	21. ABSTRACT SECURITY CLASSIFICATION
☐ UNCLASSIFIED/UNLIMITED ☐ SAME AS RPT. ☐ DTIC USERS	Unclassified
22a. NAME OF RESPONSIBLE INDIVIDUAL	22b. TELEPHONE (Include Area Code) / 22c. OFFICE SYMBOL

The period covered by the Army Grant #DAAG-29-85-0051 goes from March 1, 1985 to March 1, 1988.

The personnel sponsored by the Grant were Dr. N. Inoue from Ehime University, Japan, Dr. M. Xu from Peking University China in addition to the principal Investigator. We interacted with Prof. Edward M. Eyring of the University of Utah, Salt Lake City, with Dr. M. Salomon of the Army Research Laboratory of Ft. Monmouth N.J., and with Drs. M. Delsignore, H. Maaser and D. Saar of Colgate-Palmolive, N.J..

The activity of the research dealt with the characterization of the structure and dynamics of solutions of lithium salts relevant to secondary battery construction.

1) We started with a work dealing with $LiAsF_6$ and $LiClO_4$ in the solvent dimethylcarbonate (permittivity $\epsilon = 3.1$). It was shown that accounting for the increase in permittivity of the solvent, (and including both ion pairs and triple ions) one could extend the validity of the Fuoss-Onsager-Kraus theories to $\sim 0.1M$, as long as one used the solution permittivities. This work was published in the Journal of Physical Chemistry (P1 in the attached list).

2) A new theoretical derivation of the triple ion formation constant was presented and compared with previous theories by Fuoss and Fuoss-Kraus. This work was also published in the J. Phys. Chemistry (P2 in the attached list and correction P3 in the attached list).

3) We compared information by infrared spectra looking at the "CN" stretch of the SCN^- ion with ultrasonic relaxation spectra for the systems NaSCN and LiSCN in the solvent tetrahydrofuran (THF). One of the important conclusions reached here was that if solvent seperated species, ion-pairs and/or dimer exist in solution, vibrational spectra may give incorrect results for the corresponding formation constants. This work was published in the Journal of Phys. Chemistry (P4 in the attached list).

4) The effect of addition of a macrocycle as 18-crown-6 to NaSCN in THF was investigated by infrared spectra and by microwave dielectric relaxation. The deconvoluted IR spectra showed that only one Gaussian-Lorentzian band suffices to interpret the IR spectrum at variance with the case of NaSCN in THF where three bands are necessary. This was taken to indicate segregation of Na^+ by the macrocycle and exclusion of the anion from contacting the cation. Microwave spectra confirmed the above showing a larger apparent dipole moment of the crown ether-complex NaC^+NCS^- with respect to the Na^+, NCS^- species. This work was published in the J. Phys. Chemistry (P5 in the list).

5) Electrolytes as $LiAsF_6$ and $LiClO_4$ in the solvent 2 methyltetrahydrofuran may be used as electrolyte solutions in batteries (especially $LiAsF_6$). We therefore engaged in a study of dynamic and structure of these systems using conductance, infrared spectra ($\bar{\nu}_3$ vibrational mode of the AsF_6^- and $\bar{\nu}_4$ vibrational mode of the ClO_4^- anion respectively), microwave dielectric and ultrasonic spectra. Work at various temperatures was included as the batteries using these electrolytes may be employed at low temperature either in stratospheric conditions (missiles) or subarctic conditions (GI's in the field).

During this work, following a suggestion of Dr. Songtag of Bergen Univ., Norway we started considering an alternate model to interpret the conductance data already used in P1. We included the solution permittivities but excluded triple ions from the model description of the electrolyte solutions and we could still describe satisfactorily the conductance data. These papers were published in the Journal of Physical Chemistry (P6 and P7 in the list).

6) $LiAsF_6$ and $LiClO_4$ added of macrocycles as 12-crown-4, 15-crown-5 and 18-crown-6 in the solvent 1,3-Dioxolane (DXL) were studied by infrared spectra. The macrocycles tend to segregate Li^+ from anion contact (except 12-Crown-4 + $LiClO_4$ in DXL). In addition the stability of $LiAsF_6$ in DXL is enhanced with absence of formation of solid polymers (as in the absence of macrocycles). This is a relevant information for battery construction using these systems.

Studies by ultrasonic relaxation for both systems and by conductance and dielectric relaxation for $LiClO_4$ + Macrocycles in DXL were also reported.

Again for $LiClO_4$ alone in DXL the conductance data could be fitted by the Fuoss-Onsager theory using the solution permittivities without need of postulating the presence of triple ions. These paper were accepted by the Journal of Phys. Chem. and they are in press (P8 and P9 respectively in the list below).

7) We decided to look at the effect of a macrocycle as 18C6 when added to $LiClO_4$ in a solvent of extremely low permittivity as dimethylcarbonate (DMC). We studied infrared spectra ($\bar{\nu}_4$ mode of ClO_4^-), microwave dielectric spectra, and electrical conductivity of this system.

The conductance data for both $LiClO_4$ and $LiClO_4$+18C6 in DMC cannot be fitted by the Fuoss-Onsager equation (using the formation constant for ion pairs as a fitting parameter, the solution permittivities and excluding triple-ions) unless one resigns to change the distance parameter of contact ion-pairs.

These systems show however, formation of ion-pair dimers. We then found in the Russian Literature a suggestion that these interactions could be expressed by an ion-pair activity coefficient. We calculated these ion-pair activity coefficients from the conductance data as ratio between the experimental formation constants and the calculated ones using the Fuoss theory and a fixed contact diameter (the one at very low concentration $c<10^{-4}$ mol/dm^3). We then derived a theory of activity coefficients based on dipole-dipole potentials which reproduces satisfactorily the activity coefficients for the ion-pairs up to $c\simeq10^{-2}$ M. The conclusion of this study is that there is no need of postulating presence of triple ions characterized by their own formation constant to rationalize the minima shown by the conductance-concentration data.

It is enough to include the changes in the permittivity of the solutions due to the presence of polar ion-pairs to account for the behavior of the conductance data. In solvents of very low permittivities, it may be necessary to take into account the ion-pair to ion-pair interaction through activity coefficients to describe the conductance data.

The above does not mean that in some cases triple ions do not exist. It is known that Ag^+ tends to coordinate two ligands with covalent bonding, hence species as $AgCl_2^-$ are known. The above only indicates that the presence of triple ions is not ubiquitous at low permittivity as commonly accepted so far by electrochemists.

The above paper is going to be submitted for publication.

8) $LiAF_6$ and $LiClO_4$ in the solvent methylacetate, a system relevant to battery construction, has been studied by infrared spectra, dielectric relaxation and electrical conductivity, the latter work carried in cooperation with Dr. Salomon of the Army laboratory of Ft. Monmouth. A critical analysis of the relative precision of the fit of the conductance data using the Fuoss-Onsager theory inclusion of triple ions vs the solution permittivity and exclusion of triple ions has been carried out.

This paper is in preparation at the present time. Preliminary results have been reported in the Technical report of Jan. 1988.

List of Publications

P1. "Ionic conductivity and microwave dielectric relaxation of $LiAsF_6$ and $LiClO_4$ in dimethylcarbonate" J. Phys. Chem. 89 (1985) 4968, with M. Delsignore and H. Farber.

P2+P3. "Molecular Relaxation Dynamics and Ionic Association of $LiBF_4$ in dimethoxymethane" J. Phys. Chem 90 (1986) 66; 90 (1986) 3294 with M. Delsignore, H. Farber.

P4. "Infrared and ultrasonic spectra of sodium and lithium thiocyanates in tetrahydrofuran", J. Phys. Chem. 90 (1986) 3326, with D. Saar

P5. "Infrared and Microwave dielectric Spectra of Macrocycle-Electrolyte complexes: System NaSCN + 18C6 in THF", J. Phys. Chem. 90 (1986) 6125, with M. Xu and E.M. Eyring

P6. "Temperature dependence of ionic association and molecular relaxation dynamics of $LiAsF_6$ in 2 Methyltetrahydrofuran" J. Phys. Chem. 91 (1987) 4628 with N. Inoue, M. Xu.

P7. "Molecular Relaxation Dynamics and Structure of $LiClO_4$ solutions in 2 methyltetrahydrofuran", J. Phys. Chem. 91, (1987) 3047, with H. Maaser, M. Xu, P. Hemmis.

P8. "Infrared spectra and ultrasonic relaxation spectra of $LiAsF_6$ and macrocycles in 1,3-Dioxolane" J. Phys. Chem., May-June 1988, in press, with M. Xu, N. Inoue, E.M. Eyring.

P9. "Structure and Molecular Relaxation Dynamics of $LiClO_4$ + Macrocycle solutions in 1,3-Dioxolane" J.Phys. Chem., May 1988 in press, with M. Xu, N. Inoue, E.M. Eyring.

Reprinted from The Journal of Physical Chemistry, 1985, 89, 4968.

Ionic Conductivity and Microwave Dielectric Relaxation of $LiAsF_6$ and $LiClO_4$ in Dimethyl Carbonate

M. Delsignore,† H. Farber, and S. Petrucci*

Departments of Chemistry and Electrical Engineering, Polytechnic Institute of New York, Long Island Center, Farmingdale, New York 11735 *(Received: February 11, 1985)*

Audio-frequency electrical conductivity results are reported for the solvent dimethyl carbonate (DMC) at 25 °C in the concentration range 10^{-4} to 1 M for $LiAsF_6$ and 10^{-4} to 0.3 M for $LiClO_4$. From 10^{-4} to $\approx 10^{-2}$ M the data are interpreted by the Fuoss–Kraus triple-ion theory leading to the values of the ion-pair formation constant K_p and triple-ion formation constant K_T. For the data at higher concentration, it is shown that the change of static permittivity of the solution (due to the presence of solute ion pairs and other polar species, which increase the polarization of the solution) can account qualitatively for the behavior of the conductance data and for their deviation from the Fuoss–Kraus theory. In other words, these deviations are mostly due to changes in permittivity (not accounted for by the conventional treatment of the data) rather than by the failure of the theory, which is better than recognized so far. Introduction of the quadrupole formation constant is necessary, however, for $LiAsF_6$ for a more quantitative treatment of the conductance data. Microwave complex permittivities in the concentration range 0.05–0.3 M and frequency range ≈1–90 GHz are interpreted by two Debye relaxation processes, one due to the solute and one to the solvent. For $LiAsF_6$ the Böttcher plot (expressing a quantity related to the change of the relaxation strength ($\epsilon_0 - \epsilon_\infty$) with the concentration of electrolyte) is nonlinear with the concentration. Correction of the concentration by postulating the presence of dielectrically apolar dimers linearizes the plot with a quadrupole formation constant of the order of $K_q \approx 50\ M^{-1}$, although this figure is very tentative. For $LiClO_4$ no curvature in the Böttcher plot is visible, suggesting that the presence of quadrupoles is not significant for this electrolyte in DMC, a notion already reported in the literature. The distance separation of the charges, as calculated from the apparent dipole moment of both $LiAsF_6$ and $LiClO_4$, suggests the presence of contact ion pairs.

Introduction

Research with the electrochemically relevant electrolyte $LiAsF_6$ has been carried out so far, in this laboratory, in the ethereal solvents 1,2-dimethoxyethane[1] and 2-methyltetrahydrofuran[2] of respective permittivities $\epsilon = 7.05$ and 6.2. This electrolyte shows a high solubility (>1 M) in the solvent dimethyl carbonate of $\epsilon = 3.1$.[3] Due to its higher electrolyte strength with respect to $LiClO_4$,[4] perhaps due to steric and donicity properties of AsF_6^-, it was thought quite relevant to carry a parallel investigation of $LiAsF_6$ and[1,2] $LiClO_4$ in DMC also because of the rare chance to extend to high electrolyte concentrations a study in a medium of such low permittivity. Two experimental methods, audio-frequency electrical conductivity and microwave coaxial and rectangular waveguide reflectometry (leading to the determination of the complex permittivity $\epsilon^* = \epsilon' - j\epsilon''$), have been used at the temperature $t = 25$ °C. The present work also extends to higher concentrations of $LiClO_4$ some microwave work reported earlier.[3]

Experimental Part

$LiAsF_6$ (Agri Chemical Co., Atlanta, GA) and $LiClO_4$ (C. P. Smith Co., Cleveland, OH) were dried at 70 °C in vacuo overnight.[1] Dimethyl carbonate (Aldrich Chemical Co., 99% product) was distilled twice in a Pyrex Vigreaux column without grease on the joints. A portion of DMC was dried over activated 4 Å molecular sieves and distilled over them (about $^1/_5$ of volume of sieves with respect to the liquid). The molecular sieves were dried at ≈100 °C in vacuo overnight. A conductivity run for $LiAsF_6$ in DMC distilled over molecular sieves gave the same results as for DMC distilled without molecular sieves. For the microwave work, solutions were kept in desiccators. Contact with open atmosphere was kept to a few seconds, namely, the time necessary to fill the cells. The equipment for the conductance work has been extensively described.[5] The setups for the microwave work have been reported in previous papers.[3,6,7] The only change of significance has been in the automation and digitization of data capturing. Specifically, the 1000-Hz modulated signal from the crystal detectors is now fed to a Hewlett-Packard 3468A digital voltmeter which is sensitive to ±1 μV. The meter is part of a loop comprising a Hewlett-Packard 41CV calculator, a HP-82160A-1L interface, and a HP82162A thermal printer. The ac-modulated voltage is transmitted to the calculator upon pressing a command that induces the calculator to "listen" to the voltmeter. The calculator in turn "talks" to the printer giving the decimal log of the digitized voltage which gets hard copied. The micrometric measurements of the reflector have also been motorized with the result that the system is a semiautomatic reflectometer recording the decibel vs. distance of the reflector receding from the mica window holding the liquid at the bottom of the coaxial line (1–4 GHz) or of various waveguides (8–90 GHz).

Results and Discussion

Electrical Conductance. Table I reports the equivalent electrical conductivities Λ ($\Omega^{-1}\ cm^2\ equiv^{-1}$) and the molar concentration c (M) for $LiAsF_6$ in DMC at 25 °C. Four runs were performed with two conductance cells of cell constant $K_c = 0.1156$ and 0.2794 cm^{-1}. This last cell was used for run 4 at $c > 0.5$ M. We recalibrated the cell of lower constant with recrystallized KCl dissolved in water, measuring the cell impedance in the frequency range 1000–5000 Hz and using the Fuoss et al. equation[8] for the cell calibration

$$\Lambda = 149.93 - 94.65c^{1/2} + 58.74c \log c + 198.4c$$

The result over five solutions was

$$K_c = 0.1156 \pm 0.0004\ cm^{-1}$$

Figure 1 shows the same data in the form of log Λ vs. log c. A dramatic change, over several orders of magnitude for Λ, changing with concentration, takes place. Cleary, at ≈1 M we have a conductivity comparable to the one of $LiAsF_6$ in DME at

† Present address: Colgate-Palmolive Co., Piscataway, NJ.

(1) Farber, H.; Irish, D. E.; Petrucci, S. *J. Phys. Chem.* **1983**, *87*, 3515.
(2) Delsignore, M.; Maaser, H. E.; Petrucci, S. *J. Phys. Chem.* **1984**, *88*, 2405.
(3) Saar, D.; Brauner, J.; Farber, H.; Petrucci, S. *J. Phys. Chem.* **1978**, *82*, 545.
(4) Maaser, H. E.; Delsignore, M.; Newstein, M.; Petrucci, S. *J. Phys. Chem.* **1984**, *88*, 5100.
(5) Petrucci, S.; Hemmes, P.; Battistini, M. *J. Am. Chem. Soc.* **1967**, *89*, 5552.
(6) Farber, H.; Petrucci, S. *J. Phys. Chem.* **1975**, *79*, 1221.
(7) Farber, H.; Petrucci, S. *J. Phys. Chem.* **1981**, *85*, 1396.
(8) Lind, J. E.; Zwolenik, J. J.; Fuoss, R. M. *J. Am. Chem. Soc.* **1959**, *81*, 1557.

0022-3654/85/2089-4968$01.50/0

TABLE I: Equivalent Conductance Λ and Molar Concentration c for $LiAsF_6$ and $LiClO_4$ in Dimethyl Carbonate at t = 25 °C

$LiAsF_6$ in Dimethyl Carbonate[a]

run no.	10^4c, M	Λ, Ω^{-1} cm² equiv⁻¹	run no.	10^4c, M	Λ, Ω^{-1} cm² equiv⁻¹
1	1.8881	0.008 235	2	2.2480	0.007 718
	3.2683	0.006 724		4.9147	0.005 702
	6.6691	0.005 031		9.2272	0.004 404
	12.282	0.004 052		24.829	0.003 526
	31.446	0.003 626		58.403	0.003 832
	75.513	0.004 278		113.06	0.005 421
	142.59	0.006 703		216.50	0.011 02
	281.56	0.016 853		427.08	0.039 60
	412.96	0.036 562		692.08	0.144 2
	450.84	0.045 138		884.22	0.293 5
3	1511.9	1.1488	4	5127	6.8609
	1807.4	1.6670		10090	9.002
	3110.5	3.9865			

$LiClO_4$ in Dimethyl Carbonate[b]

run no.	10^4c, M	Λ, Ω^{-1} cm² equiv⁻¹
1	3.5683	0.002 520 3
	10.720	0.001 558 3
	20.323	0.001 328 2
	42.937	0.001 318 1
	78.760	0.001 488 5
	159.865	0.002 148 1
	412.97	0.005 878 5
	696.65	0.013 938
	863.82	0.021 501
	1059.4	0.041 264
2	1417.4	0.084 089
	2488.3	0.336 8

[a] Runs 1, 2, and 3 were performed with a cell of constant K_c = 0.1156 cm^{-1}, and run 4 was performed with a cell of constant K_c = 0.2794 cm^{-1}. [b] Both runs were performed with a cell of constant K_c = 0.1156 cm^{-1}.

$c \approx 10^{-4}$ M, a not too surprising event if one realizes that the permittivity of the solution has increased drastically from ϵ = 3.1, the value of the solvent, as shown below. In the range of electrolyte concentration 10^{-4}–10^{-2} M, the classical Fuoss–Kraus theory for triple-ion formation[9] reads

$$\Lambda g(c)c^{1/2} = \frac{\Lambda_0}{K_p^{1/2}} + \frac{\Lambda_0^T K_T}{K_p^{1/2}}\left(1 - \frac{\Lambda}{\Lambda_0}\right)c \qquad (I)$$

with

$$g(c) = \frac{\exp\left(-2.303\dfrac{\beta'}{\Lambda_0^{1/2}}(c\Lambda)^{1/2}\right)}{\left(1 - \dfrac{S}{\Lambda_0^{3/2}}(c\Lambda)^{1/2}\right)\left(1 - \dfrac{\Lambda}{\Lambda_0}\right)^{1/2}}$$

where β' is the Debye–Hückel activity coefficient term

$$\beta' = \frac{1.8247 \times 10^6}{(\epsilon T)^{3/2}}$$

and

$$S = \alpha\Lambda_0 + \beta = \frac{0.8204 \times 10^6}{(\epsilon T)^{3/2}}\Lambda_0 + \frac{82.501}{\eta(\epsilon T)^{1/2}}$$

is the Onsager conductance term. We have used ϵ = 3.12, η = 0.005 85 P, and $\Lambda_0(LiAsF_6)$ = 97.4 Ω^{-1} cm^2 $equiv^{-1}$, based on Λ_0 = 22.53 Ω^{-1} cm^2 $equiv^{-1}$ in propylene carbonate,[10] η = 0.0253 P, and the Walden rule $\Lambda_0\eta$ = constant. The results, applying eq I to the data, are determination coefficient r^2 = 0.988, intercept = 1.033×10^{-4}, and slope = 0.0306, from which $K_p = 8.9 \times 10^{11}$ M^{-1} and K_T = 445 M^{-1}, having chosen the arbitrary position $\Lambda_0^T = {}^2/_3\Lambda_0$ as done previously. Figure 2 reports an illustration of function I for the present data.

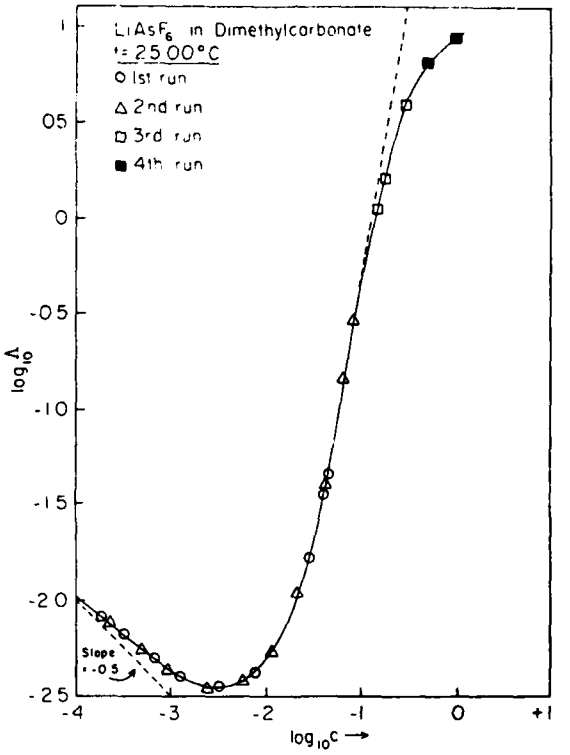

Figure 1. log Λ vs. log c for $LiAsF_6$ in DMC at 25 °C. Λ is the equivalent conductivity, and c is the molar concentration.

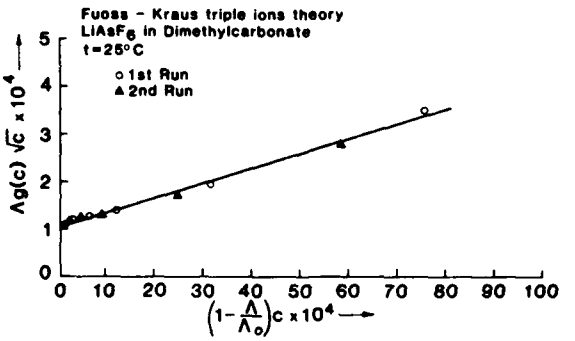

Figure 2. $\Lambda g(c)c^{1/2}$ vs. $(1 - \Lambda/\Lambda_0)c$ for $LiAsF_6$ in DMC at $c \leq 0.01$ M.

Figure 3A shows the log Λ data for $LiClO_4$ in DMC at 25 °C plotted vs. log c. Table I reports the Λ and c data for the two runs performed for $LiClO_4$ in DMC at 25 °C. One can see immediately by comparing Figures 1 and 3 that the equivalent conductance of $LiClO_4$ is 1 order of magnitude lower than that of $LiAsF_6$ at the same total concentration. Application of eq I to the data at $c < 10^{-2}$ M for $LiClO_4$ is shown in Figure 3B. Linear regressions of $\Lambda g(c)c^{1/2}$ vs. $c(1 - \Lambda/\Lambda_0)$ gives r^2 = 0.993, intercept = 0.3937×10^{-4}, and slope = 0.0110, from which $K_p = 8.6 \times 10^{12}$ M^{-1} and K_T = 418 M^{-1}, with $\Lambda_0^T = {}^2/_3\Lambda_0$, as done above.

For the above calculation we have used $\Lambda_0(LiClO_4)$ = 115.7 Ω^{-1} cm^2 $equiv^{-1}$ in DMC, based on Walden's rule and the results for $LiClO_4$ in propylene carbonate,[10] Λ_0 = 26.75 Ω^{-1} cm^2 $equiv^{-1}$ and η = 0.0253 P. By using for both $LiAsF_6$ and $LiClO_4$ the data for Λ_0 in propylene carbonate, having the same polar group as DMC

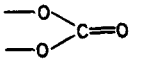

(9) Fuoss, R. M.; Kraus, C. A. *J. Am. Chem. Soc.* **1933**, *55*, 2387.
(10) Salomon, M.; Plichta, E. J. *Electrochim. Acta* **1984**, *29*, 731.

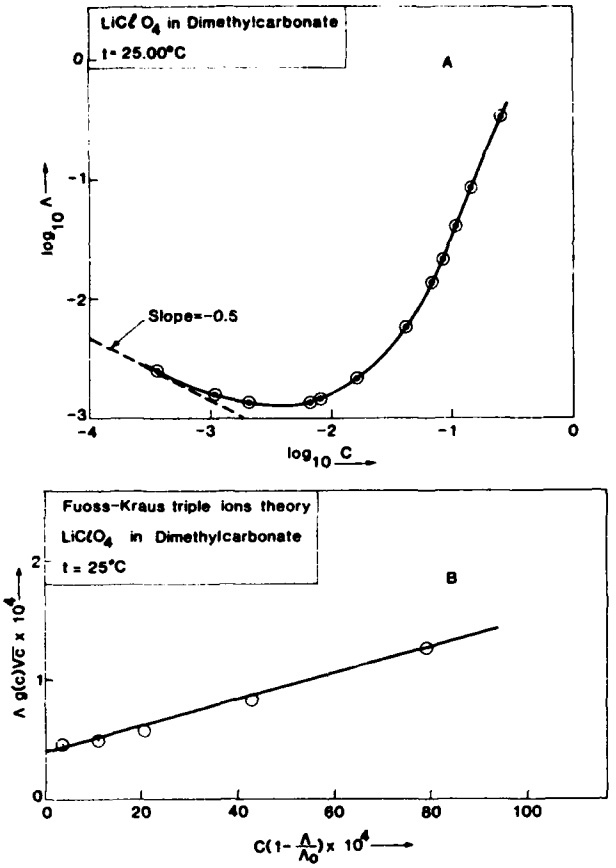

Figure 3. (A) log Λ vs. log c for DMC at t = 25 °C. (B) $\Lambda g(c)c^{1/2}$ vs. $(1 - \Lambda/\Lambda_0)c$ for $LiClO_4$ in DMC at $c \leq 0.01$ M.

we believe to have achieved a reasonable validity of Walden's rule.

An attempt has been made at this point to see whether the positive derviation of the Fuoss–Kraus $\Lambda g(c)c^{1/2}$ vs. $(1 - \Lambda/\Lambda_0)c$ plot, a trend observed before[1,2] for concentrations higher than $c \approx 10^{-2}$ M, was due to causes other than the ionic strength. It is our contention that the latter is quite low in DMC and that the apparent failure of the theory to represent the data at $c > 10^{-2}$ M is in part due to the inappropriate permittivities and viscosities used in the theoretical expressions. From the microwave portion of the work, we have fitted the static permittivities ϵ for $LiAsF_6$ solutions to the electrolyte concentration c by a cubic polynomial equation which gives by nonlinear regressions

$$\epsilon = 3.11 + 27.479c - 110.340c^2 + 199.25c^3 \quad (r^2 = 0.9993) \tag{II}$$

valid up to $c = 0.25$ M. In the same concentration range the solution densities are given by

$$\rho = 1.063 + 0.1879c - 0.2185c^2 + 0.1655c^3 \quad (r^2 = 0.99994)$$

valid within ±0.001 g/cm^{-3}. It is noteworthy to emphasize the point raised above that at 0.25 M $\epsilon = 6.20$ instead of $\epsilon = 3.11$, the solvent value. We have then decided to take the variation into account in dealing with the Fuoss–Kraus theory, a concept already expressed years ago by E. A. S. Cavell.[11] In addition, we have corrected the viscosities by the presence of the electrolyte $LiAsF_6$ by the Einstein equation, as suggested by Fuoss[12]

$$\eta^E = \eta_0\left[1 + \frac{5}{2}\phi\right] = \eta_0[1 + Fc] \tag{III}$$

where ϕ is the volume fraction $\phi = (4\pi R^3/3)Lc/1000 = {}^2/_5Fc$ and $F = 6.308 \times 10^{21}R^3$. R, the radius of the pair (taken as a sphere), has been estimated by the Debye expression $\tau = (4\pi R^3/kT)\eta$, $\tau = (2\pi f_r)^{-1}$ neglecting differences between the decay of the polarization τ_D and the real molecular relaxation time τ that enter the Debye equation. Similarly, $\eta \approx \eta_0 = 0.00585$ P has been retained. With $f_r = 1.7 \times 10^9$ Hz, it results $R = 3.7 \times 10^{-8}$, a value comparable with the sum of the crystallographic radii for $LiAsF_6$ giving $R_{cry} = 4.4 \times 10^{-8}$ cm. One should also point out that we are in complete agreement with Fuoss[12] in that eq III ought to be used instead of the experimental viscosities. The latter incorporates the Falkenhagen[13] term S_η

$$\eta = \eta_0(1 + S_\eta c^{1/2} + Fc)$$

expressing the existing velocity gradients in the solution which are absent in the conductance experiment where the solution is at rest as a whole. It results for $LiAsF_6$ in DMC that $F = 0.3$ and $\eta^E = \eta_0(1 + 0.3c)$. By the aid of eq II and III, we have calculated eq I, namely, the $g(c)$ term corrected by $\epsilon(c)$ and η^E. The data for $LiAsF_6$ in DMC are reported in Figure 4. We have then tried to calculate the right side of eq I from theory, using the expressions by Fuoss–Jagodzinski[14]

$$K_p = K_{FJ} = \frac{4\pi La^3}{3000}e^{-1/2}e^b$$

$$K_T = K_{FJ}{}^T = \frac{\pi La^3}{1000}e^{-3/2}e^{b/2} \tag{IV}$$

Specifically, we have equated eq IV to the values of K_p and of K_T for $LiAsF_6$ found experimentally in the low concentration range, namely, $K_p = 8.9 \times 10^{11}$ M^{-1} and $K_T = 445$ M^{-1} obtaining (with $\epsilon = 3.12$) $a = 6.3 \times 10^{-8}$ cm and $a_T = 16.4 \times 10^{-8}$ cm. Without assigning to these parameters physical significance, we have used these numerical values to calculate eq IV at all the concentrations using eq II to evaluate ϵ.

The results for $LiAsF_6$ solutions in DMC are reported in Figure 4 together with the calculated $[\Lambda c^{1/2}g(c)]_{calcd}$ according to the right side of eq I and also by using $\Lambda_0{}^T = {}^1/_3\Lambda_0$ as in the original version of the triple-ion theory.[3] In Figure 4 the solid lines represent these calculated values showing a qualitative trend following the data

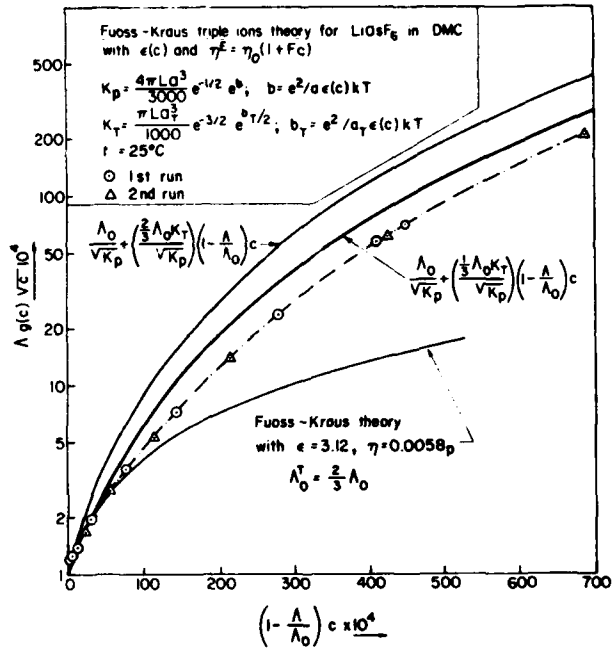

Figure 4. $\Lambda g(c)c^{1/2}$ vs. $(1 - \Lambda/\Lambda_0)c$ for $LiAsF_6$ in DMC at $c \leq 0.07$ M. $g(c)$ has been calculated with $\epsilon(c)$ and η^E (see text).

(11) Cavell, E. A. S.; Knight, P. C. *Z. Phys. Chem. (Munich)* **1968**, *57*, 3.

(12) Fuoss, R. M.; Accascina, F. "Electrolytic Conductance"; Interscience: New York, 1959; p 234.

(13) Falkenhagen, H.; Dole, M. *Z. Phys. Chem., Abt. B* **1929**, *6*, 159. Falkenhagen, H. *Phys. Z.* **1931**, *32*, 365, 745.

(14) Jagodzinski, P.; Petrucci, S. *J. Phys. Chem.* **1974**, *78*, 917.

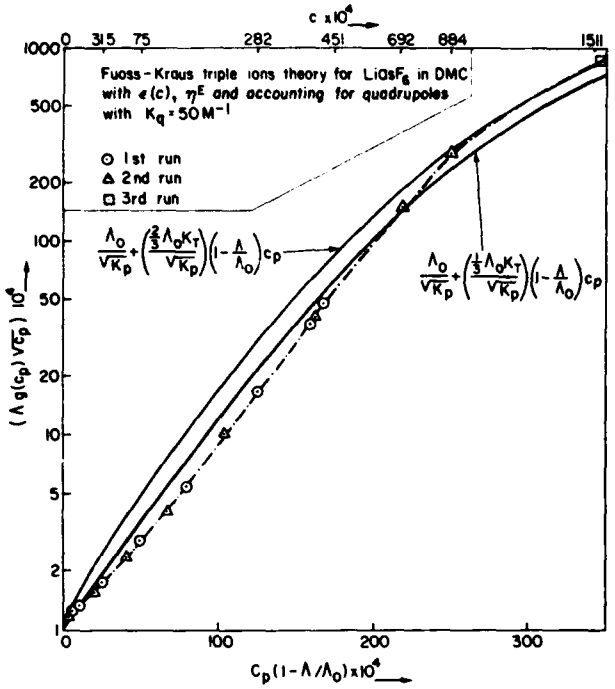

Figure 5. $\Lambda g(c_p)c_p^{1/2}$ vs. $(1 - \Lambda/\Lambda_0)c_p$ for $LiAsF_6$ in DMC at 25 °C. c_p has been calculated from the expression $c = c_p + 2K_q c_p^2$ with $K_q = 50$ M^{-1}. Also, $\epsilon(c)$ and η^E have been used for the calculation of $g(c_p)$.

at variance with the original Fuoss–Kraus theory using $\epsilon = 3.12$ and $\eta = 0.00585$ P. The introduction of $\epsilon(c)$ and η^E seems, however, to have overcorrected the $\Lambda g(c)c^{1/2}$ data. The results from the microwave data, shown below for $LiAsF_6$ in DMC, indicate that the ion pairs are not the only complex species present. The Böttcher plot[15] shows a strong concave down curvature indicating lack of proportionality of the relaxation strength $\epsilon_0 - \epsilon_\infty$ with the total concentration. This, in turn, suggests that the polarization of the solution is not proportional to c and that the total concentration is different from c_p, the ion-pair concentration. The situation is corrected by the introduction of a quadrupole equilibrium with $K_q \sim 50$ M^{-1}.

We have applied the same criterion to the conductance data of $LiAsF_6$ in DMC, expressing the total concentration by the two *major* species present (free ions and triple ions are in minor quantities)

$$c = (AB) + 2(A_2B_2) = c_p + 2c_p^2K_q$$

and using c_p rather than c in the Fuoss–Kraus scheme of association to triple ions

$$A + B \rightleftharpoons AB + B \rightleftharpoons AB_2$$

$$\rightleftharpoons AB + A \rightleftharpoons A_2B$$

with $(A) = (B) = \alpha c_p$, $(AB) = c_p(1 - \alpha - 3\alpha_T)$, and $(AB_2) = (A_2B) = \alpha_T c_p$, leading to the usual expression

$$\Lambda g(c_p)c_p^{1/2} = \frac{\Lambda_0}{K_p^{1/2}} + \frac{\Lambda_0^T K_T}{K_p^{1/2}}\left(1 - \frac{\Lambda}{\Lambda_0}\right)c_p \qquad (V)$$

which differs from eq I only by the presence of c_p instead of c. Figure 5 reports the left and right side of eq V depicted, the former by the experimental point and the latter by the solid line. Although the data for $\Lambda_0^T = {}^1/_3\Lambda_0$ are overcorrected in the lower portion of the curve and undercorrected in the upper portion, the general qualitative trend is followed up to $c \approx 0.1$ M, a large improvement over the original calculations using $\epsilon = 3.12$ and $\eta = 0.00585$ P, the solvent properties.

(15) Böttcher, C. F. "Theory of Electrical Polarization"; Elsevier: Amsterdam, 1973.

(16) Cole, K. S.; Cole, R. H. *J. Chem. Phys.* **1949**, *9*, 341.

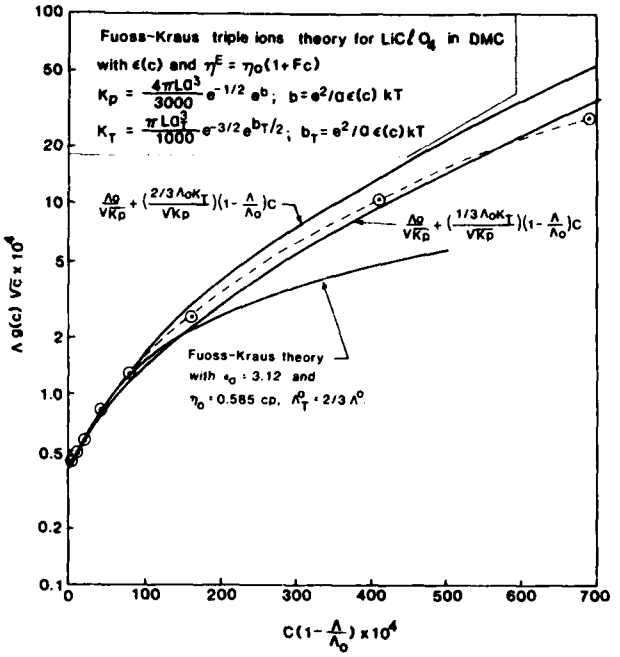

Figure 6. $\Lambda g(c)c^{1/2}$ vs. $(1 - \Lambda/\Lambda_0)c$ for $LiClO_4$ in DMC at $c \leq 0.07$ M. $g(c)$ has been calculated with $\epsilon(c)$ and η^E (see text).

The same sequence of calculations has been applied to the $LiClO_4$ data. The permittivity is expressible in terms of the concentration of $LiClO_4$ by the expression $\epsilon = 3.12 + 7.833c + 47.228c^2 - 125.61c^3$ with $r^2 = 1.0000$. The density of the solutions can be expressed by the relation $\rho = 1.063 - 0.02081c + 0.8965c^2 - 1.9036c^3$ with c the molarity of the solutions and $r^2 = 1.0000$. The average lower decay time of the polarization of the solutions is taken to be approximately equal to the relaxation time $\tau = (2\pi f_r)^{-1} = (2\pi \times 1.3 \times 10^9)^{-1} = 122.4 \times 10^{-12}$ s which, by the aid of the Debye expression $\tau = (4\pi R^3/kT)\eta$, gives $R = 4.09 \times 10^{-8}$ cm. This value introduced into the Einstein relation $\phi = (4\pi R^3/3)Lc/1000 = (2/5)Fc$ gives $F = 0.43$ and $\eta^E = \eta_0(1 + 0.43c)$.

The calculation has then been applied using eq I as for the case of the $LiAsF_6$ data, with the $\epsilon(c)$ and η^E data. The results of this calculation are depicted in Figure 6 where the solid lines correspond to the theoretical $\Lambda g(c)c^{1/2}$, calculated by the aid of equations (IV) $\Lambda_0^T = {}^2/_3\Lambda_0$ and $\Lambda_0^T = {}^1/_3\Lambda_0$. The values of $a = 5.8 \times 10^{-8}$ cm and $a_T = 16.8 \times 10^{-8}$ cm have been used based on the fit of the experimental $K_p = 8.6 \times 10^{12}$ M^{-1} and $K_T = 418$ M^{-1} from the low-concentration data. From Figure 6 the same considerations as for $LiAsF_6$ hold, namely, the agreement of the calculated and experimental data, although qualitative, encompasses a larger concentration range than in the original theory using $\epsilon = 3.12$ and $\eta = 0.00585$ P.

The difference from the $LiAsF_6$ case is that there is no need of introducing a quadrupole constant, as evidenced also by the microwave data showing no evidence of quadrupole complexation for $LiClO_4$, the Böttcher plot[15] being linear. In the above calculation of $\Lambda g(c)c^{1/2}$ the best fit is obtained by the position $\Lambda_0^T = {}^1/_3\Lambda_0$ as in the original Fuoss–Kraus theory.[9] One could surmise that by adjusting K_p, K_T, and K_q (for $LiAsF_6$) the fit may become better. Here, however, we wish only to stress the concept that, by using the information from the microwave experiments (that the permittivity of the solution changes) and by correcting viscosities, a significant improvement over the concentration range usable by the conductance theory can be obtained.

In other words, at very low permittivities, where very few ions are present, the failure of the theory is not due to ionic strength effects but rather to the neglect of the effect of the presence of large quantities of neutral species and their altering the permittivity ϵ and viscosity η. Improvements on the theory will have to be made by trying to incorporate these changes, nowadays measurable by modern tools such as microwave spectrometry for ϵ rather than

TABLE II: Dielectric Relaxation Parameters and Electrical Conductivity X for $LiAsF_6$ and $LiClO_4$ in Dimethyl Carbonate at 25 °C at the Concentrations Investigated

c	ϵ_0	ϵ_{∞_1}	ϵ_{∞_2}	f_1, GHz	f_2, GHz	X, Ω^{-1} cm^{-1}	$\lvert\bar{\Delta}\epsilon'\rvert$[a]	$\lvert\bar{\Delta}\epsilon''\rvert$[a]
				$LiAsF_6$				
0.25	6.20	3.50	2.50	1.6	22	7.38×10^{-4}	0.095	0.06
0.15	5.40	3.40	2.45	1.8	22	1.66×10^{-4}	0.04	0.05
0.10	5.00	3.30	2.40	1.6	22	3.98×10^{-5}	0.08	0.05
0.05	4.20	3.20	2.40	1.8	22	2.94×10^{-6}	0.04	0.02
				$LiClO_4$				
0.29	6.30	3.40	2.45	1.4	22	1.24×10^{-4}	0.026	0.041
0.19	5.50	3.35	2.45	1.3	22	3.22×10^{-5}	0.053	0.047
0.10[b]	4.25	3.30	2.40	1.2	18	3.46×10^{-6}	0.64	0.28
0[b]		3.12	2.35		22		0.35	0.22

[a] $\lvert\bar{\Delta}\epsilon'\rvert$ and $\lvert\bar{\Delta}\epsilon''\rvert$ are absolute average deviations ϵ'(calcd) − ϵ'(exptl) and ϵ''(calcd) − ϵ''(exptl). [b] Saar, D.; Brauner, J.; Farber, H.; Petrucci, S. *J. Phys. Chem.* **1978**, *82*, 5451.

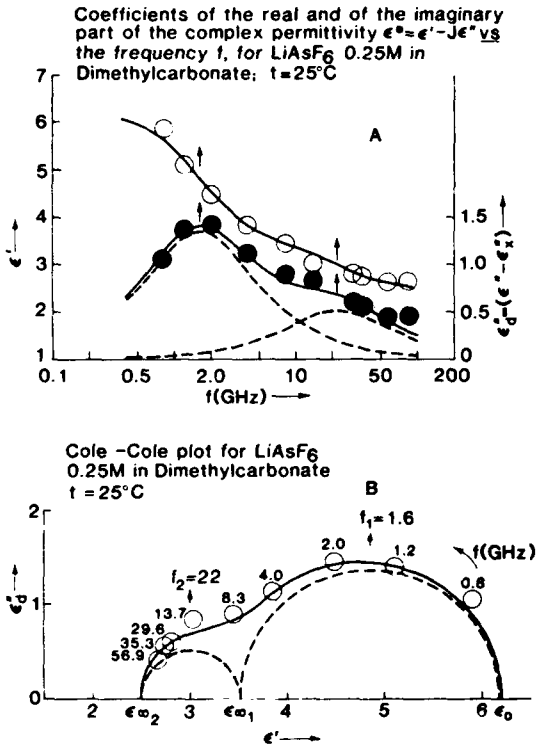

Figure 7. (A) ϵ' vs. f and $\epsilon_d'' = \epsilon'' - \epsilon_x''$ vs. f for $LiAsF_6$ (0.25 M). (B) Cole–Cole plot of $\epsilon_d'' = \epsilon'' - \epsilon_x''$ vs. ϵ' for $LiAsF_6$ (0.25 M) in DMC.

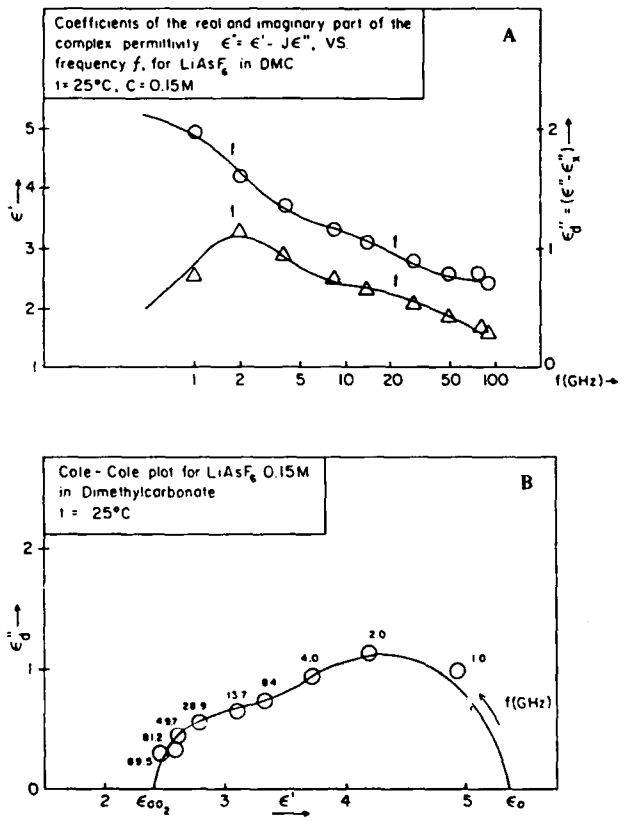

Figure 8. (A) ϵ' vs. f and ϵ'' vs. f for $LiAsF_6$ (0.15 M) in DMC at t = 25 °C. (B) Cole–Cole plot of $\epsilon_d'' = \epsilon'' - \epsilon_x''$ vs. ϵ' for $LiAsF_6$ (0.15 M) in DMC.

trying to improve on the mathematical treatment. This treatment, expressed by the Onsager–Fuoss–Kraus various editions of the theory,[12] remains an unsurpassed legacy of ingenuity, elegance, and rigor.

Microwave Complex Permittivities. Figures 7 and 8 show representative plots of the coefficient of the real part ϵ' and of the imaginary part ϵ'' of the complex permittivity $\epsilon_d^* = \epsilon' - J\epsilon_d''$, plotted vs. the frequency f for $LiAsF_6$ and $LiClO_4$ in DMC. The solid lines are the sum of two Debye single-relaxation processes according to the functions

$$\epsilon' = \frac{\epsilon_0 - \epsilon_{\infty_1}}{1 + (f/f_1)^2} + \frac{\epsilon_{\infty_1} - \epsilon_{\infty_2}}{1 + (f/f_2)^2} + \epsilon_{\infty_2}$$

$$\epsilon_d'' = (\epsilon_0 - \epsilon_{\infty_1})\frac{f/f_1}{1 + (f/f_1)^2} + (\epsilon_{\infty_1} - \epsilon_{\infty_2})\frac{f/f_2}{1 + (f/f_2)^2} \qquad \text{(VI)}$$

with ϵ_0, ϵ_{∞_1}, ϵ_{∞_2}, f_1, and f_2 the relaxation parameters. ϵ_0 is the static permittivity of the solution. $\epsilon_0 - \epsilon_{\infty_1}$ and $\epsilon_{\infty_1} - \epsilon_{\infty_2}$ are the respective relaxation strengths of solute and solvent, and f_1 and f_2 are the relaxation frequencies associated with the solute and the solvent in the solution. ϵ_{∞_1} should extrapolate at zero electrolyte concentration to the static permittivity of the pure solvent. In Figures 7 and 8 the Cole–Cole plots[16] of the quantities ϵ_d'' vs. ϵ' are also depicted. The solid lines correspond to the sum of two Debye processes according to eq VI. In the above, ϵ_d'' is the total dielectric loss ϵ'' from which has been subtracted the contribution due to the conductance $\epsilon_x'' = 1.8 \times 10^{12} X/f$ with X the specific conductance of the solutions (Ω^{-1} cm^{-1}). In Table II the dielectric relaxation parameters are reported together with the conductivity X. Equation VI have been fitted to the data by a trial and error procedure that minimizes the summations $\sum|\Delta\epsilon'| + \sum|\Delta\epsilon''|$, where $|\Delta\epsilon'| = |\epsilon'(\text{calcd}) - \epsilon'(\text{exptl})|$ and $|\Delta\epsilon''| = |\epsilon''(\text{calcd}) - \epsilon''(\text{exptl})|$ are the absolute values of the deviations.[3] We have already shown in the conductance section dealing with the $LiAsF_6$ data that the value of a obtained from the decay time of the polarization τ is comparable to the sum of the crystallographic radii, at least as an order of magnitude. In order to gain more structural information on the system, we have plotted the Böttcher function[15]

$$\epsilon_0 - \epsilon_{\infty_1} = \frac{10^{-3} 4\pi Lc}{(1 - \alpha f)^2} \frac{\mu^2}{3kT} \frac{3\epsilon_0}{2\epsilon_0 + 1} \qquad \text{(VII)}$$

in the form $\phi(\epsilon) = (\epsilon_0 - \epsilon_{\infty_1})[(2\epsilon_0 + 1)/(3\epsilon_0)]$ vs. c for $LiAsF_6$

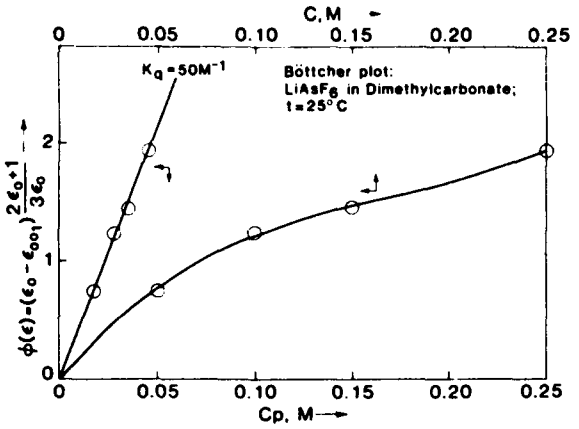

Figure 9. Böttcher function $\phi(\epsilon) = \epsilon_0 - \epsilon_{\infty 1})[(2\epsilon_0 + 1)/(3\epsilon_0)]$ vs. c and vs. $c_p = [-1 + (8K_q c + 1)^{1/2}]/(4K_q)$ for $LiAsF_6$ in DMC at $t = 25$ °C. K_q is the dimerization constant for ion pairs to quadrupoles (or dimers).

in DMC. Neglecting the polarizability α, reaction field factor of term $(1 - \alpha f)^2$ of the order of unity, one would expect a straight line. In fact, in Figure 9 one may see a strong concave down curvature.[20] This behavior becomes obvious if one realizes that in DMC one ought to expect much higher dimerization of pairs than in the dimethoxyethane and 2-methyltetrahydrofuran ethers studied so far. This is because of the lower permittivity of DMC.

If one accepts the idea that polar dimers are formed, ruled by the equilibrium $2AB \rightleftarrows (A_2B_2)$ and $K_q = (A_2B_2)/(AB)^2$, then by combining the expressions

$$c = (AB) + 2(A_2B_2)$$

$$K_q = (A_2B_2)/(AB)^2$$

$c_p = (AB)$ can be calculated for tentative values of K_q. Linear regressions of $\phi(\epsilon)$ vs. c_p should give the best straight line for the best K_q. The calculation has been done and is shown in Figure 9 leading to $r^2 = 0.990$, intercept = 0.017, and slope = 42.89 for $K_q = 50$ M^{-1}. One ought to add, however, that the optimum fit is rather insensitive on K_q, a value of $K_q = 30$ M^{-1} giving almost as good a result as $K_q = 50$ M^{-1}. With $K_q = 50$ M^{-1}, the apparent dipole moment results $\mu = 26.5 \times 10^{-18}$ esu cm, namely, $a_\mu = 5.5 \times 10^{-8}$ cm, taking a rigid sphere model $\mu = ae$ for $LiAsF_6$ in DMC. With $K_q = 30$ M^{-1}, $r^2 = 0.990$, intercept = 0.063, slope = 33.35, $\mu = 23.3 \times 10^{-18}$ esu cm, and $a_\mu = 4.9 \times 10^{-8}$ cm.

In either case one may be led to the conclusion that a_μ is of the order of magnitude of the sum of the crystallographic radii. Values for the dimerization constants have been calculated by Chabanel et al.,[17] from static dielectric data for LiBr, LiSCN, and $AgClO_4$. The calculation was based on assuming that the static dielectric increments over the solvent were due to *both* monomer pairs and dimers or quadrupoles

$$\Delta\epsilon = \delta_1(AB) + \delta_2(A_2B_2)$$

implying that the quadrupoles are polar and that $\delta_2 \neq 0$. In fact, it was reported that $\delta_2 = 1.8$ for LiBr, $\delta_2 = 10.8$ for LiSCN, and $\delta_2 = 8.6$ for $AgClO_4$ giving quadrupole constants K_q(LiBr) = 90 M^{-1}, K_q(LiSCN) = 20 M^{-1}, and $K_q(AgClO_4)$ = 45 M^{-1}. For $LiClO_4$ the effect of quadrupoles was undetectable. Later, however, it was found[18] that for both dimethyl carbonate and diethyl carbonate solvents, for LiSCN and $LiClO_4$, the microwave complex permittivity data extrapolated to static values (ϵ_0's) comparable with the data by Chabanel et al. As the microwave data were interpreted by a single Debye relaxation which was assigned to the rotation of only polar ion pairs, one had to conclude[18] that the dimers were apolar. Hence, the assumptions on the δ_2's made by Chabanel and the calculated K_q's had to be incorrect. It is also noteworthy that IR spectra in ethers in the 2040-cm^{-1} range indicated the presence of a centrosymmetric quadrupole[19]

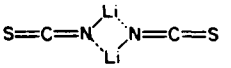

which by symmetry would have a zero dipole moment in accord with our contention for LiSCN in DMC and DEC.

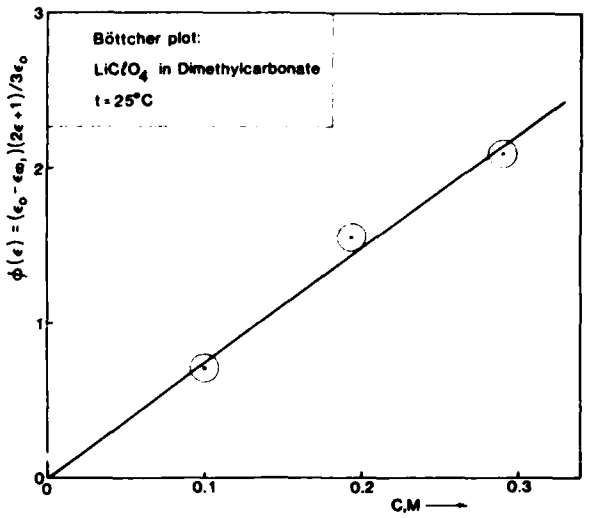

Figure 10. Böttcher function $\phi(\epsilon) = (\epsilon_0 - \epsilon_{\infty 1})[(2\epsilon_0 + 1)/(3\epsilon_0)]$ vs. c for $LiClO_4$ in DMC at $t = 25$ °C.

Figure 10 reports the Böttcher plot,[15] according to eq VII, for the dielectric data of $LiClO_4$ in DMC. Linear regressions giving 50% statistical weight to the origin give $r^2 = 0.995$ and slope = 7.413 from which one calculates the apparent dipole moment $\mu = 11.0 \times 10^{-18}$ esu cm. By taking a rigid sphere model (consistent with having neglected the polarization reaction field term) $(1 - \alpha f)^2$ gives $\mu = ae$ and $\alpha_\mu = 2.3 \times 10^{-8}$ cm, giving a strong indication of contact species for $LiClO_4$.

It is noteworthy that no curvature of the Böttcher plot is visible, at variance with the case of $LiAsF_6$ in DMC, indicating apparent absence of quadrupoles for $LiClO_4$ in DMC. This is somewhat surprising in view of $K_p(LiClO_4) > K_p(LiAsF_6)$.

Acknowledgment. The authors are grateful to the Army Office for Scientific Research (Grant No. DAAG/29/82/K0048 and DAAG/29/85/K0048) for their generous support.

Registry No. DMC, 616-38-6; $LiAsF_6$, 29935-35-1; $LiClO_4$, 7791-03-9.

(17) Menard, D.; Chabanel, M. *J. Phys. Chem.* **1975**, *79*, 1081.
(18) Saar, D.; Brauner, J.; Farber, H.; Petrucci, S. *J. Phys. Chem.* **1978**, *82*, 1943.
(19) Paoli, D.; Lucon, L.; Chabanel, M. *Spectrochim. Acta, Part A* **1978**, *34A*, 1087.
(20) Nonlinear regression of

$$\phi(\epsilon) = (\epsilon_0 - \epsilon_{\infty 1})\frac{2\epsilon_0 + 1}{3\epsilon_0}$$

vs. c gives

$$\phi(\epsilon) = -0.002 + 19.534c - 91.273c^2 + 177.023c^3 \quad (r^2 = 0.9996)$$

giving 50% statistical weight to the origin.

Reprinted from The Journal of Physical Chemistry, 1986, 90, 66.

Molecular Relaxation Dynamics and Ionic Association of $LiBF_4$ in Dimethoxymethane

M. Delsignore, H. Farber, and S. Petrucci*

Departments of Chemistry and Electrical Engineering, Polytechnic Institute of New York, Long Island Center, Farmingdale, New York 11735 (Received: June 18, 1985)

Electrical conductance data for $LiBF_4$ in dimethoxymethane (DMM) at 25 °C reveal the electrolyte to be heavily associated to ion pairs and triple ions. A theoretical expression for the triple-ion association constant similar to the Bjerrum one for ion pairs and to the Maaser–Bjerrum theory of dimers has been developed and applied to the present conductance data. Ultrasonic relaxation absorption data at much higher concentrations than the conductance data reveal association to dimers. This is also evident from the microwave dielectric data showing no electrolyte dielectric effect on the solvent and apparent lack of presence of dipoles. The ultrasonic data can be rationalized by a two-step dimerization mechanism.

Introduction

A previous conductance study of the ionic association of $LiBF_4$ in 2-methyltetrahydrofuran[1] and in 1,2-dimethoxyethane[2] of respective static permittivities $\epsilon = 6.2$ and 7.0 has been reported. In the same works,[1,2] the diffusional rotational relaxation dynamics of ion pairs was studied by dielectric relaxation. In addition, ultrasonic relaxation revealed some dimerization of the ion pairs and a kinetic investigation of this additional process was reported.

It was of interest to extend the above studies in a medium of lower permittivity as dimethoxymethane (DMM), where $\epsilon = 2.76$ at 25 °C. Presumably in DMM the electrolyte exists completely as ion pairs at all finite concentrations but the extent of triple-ion formation and quadrupule formation maybe sizable and may become preponderant at high concentrations ($c > 0.1$ and 0.2 M). On the practical side, $LiBF_4$ dissolved in ethers is a system relevant to secondary batteries construction. It was of interest to report a quantitative study in a solvent of very low permittivity as DMM ($\epsilon = 2.76$ at 25 °C) which may constitute an extreme limit for an electrolyte solution. In the process, we have derived a new Bjerrum-like expression for the association to triple ions as reported below. This expression and the corresponding one for dimer formation, already presented,[2] may give some theoretical guidelines to the extent of association up to the quadrupoles but below the larger aggregates which may precede the eventual separation of the electrolyte from the liquid phase. For the sake of clarity, after the Experimental Part the conductance and theoretical aspects leading to the triple-ion formation constant will be dealt with first, followed by the relaxation dynamics study by ultrasonic and microwave dielectric relaxation which involves itself with dimer formation.

Experimental Part

The equipment for the conductance[3] and microwave dielectric relaxation[4] has already been described. For the ultrasonic work the pulse instrumentation has been automated, in data capturing, by mounting over the dual-crystal interferometric cell a Mitutoyo Series 164 digital micrometer (resolution ±0.000 05 in.) and associated interfaced digital counter and printer, giving a hard copy of the displacements for attenuation increments (expressed in decibels) of the standard comparison signal.

For the chemicals, the solvent DMM (Aldrich) was refluxed over sodium and benzophenone until a bluish coloration indicating absence of peroxides was present. It was then distilled in the same all-Pyrex apparatus and used shortly afterward. $LiBF_4$ (Aldrich) was dried in vacuo at ~60 °C overnight.

Results and Discussion

Electrical Conductance. Figure 1A reports the electrical conductance data in the form of log Λ vs. log c at $t = 25.00$ °C for $LiBF_4$ in DMM. Several runs with independently prepared stock solutions and solvent were used in order to ensure reproducibility of the results. Figure 1B reports the same data for $c \leq 0.1$ M elaborated in accord to the Fuoss–Kraus triple-ion theory[5]

$$\Lambda g(c)c^{1/2} = \frac{\Lambda_0}{K_A^{1/2}} + \frac{\Lambda_0^T K_T}{K_A^{1/2}}\left(1 - \frac{\Lambda}{\Lambda_0}\right)c \qquad (I)$$

where $g(c)$ is a term lumping together all the interionic terms, K_A and K_T are the ion-pair and triple-ion formation constants, and Λ_0 and Λ_0^T are the limiting conductivities of the single ions and triple ions respectively. In the above, the arbitrary condition $\Lambda_0^T = {}^2/_3\Lambda_0$ has been retained as done previously.[1,2] Further, for the calculations of Λ_0, the Walden rule has been used with the following data from the literature: in THF at 25 °C (viscosity $\eta = 0.0046$ P)[6] $\lambda^\circ_{Li} = 36.6\ \Omega^{-1}\ cm^2\ equiv^{-1}$,[7] hence $\lambda^\circ_{Li}\eta = 0.168$; in nitrobenzene ($\eta = 0.01823$ P)[8a] $\lambda^\circ_{BF_4} = 22.1\ \Omega^{-1}\ cm^2\ equiv^{-1}$,[8b] hence $\lambda^\circ_{BF_4}\eta = 0.403$. It results that in DMM ($\eta = 0.00315$ P)[9] $\lambda^\circ_{Li} = 53.3\ \Omega^{-1}\ cm^2\ equiv^{-1}$ and $\lambda^\circ_{BF_4} = 127.9\ \Omega^{-1}\ cm^2\ equiv^{-1}$ or $\Lambda^\circ_{LiBF_4} = 181\ \Omega^{-1}\ cm^2\ equiv^{-1}$ and $\Lambda_0^T = {}^2/_3\Lambda_0 = 121\ \Omega^{-1}\ cm^2\ equiv^{-1}$ in DMM at 25 °C.

From Figure 1B, the solid line calculated by linear regressions gives $r^2 = 0.98$, intercept $= \Lambda_0/K_A^{1/2} = 7.20 \times 10^{-7}$, and slope $= \Lambda_0^T K_T/K_A^{1/2} = 3.98 \times 10^{-4}$, from which $K_A = 6.3 \times 10^{16}\ M^{-1}$ and $K_T = 826\ M^{-1}$.

When K_A is equated to the Fuoss–Jagodzinski expression[10]

$$K_{FJ} = \frac{4\pi L d^3}{3000} e^{-1/2} e^b \qquad (II)$$

it results in a charge-to-charge separation in the pair $d = 5.1 \times 10^{-8}$ cm. Similarly, when K_T is equated to the Fuoss–Jagodzinski[10] triple-ion theoretical expression

$$K_T^{FJ} = \frac{\pi L a^3}{1000} e^{-3/2} e^{e^2/2a\epsilon kT} \qquad (III)$$

it results to ion-to-ion pair separation $a = 16.9 \times 10^{-8}$ cm, a value that seems too high to be reconciled with the triple-ion model and

(1) M. Delsignore, H. Maaser, and S. Petrucci, *J. Phys. Chem.*, **88**, 2405 (1984).
(2) H. Maaser, M. Delsignore, M. Newstein, and S. Petrucci, *J. Phys. Chem.*, **88**, 5100 (1984).
(3) S. Petrucci, P. Hemmes, and M. Battistini, *J. Am. Chem. Soc.*, **89**, 5552 (1967).
(4) H. Farber and S. Petrucci, *J. Phys. Chem.* **85**, 1396 (1981), and previous literature quoted therein.
(5) R. M. Fuoss and C. A. Kraus, *J. Am. Chem. Soc.*, **55**, 476 (1933); R. M. Fuoss and F. Accascina, "Electrolyte Conductance", Interscience, New York, 1959.
(6) D. J. Metz and A. Glines, *J. Phys. Chem.*, **71**, 1158 (1967).
(7) D. N. Bhattacharyya, C. L. Lee, J. Smid, and M. Szwarc, *J. Phys. Chem.*, **69**, 608 (1965).
(8) (a) A. L. Powell and A. E. Martell, *J. Am. Chem. Soc.*, **79**, 2118 (1957); (b) C. R. Witschonke and C. A. Kraus, *J. Am. Chem. Soc.*, **69**, 2472 (1947).
(9) D. Saar, J. Brauner, H. Farber, and S. Petrucci, *Adv. Mol. Relax. Interact. Processes*, **16**, 263 (1980).
(10) R. M. Fuoss, *J. Am. Chem. Soc.*, **80**, 5059 (1958); P. Jagodzinski and S. Petrucci, *J. Phys. Chem.*, **78**, 917 (1974).

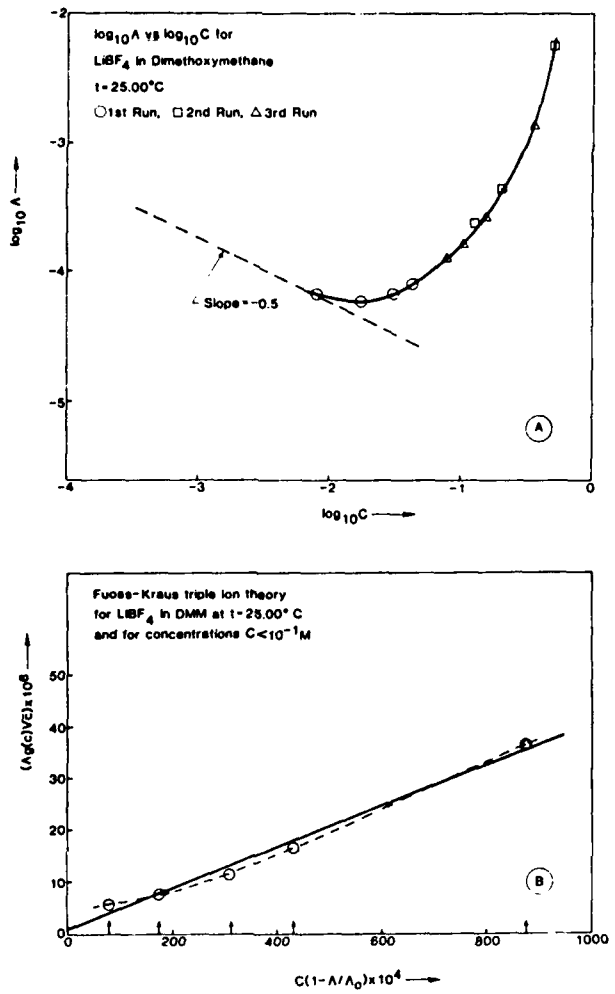

Figure 1. (A) Log Λ vs. log c for $LiBF_4$ in DMM at 25 °C. (B) $\Lambda g(c)c^{1/2}$ vs. $(1 - \Lambda/\Lambda_0)c$ for $LiBF_4$ in DMM at 25 °C according to the Fuoss–Kraus theory.

definition envisaging the three ions at contact, whereas the value $a \sim 1.5d = 7.7 \times 10^{-8}$ cm would appear to be a more reasonable parameter. Therefore, we have decided to reexamine the triple-ion theory for K_T without the constriction that the complexing ion be in contact with the pair to be defined as a triple ion. We shall follow the guidelines of the Bjerrum theory for comparison and the one for the dimers (Maaser–Bjerrum theory) already presented.[2] In the past, dealing with the three-ion interactions Fuoss and Kraus[11] have indeed derived a triple-ion expression based on the Bjerrum model. Their derivation lead to a integral which, to date, is difficult to solve, short of resolving to a graphical integration. We thought it worthwhile to try to arrive at a more manageable solution of the problem by a simplified derivation based on the interaction between an ion and a permanent dipole of moment μ.

Ion–Dipole Interaction. We will start by defining r_- as the distance between a given positive ion and the negative end of a dipole ion pair. Let r be the distance between the same ion and the center of the dipole and r_+ the distance between the ion and the positive end of the dipole ion pair. θ' is the angle between r_- and the line passing through the dipole axis, and d is the separation of the two charges in the dipole. We have then (Figure 2A) $r - r_+ = d \cos \theta'$, and the ion–dipole potential will be

$$\phi = \frac{e}{\epsilon}\left(\frac{1}{r_-} - \frac{1}{r_+}\right) = \frac{e}{\epsilon}\frac{r_+ - r_-}{r_+ r_-} \simeq -\frac{ed\cos\theta'}{\epsilon r^2}$$

(11) R. M. Fuoss and C. A. Kraus, *J. Am. Chem. Soc.*, **55**, 2387 (1933), and previous literature quoted therein.

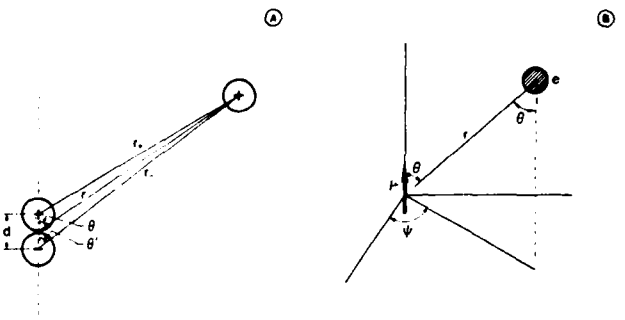

Figure 2. (A) Ion–dipole interaction. The ion is at a distance r from the center of the dipole. The segment r makes an angle θ with the axis of the dipole. (B) Polar coordinate representation of the dipole μ (taken as the origin of the Cartesian coordinate) and of an ion of charge e.

In the above, ϵ is the static permittivity of the solvent and the approximation $r_+ r_- \approx r^2$. If concomitantly one writes $\theta' \approx \theta$, where θ is the angle between r and the line passing through the dipole, one has

$$\phi = -\frac{\mu \cos\theta}{\epsilon r^2} \qquad \text{(IV)}$$

where $\mu = ed$ is the dipole moment of the dipole separated by a distance $r > d$ from the positive ion. The ion–dipole potential energy will then be

$$U = \phi e \simeq -\frac{e\mu\cos\theta}{\epsilon r^2} \qquad \text{(V)}$$

The probability of finding an ion around a dipole taken as the reference of a coordinate system will be a function of the concentration of the ions, $(Nc\sigma/1000)e^{-U/kT}$ (σ is the degree of dissociation of the electrolyte), surrounding the dipole, of the volume shell element, $4\pi r^2\,dr$, and of the solid angle ratio $dW/4\pi$, expressing the point-to-point spatial orientational probability between the ion and the central dipole (Figure 2B). In polar coordinates r, θ, and ψ, we will have

$$\frac{dW}{4\pi} = \frac{r\sin\theta\,d\psi\,r\,d\theta}{4\pi r^2} = \frac{\sin\theta\,d\theta\,d\psi}{4\pi}$$

and

$$dP(r,\theta,\psi) = \left(\frac{Nc\sigma}{1000}e^{e\mu\cos\theta/\epsilon r^2kT}\right)(4\pi r^2\,dr)\left(\frac{\sin\theta\,d\theta\,d\psi}{4\pi}\right)$$

The above expression can be integrated for $\psi = 0$ to 2π, obtaining the probability that the ion is contained in a solid annulus

$$dP(r,\theta) = \left(\frac{Nc\sigma}{1000}e^{e\mu\cos\theta/\epsilon r^2kT}\right)(4\pi r^2\,dr)\left(\frac{\sin\theta\,d\theta}{2}\right)$$

$$dP(r,\theta) = \frac{2\pi Nc\sigma}{1000}r^2\,dr\,(e^{e\mu\cos\theta/\epsilon r^2kT})\sin\theta\,d\theta \qquad \text{(VI)}$$

Call $\cos\theta = y$ and $dy = -\sin\theta\,d\theta$. Then, given

$$dP(r) = \frac{2\pi Nc\sigma}{1000}r^2\,dr\int_0^{\pi}(e^{e\mu\cos\theta/\epsilon r^2kT})\sin\theta\,d\theta$$

we shall have

$$dP(r) = \frac{2\pi Nc\sigma}{1000}r^2\,dr\int_{-1}^{1}e^{(e\mu/\epsilon r^2kT)y}\,dy$$

The integral

$$\int_{-1}^{1}e^{(\mu e/\epsilon r^2kT)y}\,dy = \frac{1}{\mu e/\epsilon r^2kT}\int_{-1}^{1}e^{(\mu e/\epsilon r^2kT)y}\,d\left(\frac{e\mu}{\epsilon r^2kT}y\right)$$

$$= \frac{e^{\mu e/\epsilon r^2kT} - e^{-\mu e/\epsilon r^2kT}}{\mu e/\epsilon r^2kT} = \frac{2\sinh[\mu e/\epsilon r^2kT]}{\mu e/\epsilon r^2kT}$$

Then

$$dP(r) = \frac{2\pi Nc\sigma}{1000} r^2\, dr \left(\frac{e^{\mu e/\epsilon r^2 kT} - e^{-\mu e/\epsilon r^2 kT}}{e\mu/\epsilon r^2 kT} \right) \quad \text{(VII)}$$

In order to integrate with respect to r, one has to set a finite upper limit to r. The above function, for a given finite thickness Δr, shows a minimum with r, defined by

$$\frac{\partial}{\partial r}\left(\frac{\Delta P(r)}{\Delta r}\right) = \frac{4\pi Nc\sigma}{1000} \frac{1}{\mu e/\epsilon kT} \frac{\partial}{\partial r}\left[r^4 \sinh\left(\frac{\mu e}{\epsilon r^2 kT}\right)\right] = 0$$

which, by operating the derivative, leads to

$$4r^3 \sinh\left(\frac{\mu e}{\epsilon r^2 kT}\right) + r^4\left[\cosh\left(\frac{\mu e}{\epsilon r^2 kT}\right)\right]\left(-\frac{2\mu e}{\epsilon r^3 kT}\right) = 0$$

$$4r^3 \tanh\left(\frac{\mu e}{\epsilon r^2 kT}\right) - \frac{2\mu e}{\epsilon r^2 kT} r^3 = 0$$

Call $Y = \mu e/\epsilon r^2 kT$. Then $2 \tanh Y - Y = 0$ and

$$\tan Y/Y = 0.5 \quad \text{(VIII)}$$

which is satisfied for $Y = 1.915 \approx 2$. The probability function will have a minimum for $Y \approx 2$ which means physically that the probability will go through a minimum for a squared distance $r^2 = q^2$ that corresponds to an aligned ($\theta = 0$) ion–dipole configuration of energy equal to $2kT$ or

$$q = \left(\frac{e\mu}{2\epsilon kT}\right)^{1/2} \quad \text{(IX)}$$

For an electrolyte such as $LiBF_4$ of $\mu = 16 \times 10^{-18}$ esu cm in the solvent 1,2-dimethoxyethane ($\epsilon = 7.0$ at 25 °C) $q = 11.5_5 \times 10^{-18}$ cm, whereas in DMM ($\epsilon = 2.76$ at 25 °C), by retaining the same μ, it results in $q = 18.4 \times 10^{-8}$ cm. Following Bjerrum, we shall integrate $dP(r)$ for r between a and q, with a being the minimum distance accessible to an ion to approach a dipole.

$$P(r) = \frac{4\pi Nc\sigma}{1000} \int_a^q \left(r^2 \frac{(e^{\mu e/\epsilon r^2 kT} - e^{-\mu e/\epsilon r^2 kT})/2}{e\mu/\epsilon r^2 kT} \right) dr$$

given

$$Y = \frac{e\mu}{\epsilon r^2 kT}, \quad r = \left(\frac{\mu e}{\epsilon kT}\right)^{1/2} Y^{-1/2}, \quad dr = -\frac{1}{2}\left(\frac{\mu e}{\epsilon kT}\right)^{1/2} Y^{-3/2}\, dY, \quad r^2\, dr = -\frac{1}{2}\left(\frac{\mu e}{\epsilon kT}\right)^{3/2} Y^{-5/2}\, dY$$

$$Y = 2 \quad \text{for } r = q$$

$$Y = \frac{e\mu}{\epsilon a^2 kT} = b \quad \text{for } r = a$$

Then

$$P(Y) = -\frac{4\pi Nc\sigma}{1000} \int_b^2 \left(\frac{\mu e}{\epsilon kT}\right)^{3/2} \frac{1}{2} Y^{-5/2} \frac{\sinh Y}{Y}\, dY$$

$$P(Y) = \frac{2\pi Nc\sigma}{1000} \int_2^b \left(\frac{\mu e}{\epsilon kT}\right)^{3/2} \frac{\sinh Y}{Y^{7/2}}\, dY \quad \text{(X)}$$

and by multiplying and dividing by a^3, we obtain

$$P(Y) = \frac{2\pi Nc\sigma a^3}{1000} b^{3/2} \int_2^b \frac{\sinh Y}{Y^{7/2}}\, dY$$

TABLE I: Calculated K_T for $LiBF_4$ in DME ($\epsilon = 7.0$) and in DMM ($\epsilon = 2.76$) at $T = 298.2$ K as a Function of the Separation Distance a between Ions and Dipoles

$10^8 a$, cm	b	K_0, M^{-1}	Q	K_T, M^{-1}	K_T(expt), M^{-1}
DME; $q = (e\mu/2\epsilon kT)^{1/2} = 11.47 \times 10^{-8}$ cm; $\mu = 15.8 \times 10^{-18}$ esu cm					
4	16.455	0.2421	398.5	6.4×10^3	50
5	10.531	0.4728	12.071	195	
5.5	8.704	0.6293	4.115	66.5	
5.6	8.395	0.6643	3.465	56.0	
5.7	8.103	0.7005	2.955	47.7	
6	7.313	0.8170	1.463	31.7	
7	5.373	1.2974	0.828	13.4	
9	3.250	2.7574	0.3055	4.94	
11	2.176	5.0345	0.0532	0.86	
DMM; $q = 18.39 \times 10^{-18}$ cm; $\mu = 16 \times 10^{-18}$ esu cm					
7	13.802	1.2974	86.34	5474	826
7.99	10.594	1.9294	12.535	834	
8	10.567	1.9366	12.336	821	
10	6.7630	3.7825	1.5071	100	
12	4.6965	6.5362	0.6283	41.8	
14	3.4505	10.379	0.3469	23.1	
16	2.6418	15.493	0.1722	11.5	
18	2.0873	22.060	0.0268	1.78	

The integral can be solved by expanding in series the convergent function

$$\sinh Y = Y + \frac{Y^3}{3!} + \frac{Y^5}{5!} + \ldots$$

$$Q = \int_2^b \frac{\sinh Y}{Y^{7/2}}\, dY = \int_2^b \left(Y^{-5/2} + \frac{1}{3!} Y^{-1/2} + \frac{1}{5!} Y^{3/2} + \frac{1}{7!} Y^{7/2} \right) dY$$

$$Q = \frac{-Y^{-3/2}}{1!(3/2)} + \frac{Y^{1/2}}{3!(1/2)} + \frac{Y^{5/2}}{5!(5/2)} + \frac{Y^{9/2}}{7!(9/2)} + \ldots \Bigg|_2^b$$

$$Q = \sum_n \frac{Y^{(n-(5/2))}}{(n-(5/2))n!} \Bigg|_2^b \quad \text{for all odd } n$$

Therefore

$$P(Y) = \frac{2\pi Nc\sigma a^3}{1000} b^{3/2} Q = \frac{2\pi Nc\sigma a^3}{1000} b^{3/2} \left| \sum_{n,\text{odd}} \frac{Y^{(n-5/2)}}{(n-5/2)n!} \right|_{Y=2}^{Y=b} \quad \text{(XI)}$$

The function Q is converging function by increasing n. By limiting n to $n = 15$, one obtains

$$Q = -\frac{b^{-3/2}}{1.5} + \frac{b^{1/2}}{(0.5)3!} + \frac{b^{5/2}}{(2.5)5!} + \frac{b^{9/2}}{(4.5)7!} + \frac{b^7}{(7)9!} + \frac{b^{17/2}}{(8.5)11!} + \frac{b^{21/2}}{(10.5)13!} + \frac{b^{25/2}}{(12.5)15!} - 0.2556, \quad (n = 15)$$

and we shall identify the ratio $P(Y)/c\sigma$ as the triple-ion formation constant K_T, associated to either of the two processes

$$AB + B^- \rightleftharpoons AB_2^-$$

$$AB + A^+ \rightleftharpoons A_2B^+$$

taken to occur to the same extent (symmetrical approximation)

$$K_T = \frac{\sigma_T c}{(1 - \sigma - 3\sigma_T)c\sigma c} \approx \frac{\sigma_T}{c\sigma}$$

namely, a degree of triple-ion formation σ_T per unit concentration of free ions. Then

$$K_T = \frac{2\pi Na^3}{1000} b^{3/2} Q = K_0 b^{3/2} Q \quad \text{(XII)}$$

Table I reports the calculated values of K_T as a function of a for

TABLE II: Experimental Values of log K_T and Calculated Values of log $K_T(a)$ for the System Isoamylammonium Nitrate in H_2O–Dioxane Mixtures at 25 °C[a]

% H_2O	ϵ	log K_T(exptl)	log $K_T(a)$	10^8a, cm	log $K_T(\bar{a})$
0.60	2.38	4.68	4.65	9.6	4.62
1.24	2.56	4.12	4.11	9.9	4.30
2.35	2.90	3.50	3.50	10.1	3.79
4.01	3.48	3.00	2.98	9.9	3.12
6.37	4.42	2.50	2.51	9.4	2.41
9.50	5.84	2.00	2.01	8.9	1.80

[a] The value $\mu = 29 \times 10^{-18}$ esu cm, corresponding to $d = 6.04 \times 10^{-8}$ cm ($\mu = de$), has been used to calculate $K_T(a)$. a is the experimental value for the ion–dipole separation distance. d is the dipole charge-to-charge separation distance. The values of log $K_T(a)$ have been approximated to log K_T(exptl) by varying a in steps of 0.1×10^{-8} cm. The value of log $K_T(\bar{a})$ corresponds to the calculated K_T for the averaged a for the system, $\bar{a} = 9.6_4 \times 10^{-8}$ cm.

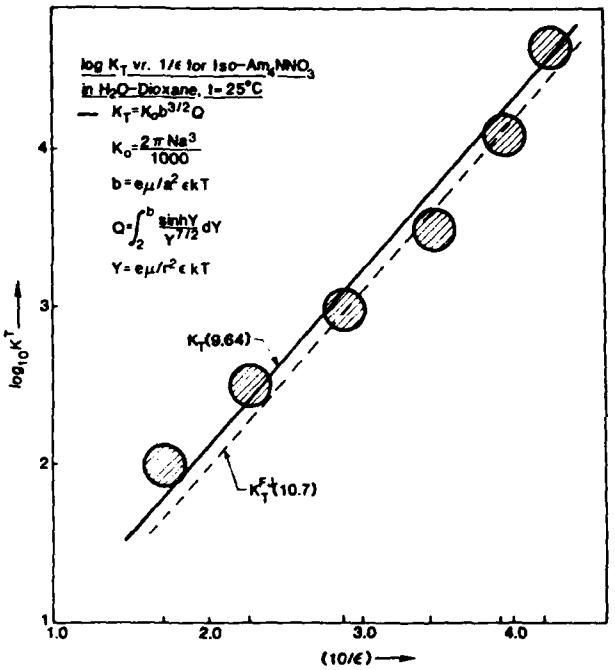

Figure 3. log K_T vs. $1/\epsilon$ for isoamylammonium nitrate in H_2O–dioxane at 25 °C. The solid line corresponds to eq XII with $a = 9.6_4 \times 10^{-8}$ cm. The dashed line corresponds to the Fuoss–Jagodzinski theory with $a = 10.7 \times 10^{-8}$ cm.

$LiBF_4$ in 1,2-dimethoxyethane (DME) of permittivity $\epsilon = 7.0$ for which $\mu = 15.8 \times 10^{-18}$ esu cm.[2] It was found[2] that K_t(exptl) = 50 M^{-1} from conductance experiments. Judging from the above figure, it would result $a \simeq 5.7 \times 10^{-8}$ cm, a very reasonable figure when compared with the charge separation of the dipole, $d = \mu/e = (15.8 \times 10^{-18}/4.8 \times 10^{-10}) = 3.3 \times 10^{-8}$ cm, and the axiom,[11] $a_T = 1.5d = 4.9 \times 10^{-8}$ cm. The last model envisages the triple ion as composed of three identical spheres in an aligned configuration (corresponding to a minimum in the potential energy). Very reliable data for K_T as a function of the permittivity exist in the literature for the system isoamylammonium nitrate in H_2O–dioxane at 25 °C.

Table II compares the experimental data for log K_T with the calculated log K_T values and the corresponding values of a used. The calculated K_T corresponds to the best fit by varying a. The values of $K_T(\bar{a})$ obtained by using the averaged a's are also shown. Figure 3 reports the log K_T vs. $1/\epsilon$ for the above system. The solid lines are the calculated values for log $K_T(9.6_4)$. The fit to the experimental data is comparable with the one obtainable with the Fuoss–Jagodzinski function K^{FJ} and the parameter $a = 10.7 \times 10^{-8}$ cm

$$K_T^{FJ} = \frac{\pi La^3 e^{-3/2}}{1000} \exp(\beta)$$

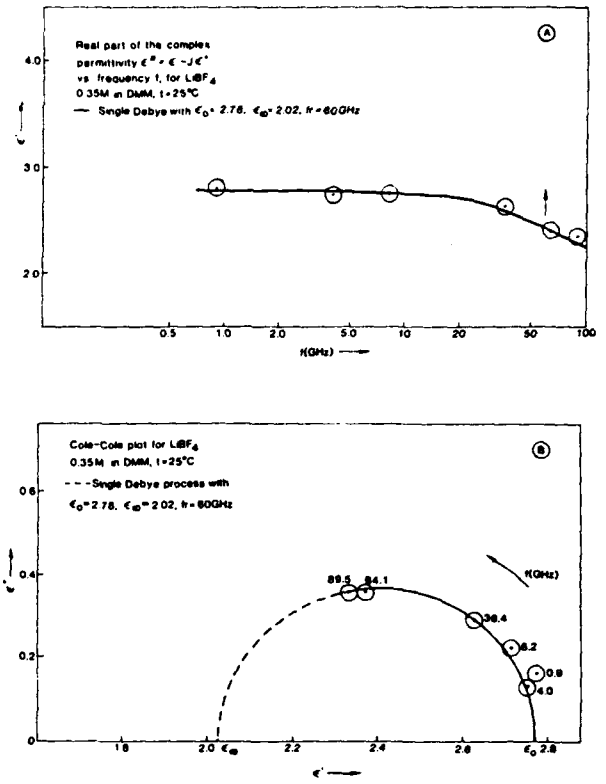

Figure 4. (A) Real part of the complex permittivity $\epsilon^* = \epsilon' - J\epsilon''$ vs. frequency f for 0.35 M $LiBF_4$ in DMM at 25 °C. (B) Cole–Cole plot for 0.35 M $LiBF_4$ in DMM at $t = 25$ °C.

with $\beta = e^2/2\epsilon akT$.

In fact, the average $|\bar{\Delta}| = |\log K_T(\text{calcd}) - \log K_T(\text{exptl})| = 0.14$ with $a = 9.6_4 \times 10^{-8}$ cm, whereas $|\bar{\Delta}| = |\log K_T^{FJ} - \log K_T(\text{exptl})| = 0.15$ with $a = 10.7 \times 10^{-8}$ cm. The present approach, however, does not contain constraints in defining a triple ion only when the ion is "in contact" with a dipole. Rather, it defines a triple ion for r varying between a and q.

We then wish to compare K_T (eq XII) with the experimental result for $LiBF_4$ in DMM at 25 °C. By use of the value $\mu = 16 \times 10^{-18}$ esu cm, obtained in DME solvent by dielectric relaxation, Table I reports the values of K_T as a function of the parameter a. The fit with the experimental value $K_T = 826$ M^{-1} is obtained for $a = 8.0 \times 10^{-8}$ cm. This value is remarkably close to the one calculable from the axiom $a = 1.5d = 7.7 \times 10^{-8}$ cm, $d = 5.1 \times 10^{-8}$ cm being calculable from the K_A obtained from the conductance data.

Dielectric and Ultrasonic Relaxation. Figure 4A reports the real part ϵ' of the complex permittivity $\epsilon^* = \epsilon' - J\epsilon''$ plotted vs. the frequency f for $LiBF_4$ (0.35 M) in DMM at 25 °C. The solid line is the fitted function which appears capable to interpret the available data according to a *single* Debye relaxation process

$$\epsilon' = (\epsilon_0 - \epsilon_\infty)\frac{1}{1 + (f/f_r)^2} + \epsilon_\infty \qquad \text{(XIII)}$$

Figure 4B is the Cole–Cole plot of ϵ'' vs. ϵ', and the semicircle corresponds to a *single* relaxation process with ϵ' given by the equation above and ϵ'' given by

$$\epsilon'' = (\epsilon_0 - \epsilon_\infty)\frac{f/f_r}{1 + (f/f_r)^2} \qquad \text{(XIV)}$$

with parameters $\epsilon_0 = 2.78$, $\epsilon_\infty = 2.02$, and $f_r = 60$ GHz. Notice that Saar et al.[9] reported for the solvent DMM $\epsilon_0 = 2.76$, $\epsilon_\infty = 2.18$, and $f_r = 75$ GHz. Hence, the presence of 0.35 M $LiBF_4$ is only detectable in a shift of the solvent relaxation to lower frequencies and a change of the relaxation strength ($\epsilon_0 - \epsilon_\infty$) which is apparently due mostly to a change in ϵ_∞. The latter one is only an extrapolated parameter because of possible effects on the

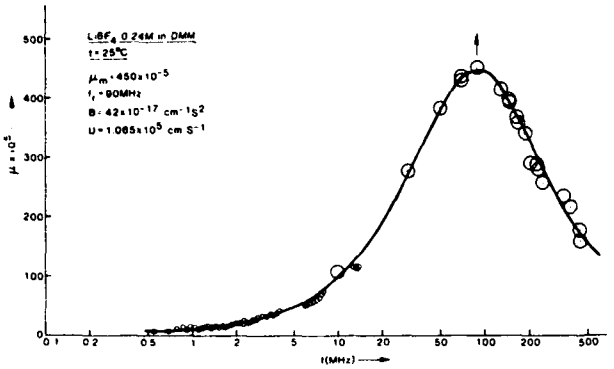

Figure 5. Ultrasonic spectrum of $\mu = \alpha_{exc}\lambda$ vs. frequency f for $LiBF_4$ in DMM at $t = 25$ °C.

TABLE III: Ultrasonic Parameters μ_m, f_r, and B and Sound Velocity u for All the Concentrations of $LiBF_4$ in DMM and Temperatures Investigated

t, °C	c, M	$10^5\mu_m$	f_r, MHz	$10^{17}B$, cm^{-1} s^2	10^5u,[a] cm s^{-1}
25	0.35	430	85	48	1.069
25	0.24	450	90	42	1.065
25	0.168	390	80	38	1.064
25	0.093	280	80	36	1.063
15	0.25	410	80	40	1.142
5	0.25	470	75	36	1.153
−1	0.25	480	70	38	1.179

[a] $10^5u = 1.179 - 0.004t$ ($r^2 = 0.9$), for 0.25 M $LiBF_4$ between 25 and −1 °C, reproduces the experimental data with a % error = $|\Delta u|/u = \pm 1\%$.

non-Debye nature at $f > 100$ GHz.[12] The rather remarkable finding for the present system is the absence of a "solute" relaxation around 1–3 GHz which has been the observed behavior of alkali salts in ethereal solvents studied so far.[12,13] This apparent invisibility of the dipolar pairs $LiBF_4$, despite the very large K_A found by conductance, can be interpreted in two ways: either the pairs are so heavily solvated that their diffusional rotational relaxation frequency is below the range accessible to our microwave measurements, or $LiBF_4$ is heavily dimerized above ~0.1 M to apolar or antiparallel dimers which are practically invisible by dielectric relaxation.

Consideration of the second hypothesis, namely a sizable dimerization, is suggested by the fact that already in DME[2] ($\epsilon = 7.0$) an ultrasonic relaxation was interpreted as due to dimerization. In DMM solvent ($\epsilon = 2.76$)[9] simple electrostatic considerations would suggest the quadrupolar or dimer formation constant to be much larger than in DME.

Figure 5 shows a representative plot of the excess sound absorption per wavelength $\mu = \alpha_{exc}\lambda$ plotted vs. f for $LiBF_4$ in DMM at 25 °C. Although the data extends to about 3 decades in frequency, a single Debye process (solid line) appears adequate to represent the data according to the function

$$\mu = 2\mu_{max}\frac{f/f_r}{1 + (f/f_r)^2} \qquad \text{(XV)}$$

where $\mu = \mu_{max}$ at the relaxation frequency $f = f_r$, $\mu = \alpha_{exc}\lambda = (\alpha - Bf^2)u/f$, α is the sound attenuation coefficient, λ is the wavelength $\lambda = u/f$, μ is the sound velocity, and $B = (\alpha/f^2)_{f>>f_r}$ is the background (α/f^2) ratio for frequencies $f >> f_r$. Table III reports the relaxation parameters μ_{max}, f_r, and B and the sound velocity u for all the solutions and temperatures investigated.

From Table III it is apparent that, within experimental error, f_r is indpendent of concentration at 25 °C but that μ_m is not linear with concentration. This last observation negates the interpretation by a scheme A ⇌ B which could represent a first-order (or pseudo-first-order) intramolecular process (involving the solvent).

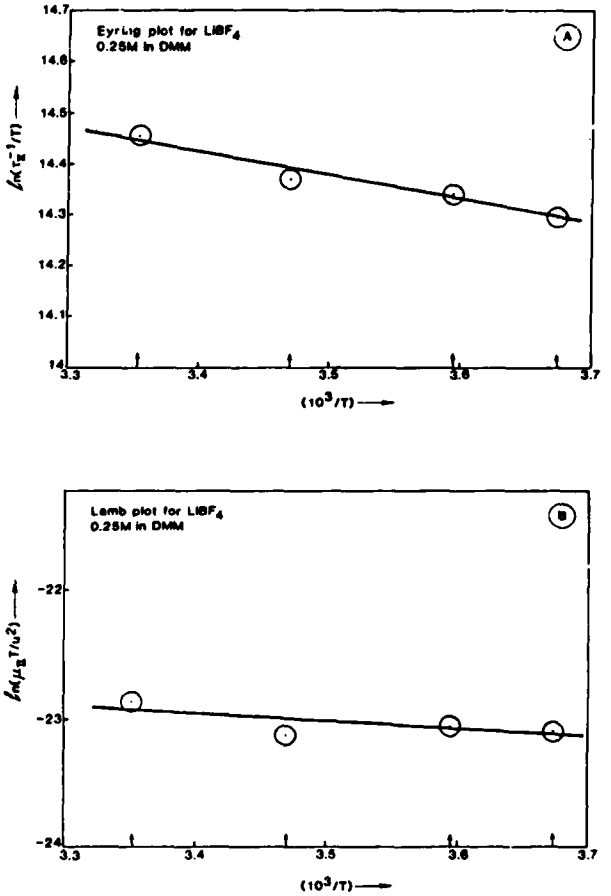

Figure 6. (A) Eyring plot for 0.25 M $LiBF_4$ in DMM. (B) Lamb plot for 0.25 M $LiBF_4$ in DMM.

Rather, we propose a multistep dimerization process of the type

$$2M \underset{k_{-1}}{\overset{k_1}{\rightleftharpoons}} M\cdots M \underset{k_{-2}}{\overset{k_2}{\rightleftharpoons}} M_2 \qquad \text{(XVI)}$$

with M = $LiBF_4$, the monomer ion pair. This scheme leads[14] to two relaxation times that for $k_1, k_{-1} >> k_2, k_{-2}$ read

$$\tau_I^{-1} = 4k_1(M) + k_{-1}$$

$$\tau_{II}^{-1} = k_2 + k_{-2}\frac{4(M)}{4(M) + K_{-1}}, \quad \text{with } K_1 = (k_1/k_{-1}) = \frac{(M\cdots M)}{(M)^2} \qquad \text{(XVII)}$$

For $4(M) >> K_{-1}$

$$\tau_{II}^{-1} = k_{-2} + k_2 = k_{-2}(1 + K_2) \quad \text{or} \quad \tau_{II}^{-1} = \frac{kT}{h}e^{\Delta S_{-2}^{\ddagger}/R}e^{-\Delta H_{-2}^{\ddagger}/RT}(1 + K_2) \qquad \text{(XVIII)}$$

with $K_2 = k_2/k_{-2}$. The above implies that a plot of $\ln(\tau_{II}^{-1}/T)$ vs. $1/T$ will have a slope[15]

$$\frac{d\ln(\tau_{II}^{-1}/T)}{d(1/T)} = -\frac{\Delta H_{-2}^{\ddagger}}{R} - \frac{K_2}{1 + K_2}\frac{\Delta H_2}{R} \qquad \text{(XIX)}$$

with $K_2 = e^{-\Delta H_2/RT}e^{\Delta S_2/R}$.

Figure 6A shows a plot of $\ln(\tau_{II}^{-1}/T)$ vs. $1/T$. The solid line was calculated by linear regression giving $r^2 = 0.95$, intercept =

(12) J. Goulon, J. L. Rivail, J. Fleming, J. Chamberlain, and P. Chantry, *C. R. Seances Acad. Sci., Ser. C*, **276**, 907 (1973).
(13) S. Onishi, H. Farber, and S. Petrucci, *J. Phys. Chem.*, **84**, 7922 (1980); H. Farber and S. Petrucci, *J. Phys. Chem.*, **79**, 1221 (1975).
(14) C. C. Chen, W. Wallace, E. E. Eyring, and S. Petrucci, *J. Phys. Chem.*, **88**, 5445 (1984).
(15) C. C. Chen and S. Petrucci, *J. Phys. Chem.*, **86**, 2601 (1982).

16.01, and slope = −466 from which $\Delta S_{-2}^{\ddagger} = -15.4$ cal/(K mol) and

$$-466 = -\frac{\Delta H_{-2}^{\ddagger}}{R} - \frac{K_2}{1 + K_2}\frac{\Delta H_2}{R} \qquad \text{(XX)}$$

Also, eq XVIII gives

$$5.28 \times 10^8 = \frac{kT}{h} e^{\Delta S_{-2}^{\ddagger}/R} e^{-\Delta H_{-2}^{\ddagger}/RT}(1 + K_2) \quad \text{or}$$

$$0.20 = e^{-\Delta H_{-2}^{\ddagger}/RT}(1 + K_2) \qquad \text{(XXI)}$$

For a two-step dimerization process (XVI), the maximum sound absorption per wavelength μ_{II} for the slow relaxation process is bound to the concentration of the various species by the relation[14]

$$\mu_{II} = \frac{\pi}{2\beta_s}\frac{\Delta V_{SII}^2}{RT}\Gamma_{II} \qquad \text{(XXII)}$$

with $\beta_S = (\rho u^2)^{-1}$ the adiabatic compressibility, ρ the density, and ΔV_{SII} the isoentropic volume change

$$\Delta V_{SII} = \Delta V_2 + \frac{1/4(M)}{1/4(M) + (M\cdots M)}\Delta V_1 \qquad \text{(XXIIa)}$$

with ΔV_1 and ΔV_2 the isoentropic volume changes associated with the steps of process XVI. Also, the function Γ_{II} is[14]

$$\Gamma_{II} = \left[\frac{1}{(M_2)} + \frac{1}{1/4(M) + (M\cdots M)}\right]^{-1} \qquad \text{(XXIII)}$$

(the factor $1/2$ instead of $1/4$ in front of (M) in eq XXIIa and XXIII reported in ref 14 was a misprint). If (M) < (M···M), (M_2), as the dielectric data seem to imply, eq XXIII can be approximated to

$$\Gamma_{II} \simeq \left[\frac{1}{(M_2)} + \frac{1}{(M\cdots M)}\right]^{-1} = \frac{K_2}{1 + K_2}(M\cdots M)$$

with $K_2 = (M_2)/(M\cdots M)$. On the other hand, one can write

$$(M\cdots M) = \frac{(M\cdots M) + (M_2)}{1 + K_2} = \frac{c^{dimer}}{1 + K_2}$$

and

$$\Gamma_{II} \simeq \frac{K_2}{(1 + K_2)^2} c^{dimer} \qquad \text{(XXIV)}$$

where $c^{dimer} = (M\cdots M) + (M_2)$. (Notice also that ΔV_{SII} is concentration dependent and that indeed μ_{II} is not linear wityh c.)

Introducing (XXIV) into (XXII)

$$\mu_{II} = \frac{\pi}{2\beta_s}\frac{(\Delta V_{SII})^2}{RT}\frac{K_2}{(1 + K_2)^2} c^{dimer}$$

$$\ln(\mu_{II}T/u^2) = \ln\left[\frac{\pi\rho c^{dimer}\Delta V_{SII}^2}{2R}\right] + \ln K_2 - 2\ln(1 + K_2) \qquad \text{(XXV)}$$

If one neglects the temperature dependence of the quantity $\rho c^{dimer}\Delta V_{SII}^2$, the above implies that

$$\frac{d\ln(\mu_{II}T/u^2)}{d(1/T)} \simeq -\frac{\Delta H_2}{R} + \frac{2K_2}{1 + K_2}\frac{\Delta H_2}{R} = \frac{\Delta H_2}{R}\frac{K_2 - 1}{K_2 + 1} \qquad \text{(XXVI)}$$

namely, the slope of a plot of $\ln(\mu_{II}T/u^2)$ vs. $1/T$ should be expressed by eq XXVI. Figure 6B shows this plot. Linear regression gives intercept = −21.05 and slope = −526.9. Therefore

$$-526.9 = \frac{\Delta H_2}{R}\frac{K_2 - 1}{K_2 + 1} \qquad \text{(XXVII)}$$

TABLE IV: Thermodynamic and Kinetic Parameters for the Slow Relaxation Dimerization Process for $LiBF_4$ in DMM

K_2	6.6	$\Delta S_{-2}^{\ddagger}$	−15.4 cal/(K mol)
ΔG_2	−1.12 kcal/mol	$\Delta H_2^{\ddagger}$	0.78 kcal/mol
ΔH_2	−1.42 kcal/mol	$\Delta S_2^{\ddagger}$	−16.4 cal/(K mol)
ΔS_2	−1.0 cal/(K mol)	k_2	4.4×10^8 s^{-1}
$\Delta H_{-2}^{\ddagger}$	2.2 kcal/mol		

TABLE V: Calculated Values of K_{qBj} according to the Expression $K_{qBj} = K_{oq}bQ_q$ as a Function of a_q, with $\mu = 16 \times 10^{-18}$ cm esu $T = 298.2$, $\epsilon = 2.76$, and $b_q = \mu^2/\epsilon a_q^3 kT$[a]

a_q	b_q	K_{oq}	Q_q	K_{qBj}
5	18.035	0.3152	5507	3.1×10^4
6	10.437	0.5447	23.34	132.7
7	6.572	0.8649	2.913	16.57
8	4.403	1.291	1.231	7.00
9	3.092	1.839	0.6935	3.94
10	2.254	2.522	0.3734	2.12
11	1.694	3.356	0.1129	0.642

[a] $K_{qBj} = 0$ for a separation distance $q = ((2/3)(\mu^2/\epsilon kT))^{1/3} = 11.4_5 \times 10^{-8}$ cm, for the above parameters.

Equations XX, XXI, and XXVII can now be correlated. Trial and error choice[15] of K_2 leads to compatibility for $K_2 = 6.6$ which leads to $\Delta H_2 = -1.42$ kcal/mol and $\Delta H_{-2}^{\ddagger} = 2.2$ kcal/mol.

Table IV reports the above and the derived thermodynamic and kinetic parameters from the relations $\Delta G_2 = -RT\ln K_2 = -1.22$ kcal at $T = 298.2$ K, $\Delta S_2 = (1/T)(\Delta H_2 - \Delta G_2) = \Delta S_2^{\ddagger} - \Delta S_{-2}^{\ddagger}$, and $\Delta H_2 = \Delta H_2^{\ddagger} - \Delta H_{-2}^{\ddagger}$.

It would appear desirable to evaluate K_q, the overall quadrupole or dimer formation constant. From scheme XVI and the definitions

$$K_1 = \frac{(M\cdots M)}{(M)^2}, \quad K_2 = \frac{(M_2)}{(M\cdots M)}, \quad K_\Sigma = \frac{(M\cdots M) + (M_2)}{(M)^2}$$

it results that

$$K_\Sigma = K_1(1 + K_2) \qquad \text{(XXVIII)}$$

and we have obtained $K_2 = 7.8$. K_1 could be evaluated in principle from the Maaser–Bjerrum[2] theoretical expression

$$K_{qBj} = K_{oq}b_qQ_q \qquad \text{(XXIX)}$$

with

$$K_{oq} = \frac{4\pi La^3}{3000}, \quad b_q = \frac{\mu^2}{\epsilon a_q^3 kT}$$

and

$$Q_q = 0.6667 - \frac{1}{b_q} + \sum_1^\infty \frac{1}{(n + 2)!\,n}(b^n - (1.5)^n) \qquad \text{(XXX)}$$

for odd n's.

For $\epsilon = 2.76$ and by retaining $\mu = 16 \times 10^{-18}$ esu cm, we have calculated Q extending n to $n = 17$. The calculation of K_{qBj} is shown in Table V. Unfortunately, K_{qBj} appears to be too sensitive to the choice of the parameter a_q, the minimum dipole–dipole separation distance, to make an assignment of $K_{qBj} = K_1$ short of being an arbitrary assumption.

Conclusion

The Fuoss–Kraus triple-ion conductance theory allows for the determination of $K_A = 6 \times 10^{16}$ M^{-1} and $K_T = 826$ M^{-1}, pending the validity of the Walden rule and the assumption $\Lambda_0 = {}^2/_3\Lambda_0$. The Fuoss–Jagodzinski association relation for K_A gives $d = 5.1 \times 10^{-8}$ cm for the charge separation of the ion pair. The theoretical expression XII derived above for K_T gives $a = 8.0 \times 10^{-8}$ cm for the minimum separation ion distance between the ion and the dipole, close to the axiom $a = 1.5d = 7.7 \times 10^{-8}$ cm. The dielectric data show absence of a dielectric relaxation for the solute in all the frequency ranges investigated. This could be rationalized either by the dipole pairs relaxing below 1 GHz or, more likely, by the

TABLE VI: Electrical Conductance Λ (Ω^{-1} cm^2 equiv^{-1}) and Concentration (mol dm^{-3}) for $LiBF_4$ in Dimethoxymethane at 25.00 °C

run	10^4c	Λ
1	78.304	6.562×10^{-5}
	174.611	5.887×10^{-5}
	311.22	6.606×10^{-5}
	430.65	8.060×10^{-5}
2	1279	2.379×10^{-4}
	2018	4.382×10^{-4}
	5026	5.662×10^{-3}
3	874.6	1.282×10^{-4}
	1080	1.589×10^{-4}
	1574	2.523×10^{-4}
	3550	1.359×10^{-3}

electrolyte being dimerized to apolar dimers.

An ultrasonic relaxation of Debye type is interpreted as due to the second step of a coupled two-step dimerization process. Kinetic and thermodynamic parameters have been extracted from the data. In particular, the formation constant for the second step of dimerization K_2 equals 6.6. The constant for the first step K_1 cannot be determined without a reliable knowledge of a_q, the pair-to-pair minimum separation distance.

Appendix

Electrical conductance and concentration data for $LiBF_4$ in DMM at 25 °C are given in Table VI.

Note Added in Proof. After the completion of the present work we have performed static permittivity measurements at $f = 3.5$ MHz with a Bontoon resonator and a cell of capacity $C_0 = 5.0_7 \pm 0.0_7$ pF of a solution 0.09_3 M $LiBF_4$ in DMM at 25 °C. The average of two experiments gave $\epsilon_0 = 2.8_2 \pm 0.0_1$, a value close to the figure extrapolated from the microwave range $\epsilon_0 = 2.78$ as reported above. This confirms that hypothesis advanced above that the electrolyte is heavily associated to apolar dimers.

Acknowledgment. We express our thanks to the Army Research Office, Research Triangle Park, NC, for their support through Grant No. DAAG/29/85/K0048.

Registry No. DMM, 109-87-5; $LiBF_4$, 14283-07-9.

Reprinted from The Journal of Physical Chemistry, 1986, 90, 3294

M. Delsignore, H. Farber, and S. Petrucci*: Molecular Relaxation Dynamics and Ionic Association of $LiBF_4$ in Dimethoxymethane.

Pages 66–72. Recently[1] the equation describing the formation constant of triple ions K_T in a medium of permittivity ϵ has been proposed

$$K_T = K_0 b^{3/2} Q$$

with

$$K_0 = \frac{2\pi N a^3}{1000}, \quad b = \frac{e\mu}{\epsilon a^2 kT}$$

and

$$Q = \sum_n \frac{Y^{(n-(5/2))}}{(n-(5/2))n!}\Bigg|_2^b$$

for all odd n's, and $Y = e\mu/\epsilon r^2 kT$. a is the minimum distance between the ion and the dipole ion-pair of moment μ. For n up to $n = 15$, Q should read

$$Q = -\frac{b^{-3/2}}{1.5} + \frac{b^{1/2}}{(0.5)3!} + \frac{b^{5/2}}{(2.5)5!} + \frac{b^{9/2}}{(4.5)7!} + \frac{b^{13/2}}{(6.5)9!} + \frac{b^{17/2}}{(8.5)11!} + \frac{b^{21/2}}{(10.5)13!} + \frac{b^{25/2}}{(12.5)15!} - 0.2556$$

instead of

$$\ldots + \frac{b^7}{(7)9!} + \ldots$$

in the fifth term on the right side, as previously reported.[1]

(1) Delsignore, M.; Farber, H.; Petrucci, S. *J. Phys. Chem.* **1986**, *90*, 66.

TABLE I: Calculated K_T for $LiBF_4$ in DME (ϵ = 7.0) and in DMM (ϵ = 2.76) at T = 298.2 K as a Function of the Separation Distance a between Ions and Dipoles

$10^8 a$, cm	Q	K_T, M^{-1}	K_T(exptl), M^{-1}
	DME		
4	305.11	4931	
5	8.3013	134.2	
5.5	3.1719	51.3	50
5.6	2.7396	44.3	
5.7	2.3949	38.7	
6	1.6988	27.5	
7	0.8012	12.9	
9	0.3050	4.93	
11	0.05329	0.86	
	DMM		
7	59.728	3973	
7.7	13.776	916.5	
7.76	12.419	826.2	826
7.8	11.610	772.4	
8	8.4640	563.1	
10	1.3581	90.4	
12	0.6187	41.2	
14	0.3463	23.0	
16	0.1725	11.5	
18	0.02717	1.81	

Consequently, the values of Q and K_T of Table I[1] should be corrected as indicated in the revised Table I reported here.

For $LiBF_4$ in DME, a fit with K_T(exptl) is obtained for $a \simeq 5.5 \times 10^{-8}$ cm and for $LiBF_4$ in DMM, a fit is obtained for $a = 7.76 \times 10^{-8}$ cm. Both figures are in reasonable agreement with the axiom $a = 1.5d$, with d the ion pair separation distance.[1]

Similarly, the fit with K_T for tetraisoamylammonium nitrate of Table II is obtained for $\bar{a} = 9.38 \times 10^{-8}$ cm instead of $\bar{a} = 9.64 \times 10^{-8}$ cm as reported.[1] The conclusions of the work[1] thus remain the same.

Reprinted from The Journal of Physical Chemistry, 1986, 90, 3326

Infrared and Ultrasonic Spectra of Sodium Thiocyanate and Lithium Thiocyanate in Tetrahydrofuran

D. Saar[†] and S. Petrucci*

Department of Chemistry, Polytechnic University, Long Island Center, Farmingdale, New York 11735
(Received: December 17, 1985)

Infrared spectra of sodium thiocyanate solutions and lithium thiocyanate solutions in tetrahydrofuran (THF) in the wavenumber range 2000–2200 cm^{-1} are reported. The digitized spectral envelope, which is due to the out-of-phase stretch of the SCN anion, is quantitatively described by the sum of three Gaussian–Lorentzian product functions. The three spectral bands are assigned respectively to the N-bonded ion pairs (~2057 cm^{-1} for NaNCS, ~2064 cm^{-1} for LiNCS), to the dimers or quadrupoles (~2043 cm^{-1} for $(NaNCS)_2$, 2040 cm^{-1} for $(LiNCS)_2$), and tentatively to triple ions (2074 cm^{-1} for sodium thiocyanate, ~2086 cm^{-1} for lithium thiocyanate). The maximum absorbances per unit length of cell are expressed as a function of concentrations by cubic polynomial functions. Ultrasonic spectra for sodium thiocyanate solutions in THF in the frequency range 0.5–400 MHz are described by the sum of two Debye relaxation functions. The ultrasonic spectra for sodium thiocyanate in THF are interpreted as due to a two-step process, $2NaNCS \rightleftharpoons NaNCS\cdots NaNCS \rightleftharpoons (NaNCS)_2$, depicting the two-step dimerization of the ion pair NaNCS, the intermediate being a solvent-separated species. For lithium thiocyanate solutions in THF, the ultrasonic spectra are described by a single Debye relaxation function and interpreted by the dimerization scheme $2LiNCS \rightleftharpoons LiNCS\cdots LiNCS$, the product of the reaction being mostly a solvent-separated species, the "contact" species being probably in lesser amounts than for $(NaNCS)_2$ in accordance with the evidence from the infrared spectra. The limitations of the infrared method in giving reliable formation stoichiometric constants in media of low permittivity are discussed. The advantage of combining the structural information from vibrational spectra to the kinetic results of the ultrasonic spectra for a molecular interpretation of the latter ones is reiterated.

Introduction

Recently there has been a renewed interest,[1] after the classical work of Fuoss and Kraus[2] of the thirties, in the association and dimerization of electrolytes in media of low permittivity. The practical relevance of these systems, especially lithium salts in ethereal solutions, is due to their use in the construction of secondary batteries. Knowledge of the state of association of the electrolyte and of the lifetime of the complex species is essential for the optimal choice of solvent and electrolyte. Despite recent advances in application of transport theories of electrolytes[3] and theoretical new expressions for the formation constant of dimers ion pairs[4] and triplets,[5] our knowledge of the *structure* of the complex species in solution is scarce or nonexistent.

To this end a program by vibrational IR spectra combined to the already existing molecular relaxation dynamic methods (microwave dielectric relaxation and/or ultrasonic relaxation) has been initiated. For the present work the electrolytes sodium thiocyanate and lithium thiocyanate in the solvent THF have been examined. For the IR spectra the intramolecular vibration of the anion, specifically the out-of-phase stretch of the SCN^- anion[6] (or, in the group frequency jargon, the "CN stretch"), and its changes due to molecular environments have been used as a probe to study the molecular complexation of the electrolytes.

Ultrasonic relaxation spectra of the same systems are also reported, using the structural information from the IR spectra, for their interpretation.

Experimental Section

The IR spectra have been recorded by a Perkin-Elmer 983G spectrometer, using scan times and noise filter modes (4 and 16, respectively) slow enough that no spectral distortion was noticed with respect to slower modes. The cells were calibrated by the fringe method[7] before each collected spectrum. They were demountable Perkin-Elmer cells with 0.05-mm Teflon spacers. Both CaF_2 and NaCl windows were used, ensuring independence of the spectra from the material of the windows, and hence their inertness to possible dissolution into the liquid. The ultrasonic instrumentation, data collection, and method have been described extensively in previous work.[8] Sodium thiocyanate and lithium thiocyanate (Baker reagents with analysis certificate) were redried at ~70 and 110 °C, respectively, in vacuo (~1 mm), in volumetric flasks until constancy of weight. Solutions were prepared by volume addition of tetrahydrofuran (THF) (Baker ACS) dried over molecular sieves (5Å). The molecular sieves had been dried for many hours at ~140 °C and cooled in vacuo. Infrared spectra of the THF product as received showed a faint band at ~3300 cm^{-1} which disappeared after a few days' exposure to molecular sieves. This indicated absence of water in this product within the resolution of the 983G spectrometer set with an ordinate scale of 0.25 in absorbance (A = 0.0025/minimum division).

Results and Calculations

Some of the infrared spectra expressed in absorbance vs. wavenumber (cm^{-1}) are depicted in Figures 1 and 2. The spectra for sodium thiocyanate show rather dramatically the relative change of the two visible bands with total concentration of electrolyte.

For lithium thiocyanate the satellite band is the one at lower wavenumbers at variance with the case of sodium thiocyanate, indicating qualitatively a different molecular distribution of the species present for the two electrolytes.

For the quantitative interpretation of the spectra they were digitized with a resolution of 2.5 cm^{-1} (1.25 cm^{-1} near the peaks and shoulders). It is known that Lorentzian functions are particularly applicable to gases and Gaussian functions are particularly applicable[9] to solids in terms of the band shape of vibrational

[†] Colgate-Palmolive Co., Piscataway, N.J.

(1) Farber, H.; Irish, D. E.; Petrucci, S. *J. Phys. Chem.* **1983**, *87*, 3515. Harada, Y.; Salomon, M.; Petrucci, S. *J. Phys. Chem.* **1985**, *88*, 2005 and literature quoted therein.
(2) Fuoss, R. M. *J. Am. Chem. Soc.* **1934**, *56*, 1127, 1031; **1936**, *58*, 982. Fuoss, R. M.; Kraus, C. A. *J. Am. Chem. Soc.* **1935**, *57*, 1; **1933**, *55*, 3614.
(3) Delsignore, M.; Farber, H.; Petrucci, S. *J. Phys. Chem.* **1985**, *89*, 4968.
(4) Maaser, H.; Delsignore, M.; Newstein, M.; Petrucci, S. *J. Phys. Chem.* **1984**, *88*, 5100.
(5) Delsignore, M.; Farber, H.; Petrucci, S. *J. Phys. Chem.* **1986**, *90*, 66.
(6) Colthup, N. B.; Daly, L. H.; Wiberley, S. E. *Introduction to Infrared and Raman Spectroscopy*, 2nd ed.; Academic: New York, 1975; Chapter 4.
(7) Reference 6, Chapter 2.
(8) Petrucci, S. *J. Phys. Chem.* **1967**, *71*, 1174. Darbari, G. S.; Richelson, M. R.; Petrucci, S. *J. Chem. Phys.* **1970**, *53*, 859. Bonsen, A.; Knoche, W.; Berger, W.; Giese, K.; Petrucci, S. *Ber. Bunsenges. Phys. Chem.* **1978**, *82*, 678. Chen, C.; Wallace, W.; Eyring, E.; Petrucci, S. *J. Phys. Chem.* **1984**, *88*, 2541.
(9) Dogonadze, R. R.; Itskovitch, E. M.; Kuznetsov, A. M.; Vorotyntsev, M. A. *J. Phys. Chem.* **1975**, *79*, 2827.

TABLE I: Calculated Infrared Parameters from Fitting the Digitized Infrared Spectra to the Gaussian–Lorentzian Product Function[a]

$$A = \sum_j A_j^0 \left[\exp\left(-\frac{(\bar{\nu} - \bar{\nu}_j)^2}{2\sigma_j^2} \right) \right] \left[1 + \frac{(\bar{\nu} - \bar{\nu}_j)^2}{\sigma_j^2} \right]^{-1}$$

NaSCN

c, M	l, mm	A^0_{2043}	$\bar{\nu}_{2043}$	$(\Delta\nu)_{1/2}$	A^0_{2057}	$\bar{\nu}_{2057}$	$(\Delta\nu)_{1/2}$	A^0_{2074}	$\bar{\nu}_{2074}$	$(\Delta\nu)_{1/2}$
0.198	0.057	0.79	2043.5	13	0.47	2057	13	0.10	2074	13
0.148	0.057	0.60	2043	13	0.42	2056	13	0.06	2074	13
0.103	0.050	0.40	2042.5	13	0.25	2057	13	0.02	2074	13
0.050	0.051	0.17	2042	13	0.14	2056.5	13	0.005	2074	13
0.025	0.059	0.080	2042	13	0.087	2057	13			

LiSCN

c, M	l, mm	A^0_{2040}	$\bar{\nu}_{2040}$	$(\Delta\nu)_{1/2}$	A^0_{2064}	ν_{2064}	$(\Delta\nu)_{1/2}$	A^0_{2086}	$\bar{\nu}_{2086}$	$(\Delta\nu)_{1/2}$
0.268	0.056	0.20	2038	14	1.70	2065	14	0.12	2088	14
0.210	0.056	0.14	2040	14	1.26	2065	14	0.12	2086	14
0.100	0.057	0.05	2040	14	0.67	2064	14	0.04	2086	14
0.066	0.061	0.03	2040	13	0.58	2063	13	0.015	2086	13
0.042	0.056	0.016	2040	13	0.29	2064	13	0.018	2086	13

[a] $\sigma_j = (\Delta\nu_j)_{1/2}/1.46$ for NaSCN and LiSCN in THF. $\bar{\nu}_j$ and $(\Delta\nu_j)_{1/2}$ are expressed in cm^{-1}.

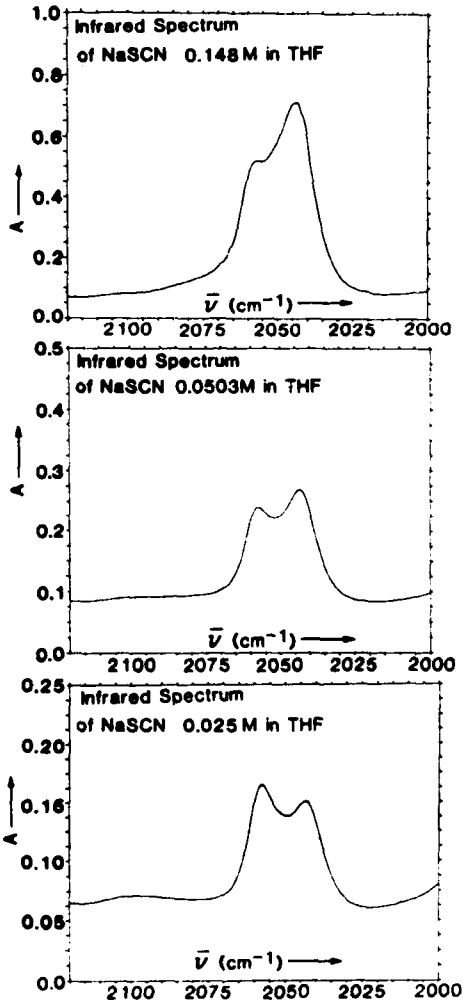

Figure 1. Representative infrared spectra for the CN stretch of sodium thiocyanate in THF at various concentrations.

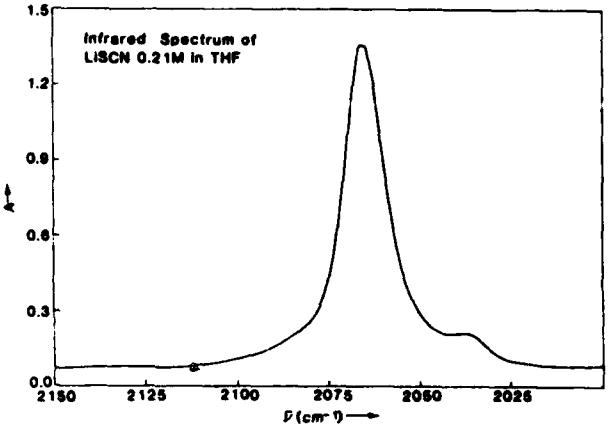

Figure 2. Representative infrared spectrum for the CN stretch of lithium thiocyanate in THF.

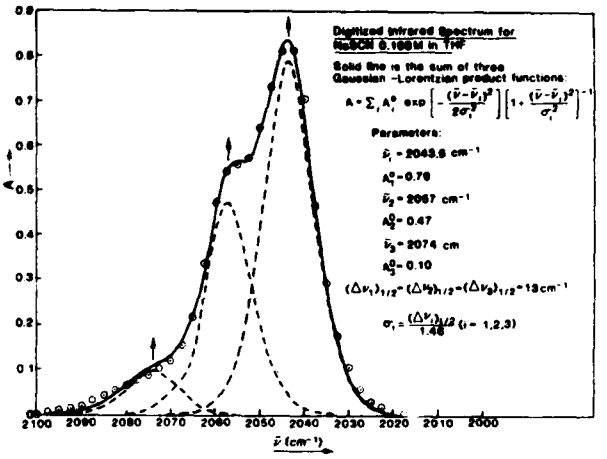

Figure 3. Digitized infrared spectrum and calculated spectrum sum of three Gaussian–Lorentzian product functions for sodium thiocyanate in THF. Cell length $l = 0.057$ mm.

spectra. For the present case the empirical Gaussian–Lorentzian product function already used before[10] has been applied

$$A_j = A_j^0 \left(\exp\left[\frac{-(\bar{\nu} - \bar{\nu}_j)^2}{2\sigma_j^2} \right] \right) \left(1 + \frac{(\bar{\nu} - \bar{\nu}_j)^2}{\sigma_j^2} \right)^{-1} \quad (I)$$

with A_j^0 the absorbance at the center-band wavenumber $\bar{\nu}_j$, σ_j the variance $\sigma_j = (\Delta\nu)_{1/2}/1.46$, with $(\Delta\nu)_{1/2}$ the bandwidth at $(1/2)A_j^0$ for each band. For the spectra of the present work it has proven to be necessary to use three Gaussian–Lorentzian bands for a quantitative interpretation of the absorbance envelope; hence

$$A = \sum_j A_j \qquad (j = 1, 2, 3) \qquad (II)$$

The parameters used to interpret the spectra are collected in Table

(10) Irish, D. E.; Tang, S. Y.; Talts, H.; Petrucci, S. *J. Phys. Chem.* **1979**, *83*, 3268.

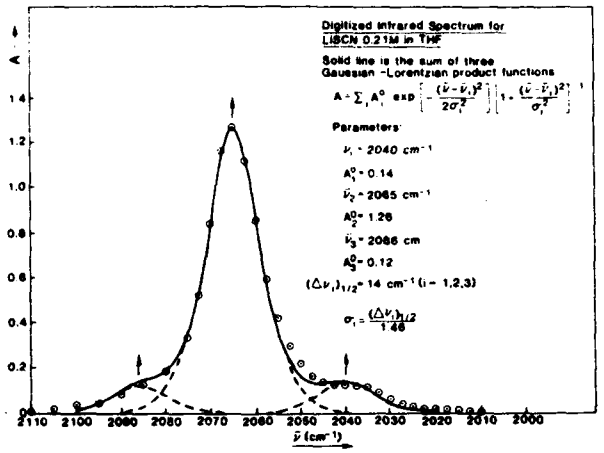

Figure 4. Digitized infrared spectrum and calculated spectrum sum of three Gaussian–Lorentzian product functions for lithium thiocyanate in THF. Cell length l = 0.056 mm.

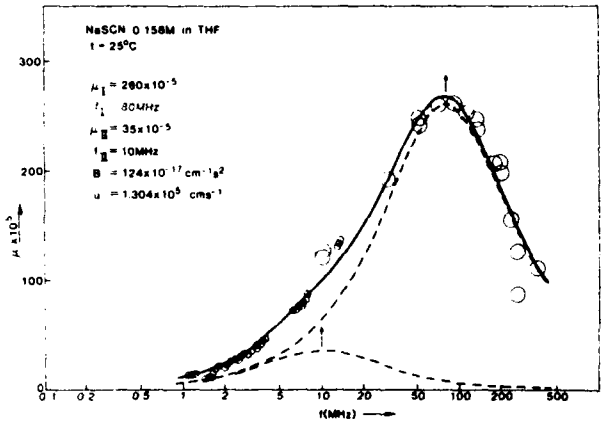

Figure 5. Excess sound absorption per wavelength μ vs. frequency f for a representative ultrasonic spectrum of sodium thiocyanate in THF at 25 °C.

I for all the concentrations of sodium thiocyanate and of lithium thiocyanate investigated in THF. Figures 3 and 4 report representative plots of the digitized spectra for sodium thiocyanate and lithium thiocyanate in THF with the indicated band components (dashed lines) and their sum (solid lines) describing the absorbance envelope.

Representative plots of the ultrasonic spectra for sodium thiocyanate and lithium thiocyanate in THF are reported in Figures 5 and 6. For the case of sodium thiocyanate two Debye processes are necessary to interpret the spectra expressed as excess sound absorptions per wavelength $\mu = (\alpha - Bf^2)u/f$ vs. the frequency f. In the above, α is the sound attenuation coefficient, B is the background sound absorption ratio α/f^2 at $f \gg f_I f_{II}$ with f_I and f_{II} the two relaxation frequencies, $B = (\alpha/f^2)_{f \gg f_I f_{II}}$, and u is the sound velocity. Therefore

$$\mu = 2\mu_I \frac{(f/f_I)}{1 + (f/f_I)^2} + 2\mu_{II} \frac{(f/f_{II})}{1 + (f/f_{II})^2} \qquad \text{(III)}$$

where μ_I and μ_{II} are the maximum sound excess absorptions for the two Debye processes centered at f_I and f_{II}, respectively.

Table II collects all the calculated relaxation parameters and the sound velocities u for the concentrations investigated for sodium thiocyanate and lithium thiocyanate in THF at 25 °C.

Discussion

(*a*) *Vibrational Spectra.* The thiocyanate anion is konwn to be a potentially ambidentate ligand. It is a linear ion which may ligate through the nitrogen or sulfur atom. The three frequencies of the thiocyanate ion are the out-of-phase stretch $\tilde{\nu}_1$, with characteristic frequency at 2050 cm⁻¹, the in-phase stretch $\tilde{\nu}_3$ with

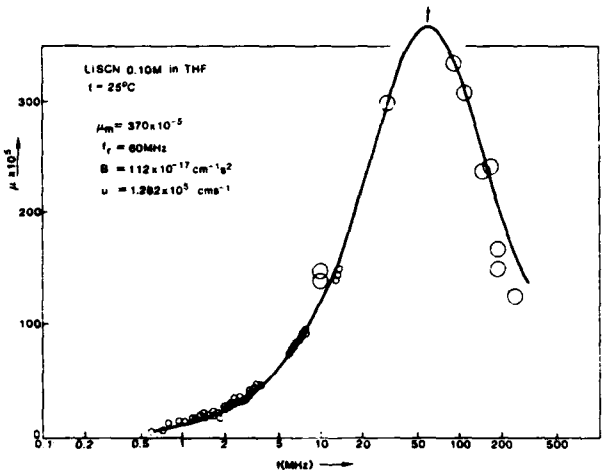

Figure 6. Excess sound absorption per wavelength μ vs. frequency f for a representative ultrasonic spectrum of lithium thiocyanate in THF at 25 °C.

TABLE II: Ultrasonic Relaxation Parameters and Sound Velocities for NaSCN and LiSCN in THF at t = 25 °C

c, M	$10^5\mu_I$	f_I, MHz	$10^5\mu_{II}$	f_{II}, MHz	$10^{17}B$, cm⁻¹ s²	$10^{-5}u$, cm s⁻¹
			NaSCN			
0.20	315	90	40	12	124	1.289
0.158	260	80	35	10	124	1.304
0.11	210	70	15	7	126	1.284
0.056	95	65	10	6	130	1.291
			LiSCN			
0.10	370	60			112	1.282
0.066	140	50			122	1.279
0.042	150	45			126	1.283
0.024	85	35			124	1.283

characteristic frequency at 735 cm⁻¹, and the bending (double degenerate) mode $\tilde{\nu}_2$ with frequency $\tilde{\nu}_2$ = 480 cm⁻¹. These group frequencies (used here as a jargon in place of the more correct term wavenumber) change characteristically depending on the coordination mode. Specifically, N-bonded complexes cause an increase of $\tilde{\nu}_1$, $\tilde{\nu}_2$ does not change, and $\tilde{\nu}_3$ increases, whereas S-bonded complexes show a larger $\tilde{\nu}_1$ increase but a decrease of both $\tilde{\nu}_2$ and $\tilde{\nu}_3$, both being more diagnostic than $\tilde{\nu}_1$ in determining the bonding end of the anion. However, solvent bands often obscure the $\tilde{\nu}_2$ and $\tilde{\nu}_3$ regions. Previous work[10-12] has established that with "hard" poorly polarizable ions as Na^+ and Li^+ the ion pairs contact complexes are N-bonded with a respective increase of ~8 and ~15 cm⁻¹ of the center-band frequency with respect to the spectroscopically free (ion and outer-sphere ion-paired) SCN^- anion.

On the basis of the above, one would attribute the band at ≈2057 cm⁻¹ for NaNCS and ≈2064 cm⁻¹ for LiNCS in THF (Table I) to contact ion pairs. No free ions or outer-sphere ion pairs are detectable. Indeed both these species, if present, would cause the appearance of an additional band at ~2050 cm⁻¹, which is absent for the present systems. In past work in this laboratory[13] and previously by Chabanel et al.[12] the band at ~2040 cm⁻¹ has been attributed to contact dimer ion pairs or quadrupoles $(NaNCS)_2$ and $(LiNCS)_2$.

One has to keep in mind however that the bands at 2057 and 2064 cm⁻¹, respectively, could also be accounted for by solvent-separated dimers $(NaNCS\cdots NaNCS)_2$ and $(LiNCS\cdots LiNCS)_2$ which would be spectroscopically indistinguishable from the monomer species NaNCS and LiNCS.

(11) Gans, P. *Vibrating Molecules*; Chapman and Hall: London, 1971; Chapter 9.
(12) Paoli, D.; Lucon, M.; Chabanel, M. *Spectrochim. Acta, Part A* **1978**, *34*, 1087 and previous literature quoted therein.
(13) Saar, D.; Brauner, J.; Farber, H.; Petrucci, S. *J. Phys. Chem.* **1978**, *82*, 545.

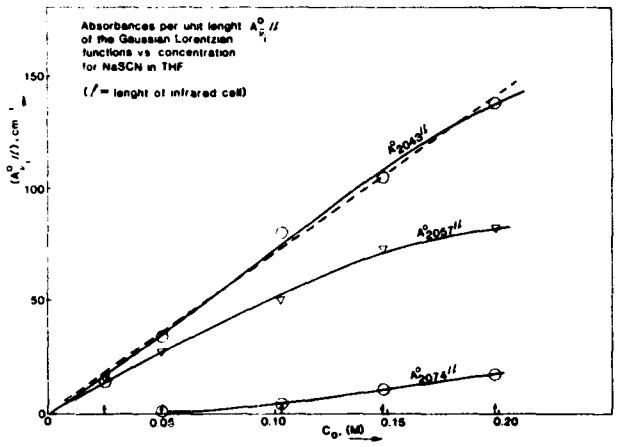

Figure 7. Maximum absorbances vs. concentration of the Gaussian–Lorentzian bands for sodium thiocyanate in THF.

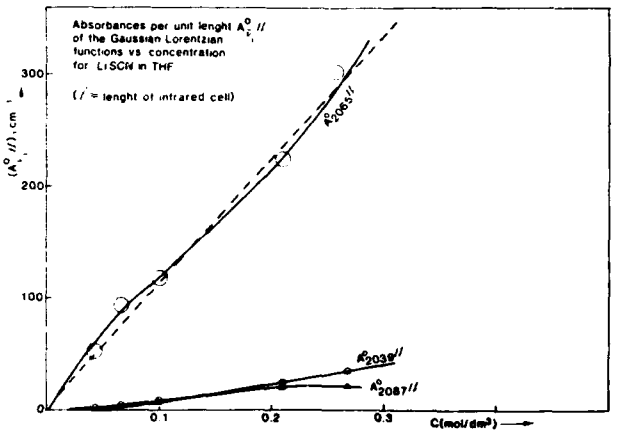

Figure 8. Maximum absorbances vs. concentration of the Gaussian–Lorentzian bands for lithium thiocyanate in THF.

Therefore, for instance for sodium thiocyanate solutions any calculation of formation constants based on relations as $A^0_{2057} = \epsilon_p/c_p$ and $A^0_{2040} = \epsilon_q/c_q$ is destined to fail if outer-sphere dimers are present. In the above ϵ_p and ϵ_q are the extinction coefficients or molar absorptivities of the ion pair and quadrupole, respectively, c_p and c_q the corresponding concentrations, and l is the length of the cell. In other words, even if assumptions as $2\epsilon_p = \epsilon_q$ are correct, the calculated $K_q = c_q/c_p^2$ is going to be void of significance if outer-sphere dimers are present. This is because, in this case, $A^0_{2040} = \epsilon_q c_q^{\text{contact}}$ and $A^0_{2057} = \epsilon_p(c_p + c_q^{\text{outersphere}})$. The calculated $K_q = c_q^{\text{contact}}/(c_p + c_q^{\text{outersphere}})^2$ would then become *strongly* concentration-dependent. The presence of solvent-separated dimers is consistent with the results of the ultrasonic analysis of the data given below.

The small bands at 2074 and 2086 cm^{-1} respectively for sodium thiocyanate and lithium thiocyanate have a less definite interpretation than the ones for the other two bands which has also been confirmed by normal-coordinate analysis.[12] We tentatively attribute these bands at 2074 and 2086 cm^{-1} to triple ions existing at lower concentration than the other species. The latter is suggested by the smallness of the A^0's.

Because of the above considerations, we think that it is safe not to overextend vibrational spectrometry beyond its present capability in trying to calculate formation constants at low permittivities where, because of electrostatic forces, a larger population of outer-sphere dimers may exist. The same warning referred to ion pairs, in solvents of intermediate permittivity, was given by some of us in a past work.[10] The method may be approximately correct for ion pairs in aqueous solutions because of its large permittivity, although even in this case for metal(II) sulfates, a large concentration of outer species ion pair appears to exist.[14] Accordingly, we have only calculated the concentration dependence of the individual maximum absorbances per unit length of cells l by fitting the data to cubic polynomials as reported below.

For sodium thiocyanate in THF

$$A^0_{2043}/l = -0.31 + 603.1c + 2187.5c^2 - 8649c^3; \quad r^2 = 0.998$$

$$A^0_{2057}/l = 0.1996 + 516.6c + 483c^2 - 4942c^3; \quad r^2 = 0.998$$

$$A^0_{2074}/l = 0.0131 - 56.34c + 1195c^2 - 2334c^3; \quad r^2 = 0.999$$

For lithium thiocyanate solutions in THF

$$A^0_{2040}/l = -0.0006 + 51.980c + 379.80c^2 - 285.95c^3; \quad r^2 = 0.99999$$

$$A^0_{2064}/l = -0.252 + 1610.7c + 5395.9c^2 + 13.490c^3; \quad r^2 = 0.9987$$

$$A^0_{2086}/l = 0.1170 - 17.480c^2 + 1254.4c^2 - 3320.8c^3; \quad r^2 = 0.9925$$

The above expressions have been calculated by nonlinear regression giving 50% statistical weight to the origin. It is noteworthy that the bands at 2043 and 2065 cm^{-1} for sodium thiocyanate and lithium thiocyanate solutions may also be expressed as simple linear functions of c with an almost comparable determination coefficient r^2 (dashed lines in Figures 7 and 8).

For sodium thiocyanate in THF

$$A^0_{2043}/l = -0.34 + 714.2c; \quad r^2 = 0.997$$

For lithium thiocyanate in THF

$$A^0_{2065}/l = 3.08 + 111.1c; \quad r^2 = 0.9948$$

From the analysis of the IR spectra it would appear therefore that contact dimers are the dominant species for sodium thiocyanate in THF with an almost comparable amount of "spectroscopically" free monomers (free ion pairs and outer-sphere dimers). On the contrary for lithium thiocyanate in THF, the latter two species appear as the dominant species. This is in line with the relative solvation tendencies of Li^+ vs. Na^+ ions.

(*b*) *Ultrasonic Spectra.* The ultrasonic spectra and the data collected in Table II for sodium thiocyanate in THF can now be interpreted on the basis of the structural information gathered through the IR spectra. Simple concentration distribution calculations of the various species present in THF with reasonable formation constant parameters as $K_p = 10^8$ M^{-1}, $K_T = 10^2$ M^{-1}, and $K_q = 10$ M^{-1} (for the ion pair, triple, and quadruple formation constants) reveal that in the concentration range 0.05–0.2 M the ion pair and quadrupole concentrations are of the same order of magnitude but that $c_p, c_q \gg c_T$, the triple ion concentration.

It is therefore unlikely that the source of any of the two Debye relaxation processes be due to equilibria involving triple ions. Accordingly, we have interpreted the ultrasonic relaxation spectra for sodium thiocyanate in THF according to the two-step dimerization equilibrium

$$2AB \underset{k_{-1}}{\overset{k_1}{\rightleftharpoons}} AB\cdots AB \underset{k_{-2}}{\overset{k_2}{\rightleftharpoons}} (AB)_2$$

where AB = NaNCS, AB···AB = NaNCS···NaNCS, and $(AB)_2 = (NaNCS)_2$. The above leads[15] to two relaxation times τ_I and τ_{II}, where

$$\tau_{I,II}^{-1} = \tfrac{1}{2}[S \pm (S^2 - 4P)^{1/2}]$$

$$S = \tau_I^{-1} + \tau_{II}^{-1} = 4k_1(AB) + k_{-1} + k_2 + k_{-2}$$

$$P = \tau_I^{-1}\tau_{II}^{-1} = 4k_1(AB)(k_2 + k_{-2}) + k_{-1}k_{-2}$$

$$\tau_I^{-1} = 2\pi f_I, \quad \tau_{II}^{-1} = 2\pi f_{II}$$

Assuming as a first approximation $AB \approx c$, the stoichiometric concentration, Figure 9, A and B has been constructed. Linear

(14) Eigen, M.; De Maeyer, L. In *Investigation of Rates and Mechanisms of Reaction*. Weissberger, A., Ed.; Wiley: New York, 1962; Vol. VIII, Part II.

(15) Delsignore, M.; Maaser, H.; Petrucci, S. *J. Phys. Chem.* **1984**, *88*, 2405.

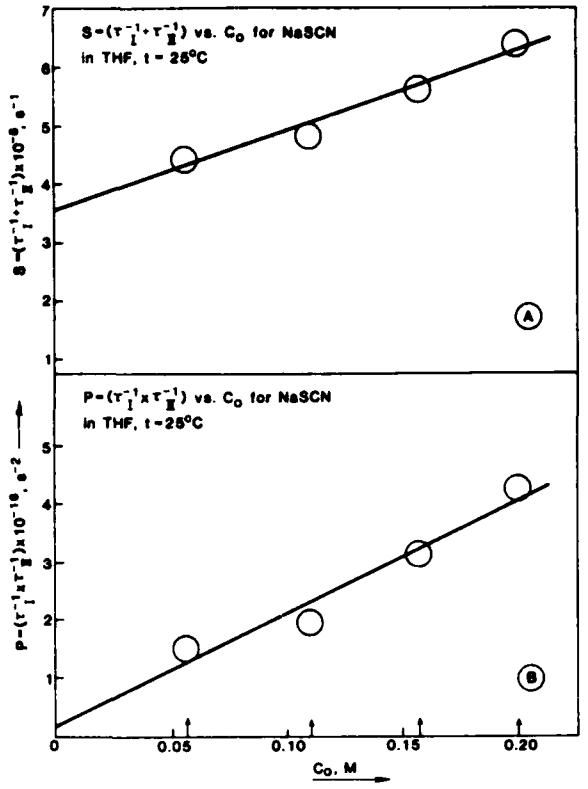

Figure 9. (A) S ($=\tau_I^{-1} + \tau_{II}^{-1}$) vs. c for sodium thiocyanate in THF at 25 °C. (B) P ($=\tau_I^{-1}\tau_{II}^{-1}$) vs. c for sodium thiocyanate in THF at t = 25 °C.

TABLE III: Rate Constants and Equilibrium Constants[a] for the Dimerization of NaSCN in THF according to the Scheme

$$2\text{NaSCN} \underset{k_{-1}}{\overset{k_1}{\rightleftharpoons}} (\text{NaNCS}\cdots\text{NaNCS}) \underset{k_{-2}}{\overset{k_2}{\rightleftharpoons}} (\text{NaNCS})_2$$

k_1, M^{-1} s^{-1}	$= 3.4_3 \times 10^8$
k_{-1} s^{-1}	$= 2.1_3 \times 10^8$
K_1, M^{-1}	$= 1.6$
k_2, s^{-1}	$= 1.3_3 \times 10^8$
k_{-2}, s^{-1}	$= 8.7 \times 10^6$
K_2	$= 15._3$
$K_q = K_1(1 + K_2)$, M^{-1}	$= 26._1$

[a] 1st app. (NaNCS) = c.

regression of S vs. c gives slope = 1.37×10^9, intercept = 3.55×10^8, and $r^2 = 0.96$. Linear regression of P vs. c gives slope' = 1.94×10^{17}, intercept' = 1.86×10^{15}, and $r^2 = 0.94$, from which the four kinetic rate constants k_1, k_{-1}, k_2, and k_{-2}, the formation constants $K_1 = k_1/k_{-1}$ and $K_2 = k_2/k_{-2}$, and the dimerization constant $K_q = K_1(1 + K_2)$ have been calculated (Table III).

A second approximation has been performed by using $K_q = 26$ M^{-1} to calculate c_p = (AB).

The new sequence gives slope = 6.74×10^9., intercept = 2.62×10^8, and $r^2 = 0.93$ for S vs. c, but slope' = 9.49×10^{17}, intercept' ≈ 0, and $r^2 = 0.90$ for P vs. c, making impossible further progress without a reliable figure for K_q.

For lithium thiocyanate in THF, a single Debye process suffices to interpret the ultrasonic relaxation data. The infrared data indicate that the contact species $(LiNCS)_2$ are in minor concentration (as well as the assigned triple ion species), the major species being the "spectroscopically free" LiNCS pair. The latter maybe a combination of LiNCS and (LiNCS···LiNCS) species.

Consequently we have interpreted the ultrasonic spectra for lithium thiocyanate in THF as due to the process

$$2\text{LiNCS} \underset{k_r}{\overset{k_f}{\rightleftharpoons}} (\text{LiNCS}\cdots\text{LiNCS}) \qquad \text{(IV)}$$

where the product of the reaction maybe mainly (LiNCS···LiNCS)

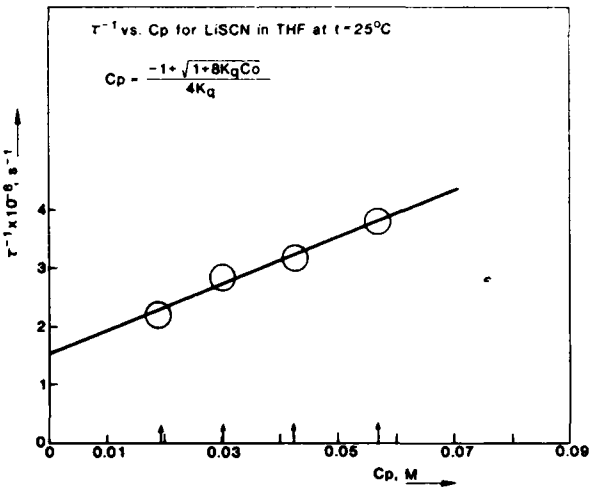

Figure 10. τ^{-1} vs. c for lithium thiocyanate in THF at t = 25 °C.

with a minor percentage of contact $(LiNCS)_2$. Both species will be symbolized here as (LiNCS···LiNCS). Notice in fact from Table II that the visible relaxation frequency for lithium thiocyanate solutions 0.1 M (f_r = 60 MHz) is comparable with f_I = 70 MHz for 0.1 M sodium thiocyanate solutions, whereas f_{II} = 7 MHz. Scheme IV leads to the relation[16]

$$\tau^{-1} = 4k_f(\text{LiNCS}) + k_r = 4k_f(\text{AB}) + k_r \qquad \text{(V)}$$

with

$$K_1 = \frac{(\text{AB})_2}{(\text{AB})^2} = k_f/k_r; \quad (\text{AB})_2 = (\text{LiNCS}\cdots\text{LiNCS})$$

In the zeroth approximation (AB) = c, linear regression of τ^{-1} *vs.* c *gives* $r^2 = 0.97$, *slope* = 1.96×10^9, *and intercept* = 1.85×10^8, from which one calculates $k_f = 4.9 \times 10^8$ M^{-1} s^{-1}, $k_r = 1.8_5 \times 10^8$ s^{-1}, and $K_1 = 2.6_5$ M^{-1} (Figure 10).

A series of successive approximations is started with the initial $K_1 = 2.6_5$ M^{-1}. After seven approximations convergence is obtained with $K_1 = 6.6$ M^{-1}, $k_f = 9.9 \times 10^8$ M^{-1} s^{-1}, and $k_r = 1.5 \times 10^8$ s^{-1}.

Notice that the zeroth approximation $k_f = 4.9 \times 10^8$ M^{-1} s^{-1} is comparable with the value of $k_1 = 3.4 \times 10^8$ M^{-1} s^{-1} calculated for sodium thiocyanate in THF, reinforcing the above interpretation of the ultrasonic relaxation of lithium thiocyanate leading mainly to outer-sphere dimers.

Conclusions

The combination of vibrational spectrometry and ultrasonic spectrometry in electrolyte solutions of low permittivity leads to complementary information of invaluable importance in the interpretation of the relaxation spectra by ultrasonics. Instead of guessing the species participating in the chemical equilibria being disturbed by the sound wave, one has indicatio of their presence by infrared spectra in a comparable concentration range. On the other hand, as in any other method, vibrational spectra seem to have limitations in their apparent inability to distinguish between "free species" and "solvent-separated species" leading to interpretation errors if one ignores the possible presence of the latter ones.

Work is now in progress with other lithium electrolytes more likely to be employed in solutions used for battery construction.

Acknowledgment. We thank the Army Office of Scientific Research, Durham, NC, for their generous support through Grant No. DAAG-29-85-K0048. Thanks are also due to Mr. Charles Christie of Perkin-Elmer Co., Elmwood Park, NJ, for technical advice during the use of the 983G IR spectrometer.

Registry No. THF, 109-99-9; NaNCS, 540-72-7; LiNC: 556-65-0.

(16) Onishi, S.; Farber, H.; Petrucci, S. *J. Phys. Chem.* **1980**, *84*, 2922 Farber, H. Petrucci, S. *Ibid.* **1981**, *85*, 2987.

Reprinted from The Journal of Physical Chemistry, 1986, 90, 6125

Infrared and Microwave Dielectric Spectra of Macrocycle–Electrolyte Complexes: NaSCN + 18C6 in THF

Meizhen Xu, Edward M. Eyring,† and S. Petrucci*

Polytechnic University, Department of Chemistry, Long Island Center, Farmingdale, New York 11735
(Received: May 16, 1986)

Infrared spectra in the 2100–2000-cm^{-1} frequency range for NaSCN + 18C6 in THF, related to the "CN stretch" of the SCN^- ion, reveal dramatic differences when compared to similar spectra obtained without addition of the macrocycle. A single Gaussian–Lorentzian band centered at ~2060 cm^{-1} suffices to describe quantitatively the spectra at variance with NaSCN in THF, requiring three bands as reported also previously. Similarly dramatic differences are also found in the dielectric spectra. The Böttcher plots are drastically different when the macrocycle is present. Both these results are quantitatively interpreted by the crown ether complexing the cation. Whereas the ion pairs of Na^+ with ^-NCS persist, the large population of dimers or quadrupoles in the absence of the macrocycle is disrupted by the latter.

Introduction

It is well-known that interaction of electromagnetic waves with liquid solutions may yield different information depending on the frequency band, or energy employed. Thus microwaves, in the frequency range 0.1 to 100 GHz (10^8 to 10^{11} Hz), may cause the rotational relaxation of complex dipolar species of the solute as well as of the solvent dipoles (at higher frequencies than the former ones).[1] Similarly, infrared radiation in the wavenumber range 4000 to 200 cm^{-1} (10^{14} to 6×10^{12} Hz) may be selectively absorbed at frequencies corresponding to various intermolecular and intramolecular vibrations.[2] These may range from intermolecular vibrations of cations rattling against their solvation cages to polyatomic anion intramolecular vibrations. As these vibrations are sensitive to molecular neighbors in contact, infrared spectroscopy is a powerful tool for a diagnostic structural analysis of the species in solution. Information from vibrational spectra may be of fundamental importance for the interpretation of the microwave rotational spectra.

To the knowledge of the authors, the above combination of techniques has never been applied to the study of macrocyclic complexes with alkali metal ions in solutions of low permittivity. In the present first such study by microwave dielectric relaxation and infrared spectrometry the system NaSCN + 18C6 in the solvent tetrahydrofuran is reported.

Experimental Section

Infrared spectra were recorded by a Perkin-Elmer 983G spectrophotometer equipped with demountable cells with CaF_2 or NaCl windows as described previously.[3] Teflon spacers 0.05 mm thick were employed. The cells were calibrated by the fringe method before each run. The spectrometer prints the values of "peaks" in terms of their wavenumbers. These figures were employed in a linear regression calculation to give the average wavenumber difference between neighboring fringes. From this, the cell thickness l was calculated. The spectrometer also displays wavenumber and absorbance, from the memory of a recorded spectrum, by moving a cursor stepwise. These values were recorded and used for the deconvolution of the digitized spectra in terms of a Gaussian–Lorentzian band, as described below. Manually digitized spectra, from recorded plots given by the spectrometer, gave results identical with the automatically digitized spectra. The latter, however, were superior in terms of the number of decimals that were otherwise unreadable from the plots. The electronics and cells of the microwave spectrometers were described previously.[4] For the data capturing, however, the dielectric spectrometers have now been automated, both in terms of the reflector distance from the window and of the reflected powers as follows:

A Mitutoyo digimatic indicator, Model 543–425 (precision ± 0.0001 in) is connected through a multiplexer Mux-10 and Hewlett-Packard S-232 interface to an 85 Hewlett-Packard computer. The data are transferred to the computer by pressing a foot switch (Mitutoyo 937179) connected to the "external load" terminal of the Mux-10 multiplexer.

Similarly the voltage readings (from the 1000-Hz modulated, reflected voltage sensed by a crystal detector) of the HP-3468A digital voltmeter are transferred via a HP-IL interface loop to the same HP-85 computer (HP-82938A-IL interface). A thermal printer (82162A) that is part of the IL-loop collects both sets of data, namely lengths and voltages. A simple program has been written, which allows for the simultaneous recording of the distances from the indicator and of the logarithm of the voltages from the voltmeter, the results being given as a hard copy from the printer. The authors believe that the program offered by Mitutoyo Co.[5] with the indicator and multiplexer is unnecessary for the present purpose. The present program will be sent to the interested reader upon request.

The macrocycle 18C6 (Aldrich) was recrystallized from acetonitrile from which it precipitates forming a weak adduct. Pure

† University of Utah, Department of Chemistry, Henry Eyring Building, Salt Lake City, UT 84112.

(1) Davies, M. In *Dielectric Properties and Molecular Behavior*, Hill, N., Ed.; Van Nostrand: London, 1969.
(2) Gans, P. *Vibrating Molecules*; Chapman and Hall: London, 1971; Chapter 9.
(3) Saar, D.; Petrucci, S. *J. Phys. Chem.* **1986**, *90*, 3326.
(4) Delsignore, M.; Farber, H.; Petrucci, S. *J. Phys. Chem.* **1985**, *89*, 4968.
(5) Mitutoyo SPC software, Bulletin No. 4090 of Mitutoyo Co.

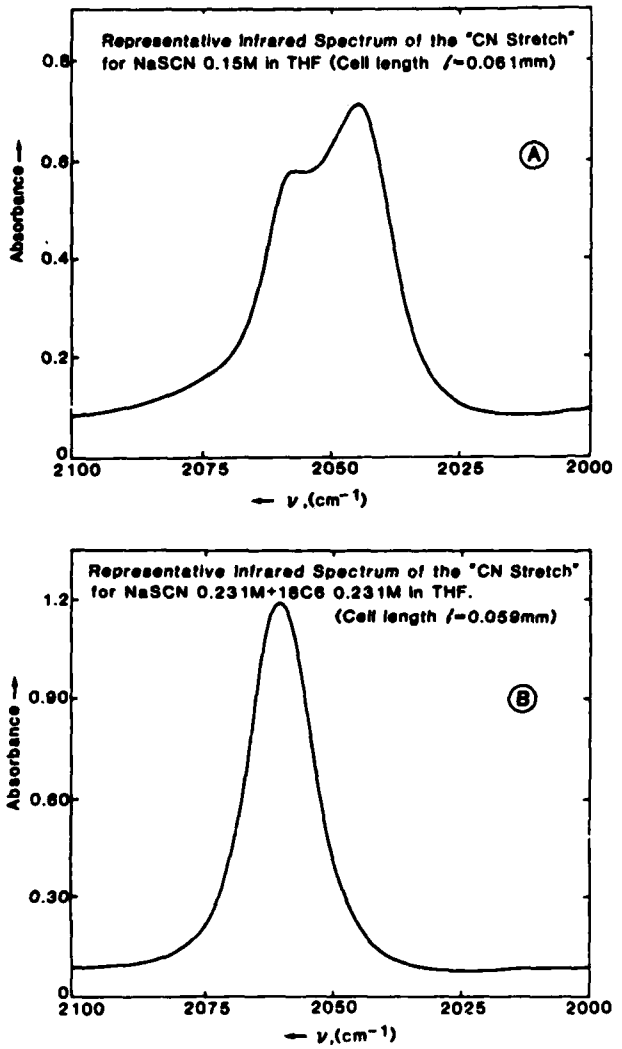

Figure 1. A. Representative infrared spectrum of the "CN stretch" of NaNCS in THF. B. Representative infrared spectrum of the "CN stretch" of NaNCS + 18C6 ($R \simeq 1$) in THF.

18C6 can then be obtained by exposure of the material to vacuum for a few hours. NaSCN (Aldrich) was redried in vacuo (~1 Torr) at ~60 °C overnight. THF (ACS) was dried over predried molecular sieves for about 1 week. Absence of water was checked by IR spectroscopy in the region 3500–3100 cm^{-1} with a 983G Perkin-Elmer spectrometer set at high resolution full scale absorbance as done before.[3] No trace of a water band at ~3300 cm^{-1} was visible in contrast with the original product before exposure to molecular sieves. The solutions were prepared by drying NaSCN directly in volumetric flasks at 60 °C in vacuo overnight, adding the crown ether and exposing to vacuum at room temperature overnight, followed by addition of THF to the weighed flask up to the volume mark.

Results

Figure 1A reports a representative infrared spectrum in the frequency range 2100–2000 cm^{-1} of sodium thiocyanate in THF. Figure 1B reports a similar spectrum of NaSCN + 18C6 in THF in the molar ratio $R = [18C6]/[NCS^-] \simeq 1$. It is obvious that dramatic differences occur. The satellite band at ~2074 cm^{-1}, attributed to the triple ions,[3] and the band at ~2043 cm^{-1}, attributed[3] to dimers or quadrupoles $(NaNCS)_2$, have disappeared upon addition of 18C6. A single band at ~2060 cm^{-1}, attributable to contact ion pairs NaC, NCS, is visible. [This band in the absence of the macrocycle appears at ~2057 cm^{-1}.] Free ions NCS^- (or solvent separated $NaC^+ \cdots NCS^-$ species, spectroscopically indistinguishable from NCS^-) would show a band at ~2050 cm^{-1}.

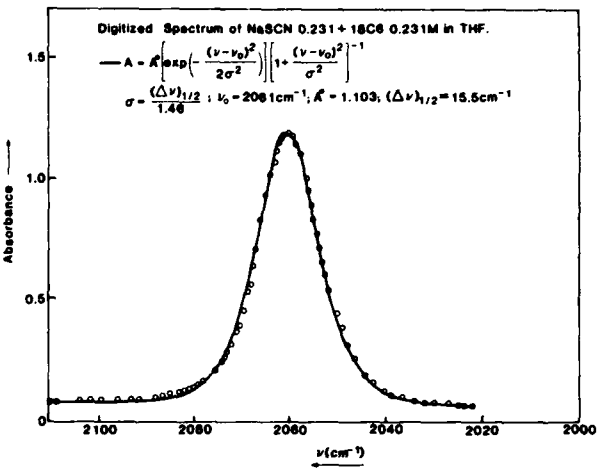

Figure 2. Digitized infrared spectrum for the system 0.231 M NaSCN + 0.231 M 18C6 in THF. The solid line is the Gaussian–Lorentzian function (I) with parameters $A_0 = 1.103$, $\nu_0 = 2061$ cm^{-1}, $(\Delta\nu)_{1/2} = 15.5$ cm^{-1}.

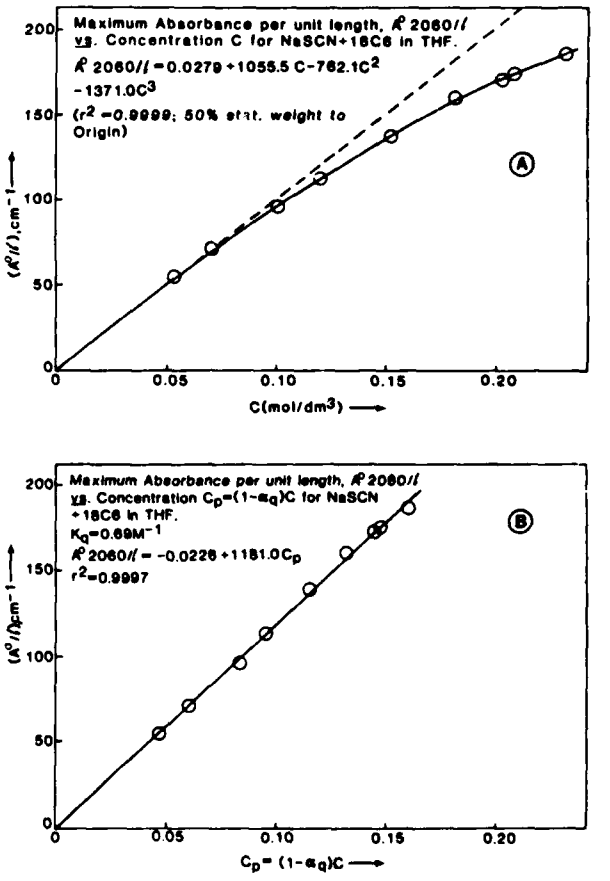

Figure 3. A. (A_0/l), the maximum absorbance per unit length of cell, vs. the electrolyte concentration of NaSCN + 18C6 in THF. B. (A_0/l) vs. $C_p = (1 - \alpha_q)C$, the ion pair concentration, where α_q has been evaluated with $K_q = 0.7$ M^{-1}.

Figure 2 reports a digitized spectrum for the system NaSCN + 18C6 in THF. The solid line corresponds to the interpretation of the spectrum by a single Gaussian–Lorentzian function[3]

$$A = A_0\left[\exp\left(-\frac{(\nu-\nu_0)^2}{2\sigma^2}\right)\right]\left[1+\frac{(\nu-\nu_0)^2}{\sigma^2}\right]^{-1} \quad (1)$$

centered at the wavenumber $\nu_0 \simeq 2060$ cm^{-1}. A_0 is the ordinate or maximum absorbance at ν_0. σ is the variance $\sigma = (\Delta\nu)_{1/2}/1.46$, where $(\Delta\nu_{1/2})$ is the width of the band at $A_0/2$.

TABLE I: Calculated Parameters A_0, ν_0, and $(\Delta\nu)_{1/2}$ for All the NaSCN + 18C6 Solutions in THF Investigated by Infrared Spectrometry according to the Gaussian–Lorentzian Function:[a]

$$A = A_0\left[\exp\left(-\frac{(\nu-\nu_0)^2}{2\sigma^2}\right)\right]\left[1+\frac{(\nu-\nu_0)^2}{\sigma^2}\right]^{-1}$$

l, mm	C_{NaSCN}, M	C_{18C6}, M	A_0	ν_0, cm^{-1}	$(\Delta\nu)_{1/2}$, cm^{-1}	C_p, M
0.0611	0.05292	0.05480	0.331	2060	14	0.0469
0.0607	0.07046	0.0704	0.430	2060	14	0.0604
0.0628	0.1015	0.1016	0.607	2060	14	0.0827
0.0586	0.121	0.128	0.664	2060	14	0.0955
0.0597	0.152	0.144	0.828	2060	14.5	0.115
0.0517	0.182	0.185	0.826	2060	14.5	0.133
0.0590	0.203	0.215	1.008	2060	14.5	0.145
0.0608	0.208	0.210	1.058	2060	14.5	0.148
0.0592	0.231	0.231	1.103	2061	15.5	0.160

[a] l is the cell length expressed in mm. $C_p = (1-\alpha_q)C$, where $K_q = 0.69 = \alpha_q/[4(1-\alpha_q)^2C]$. $(A_0/l) = 0.0279 + 1055.5C - 762.1C^2 - 1371.0C^3$ by nonlinear regression with 50% statistical weight to the origin; $r^2 = 0.9999$. $(A_0/l) = -0.0226 + 1181.0(1-\alpha_q)C = -0.0226 + 1181.0C_p$ by linear regression with 50% statistical weight to the origin; $r^2 = 0.9997$. *In the above functions* (A_0/l), l *is expressed in cm.*

Table I reports the calculated parameters A_0, ν_0, and $(\Delta\nu)_{1/2}$ for all the concentrations of electrolyte and 18C6 investigated in THF. The fit has been achieved by a computer calculation which minimizes the quantity: $\sum_\nu|A^{calcd} - A^{exptl}|$.

Table I also reports the optical length of the infrared cells, l (mm), calibrated before each experiment. Figure 3 reports the quantity A_0/l, the absorbance per unit length of IR cell plotted vs. the total electrolyte concentration C. A slight curvature occurs. This indicates that, although species such as $(NaNCSNa)^+$ and $(NaNCS)_2$ present in the system sodium thiocyanate in THF have been disrupted by the crown ether, the simplistic interpretation of the spectrum as corresponding to the function

$$A_0/l = \epsilon_p C_p \simeq \epsilon_p C \qquad (2)$$

(with ϵ_p the extinction coefficient or molar absorptivity of the contact pair NaC^+, $NCS)^-$ does not suffice to interpret the spectrum.

As only one band is observable, we advance the hypothesis that some dimers $(NaC, NCS)_2$ exist in small concentration, sufficient to cause the curvature in the A_0/l vs. C plot. A calculation has been attempted according to the scheme:

$$\underset{2(1-\alpha_q)C}{2NaC,NCS} \rightleftharpoons \underset{\alpha_q C}{(NaC,NCS)_2} \qquad (3)$$

with

$$K_q = \frac{\alpha_q}{4(1-\alpha_q)^2C}$$

calculating, by trial and error, the best K_q which gives a linear plot of (A_0/l) vs. $(1-\alpha_q)C = C_p$ with the determination coefficient r^2 closest to unity and intercept closest to zero. The fit is shown in Figure 3 which corresponds to $K_q = 0.7$ M^{-1}. One ought to realize, however, that, even if the rationalization of the curvature of (A_0/l) vs. C is correct, the value of K_q is very tentative. The linearization of the (A_0/l) vs. $(1-\alpha_q)C = C_p$ plot is not a very sensitive procedure.

Another serious objection could be voiced against eq 3. It implicitly ignores the possible presence of solvent-separated dimers of the type NaC, NCS···NaC, NCS. This would imply an alternative scheme of dimerization

$$\underset{C_1}{2NaC,NCS} \rightleftharpoons \underset{C_2}{NaC,NCS\cdots NaC,NCS} \rightleftharpoons \underset{C_3}{(NaC,NCS)_2} \qquad (3a)$$

Equation 3a would carry as a consequence the fact that A_0/l would account for both NaC,NCS and NaC,NCS···NaC,NCS which *are indistinguishable spectroscopically and that*

$$K_q' = \frac{C_2 + C_3}{C_1^2}$$

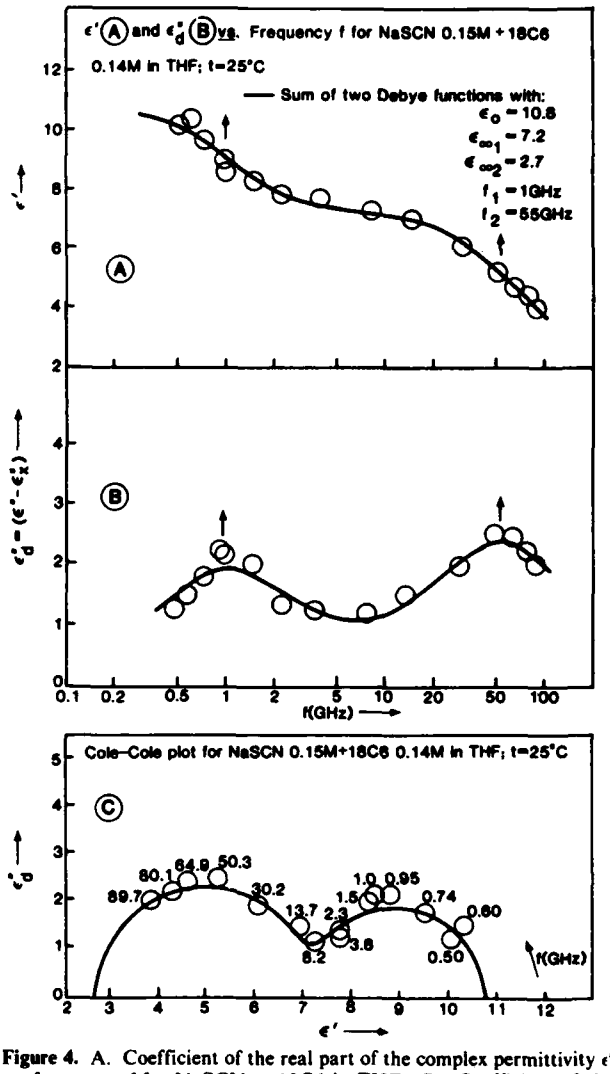

Figure 4. A. Coefficient of the real part of the complex permittivity ϵ' vs. frequency f for NaSCN + 18C6 in THF. B. Coefficient of the imaginary part of the complex permittivity $\epsilon_d'' = \epsilon'' - \epsilon_x''$ vs. the frequency f. $\epsilon_x'' = 1.8 \times 10^{12}\,\chi/f$; χ is the specific conductivity. C. Cole–Cole plot, ϵ_d'' vs. ϵ' at $t = 25$ °C.

instead of the one we have calculated which implies $C_2 = 0$. This objection has already been spelled out before[3] in evaluating K_q's obtained from vibrational spectrometry.

In the present case, however, it is likely that $C_2 \sim 0$ and that (A_0/l) reflects only the contribution of C_1 because a single value of $K_q = 0.7$ is able to linearize the plot (A_0/l) vs. C. Were the C_2 values different from zero a significant change of K_q with C in order to linearize the (A_0/l) vs. C_p plot would have been necessary, having retained eq 3.

Figure 4 shows a representative plot[4] of the coefficient of the real part of the complex permittivity ϵ' vs. the frequency f. A plot of the coefficient of the imaginary part of the complex permittivity ϵ'', corrected by the conductance $X(\Omega^{-1}$ cm$^{-1})$, $\epsilon''_d = [\epsilon'' - (1.8 \times 10^{12})/f]$, vs. the frequency f is also shown.[4] In the above the complex permittivity is $\epsilon^* = \epsilon' - J\epsilon''$.

In Figure 4, for the same system, NaSCN + 18C6 in THF, the Cole–Cole plot[1] of ϵ''_d vs. ϵ' is reported. The solid lines in Figure 4 correspond to the sum of the two Debye processes, according to the function:

$$\epsilon' = (\epsilon_0 - \epsilon_{\infty_1})\frac{1}{1+(f/f_1)^2} + (\epsilon_{\infty_1} - \epsilon_{\infty_2})\frac{1}{1+(f/f_2)^2} + \epsilon_{\infty_2} \qquad (4)$$

$$\epsilon''_d = (\epsilon_0 - \epsilon_{\infty_1})\frac{f/f_1}{1+(f/f_1)^2} + (\epsilon_{\infty_1} - \epsilon_{\infty_2})\frac{f/f_2}{1+(f/f_2)^2}$$

Table II reports the calculated parameters ϵ_0, ϵ_{∞_1}, ϵ_{∞_2}, f_1, and f_2

TABLE II: Calculated Parameters ϵ_0, ϵ_{∞_1}, ϵ_{∞_2}, f_1, and f_2 and Measured Specific Conductance χ (Ω^{-1} cm^{-1}) for All the Systems NaSCN + 18C6 and NaSCN Investigated in THF at 25 °C by Dielectric Spectrometry

C_{NaSCN}, M	C_{18C6}, M	ϵ_0	ϵ_{∞_1}	ϵ_{∞_2}	f_1, GHz	f_2, GHz	χ, Ω^{-1} cm^{-1}
			NaSCN + 18C6 in THF				
0.0529	0.0541	8.7	7.2	2.7	1	55	$9.7_5 \times 10^{-5}$
0.104	0.105	9.7	7.2	2.7	1	55	$2.4_2 \times 10^{-4}$
0.15	0.14	10.8	7.2	2.7	1	55	$3.5_8 \times 10^{-4}$
			NaSCN in THF				
0.10		8.3	7.3	2.4_5	2	60	$1.8_9 \times 10^{-5}$
0.152		8.5	7.3	2.5	2	60	$2.9_6 \times 10^{-5}$
0.19_3		8.8	7.3	2.5	2	60	$4.0_2 \times 10^{-5}$

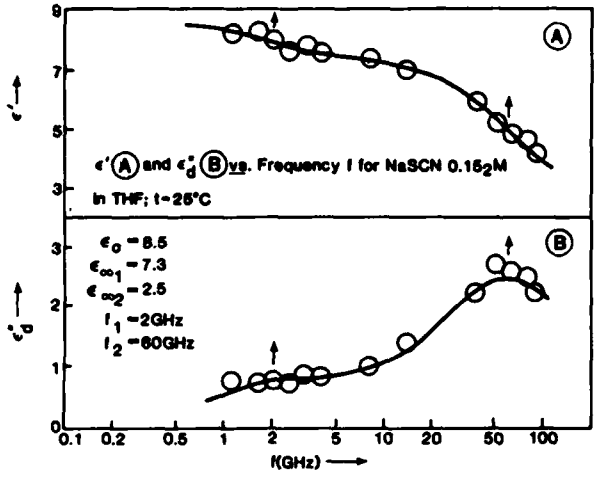

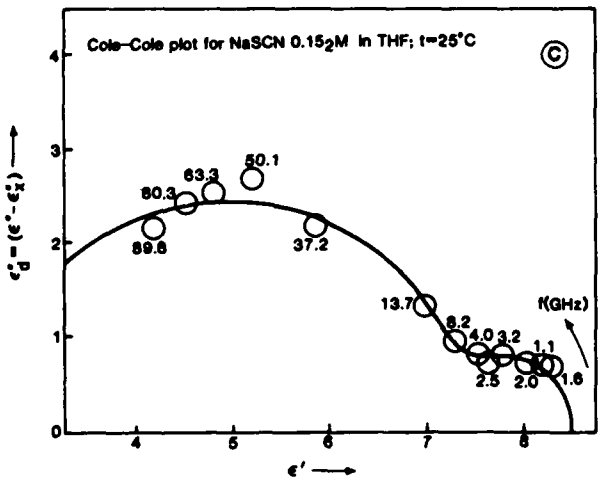

Figure 5. A. Coefficient of the real part of the complex permittivity ϵ' vs. frequency for NaSCN in THF; t = 25 °C. B. Coefficient of the imaginary part of the complex permittivity $\epsilon_d'' = \epsilon'' - \epsilon_s''$ vs. frequency at t = 25 °C. C. Cole–Cole plot, ϵ_d'' vs. ϵ' at t = 25 °C.

and the measured specific conductance χ for all the systems NaSCN + 18C6 investigated in THF at 25 °C. The fit of eq 4 to the data has been achieved by minimizing the summation:

$$\Sigma|\epsilon'_{calcd} - \epsilon'_{exptl}| + \Sigma|\epsilon''_{calcd} - \epsilon''_{exptl}|$$

From the position of the dielectric relaxation at high frequency and from comparison with previous work,[6] we attribute the relaxation at high frequency to the solvent. The lower relaxation, absent in the case of the solvent, is attributed to the solute complex dipole NaC^+, NCS^-. In order to draw a parallel with the infrared

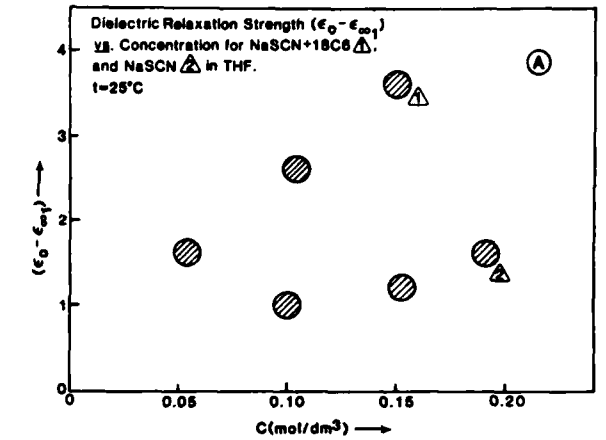

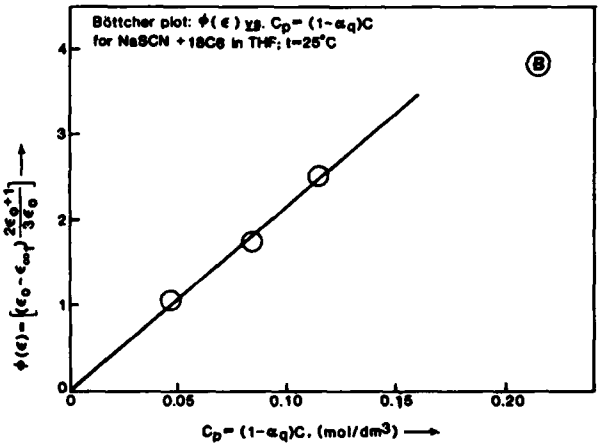

Figure 6. A. Relaxation strength ($\epsilon_0 - \epsilon_{\infty_1}$) vs. electrolyte concentration C for the systems NaSCN + 18C6 and NaSCN in THF at t = 25 °C. B. Böttcher plot $\phi(\epsilon) = (\epsilon_0 - \epsilon_{\infty_1})[(2\epsilon_0 + 1)/3\epsilon_0]$ vs. $C_p = (1 - \alpha_q)C$ for NaSCN + 18C6 in THF at t = 25 °C.

research reported above, dielectric spectra of the system NaSCN in THF have also been recorded.

Figure 5A shows a representative plot of ϵ' vs f, Figure 5B of ϵ''_d vs. f, and Figure 5C of ϵ''_d vs. ϵ' for NaSCN in THF. The solid lines are the fitted functions (eq 4), according to the sum of two Debye relaxation processes.

Table II reports the calculated dielectric parameters for all the NaSCN solutions investigated in THF.

Figure 6 reports the "relaxation strength" ($\epsilon_0 - \epsilon_{\infty_1}$) for the relaxation due to the solute at lower frequency (1 and 2 GHz, respectively) for NaSCN + 18C6 and NaSCN in THF at 25 °C. A dramatic difference is noticeable.

Figure 6B reports the Böttcher plot[7]

$$\Phi(\epsilon) = (\epsilon_0 - \epsilon_{\infty_1})\frac{2\epsilon_0 + 1}{3\epsilon_0} = \frac{4\pi L \times 10^{-3}}{(1 - \alpha f)^2}\frac{\mu^2}{3kT}C_p \qquad (5)$$

where the polarizability α and internal field factor f term[1,8] $(1 - \alpha f)^2$ has been approximated to unity. The ion-pair concentration $C_p = (1 - \alpha_q)C$ has been calculated by using the value k_q = 0.7 M^{-1}, obtained from the IR spectra above. Linear regression of $\Phi(\epsilon)$ vs. C_p (50% statistical weight to the origin) gives Intercept = 0.002, slope 21.67, r^2 = 0.999, from which $\mu = 18.8 \times 10^{-18}$ esu cm. Here we have taken a rigid sphere model, $\mu = a_\mu e$, and $a_\mu = 3.9 \times 10^{-8}$ cm, the charge-to-charge separation distance in the ion pair.

Unfortunately a similar calculation is not feasable for the NaSCN system in THF due to the unknown value of K_q and the

(6) Saar, D.; Brauner, J.; Farber, H.; Petrucci, S. *J. Phys. Chem.* **1978**, *82*, 1943.

(7) Böttcher, C. F. *Theory of Electrical Polarization*; Elsevier: Amsterdam, 1973.

(8) Farber, H.; Petrucci, S. *J. Phys. Chem.* **1975**, *79*, 1221. **1976**, *80*, 327.

evidence from IR spectra (Figure 1A) that a large proportion of the electrolyte exists as dimers. If the latter are apolar ($\epsilon_0 - \epsilon_{\infty_1}$) will reflect only the C_p contribution to the polarization of the solution. More information can, however, be extracted from the relaxation frequencies f_1. By neglecting differences between the microscopic relaxation time $\tau' = [4\pi a_\tau^3/(kT)]\eta$ (according to Debye) and the decay time of the solute polarization $\tau = (2\pi f_1)^{-1}$, by retaining the solvent viscosity $\eta = 0.0046$ P,[9] one calculates for the system NaSCN + 18C6 in THF a rotational radius of the ion pair NaC^+, NCS^- that is $a_\tau = 4.8 \times 10^{-8}$ cm, given $\tau = 159.2$ ps. This figure is comparable to $a_\mu = 3.9 \times 10^{-8}$ cm obtained above, when one recalls that a_μ reflects the charge-to-charge separation and a_τ the diffusional rotation radius of the solvated complex.[6] For NaSCN in THF $\tau = 79.6$ ps, $a_\tau = 3.8 \times 10^{-8}$ cm, reflecting the less bulky rotating entity in the absence of the coordinated crown ether. As remarked above, no inferences can be drawn for a_μ given a lack of knowledge of K_q for NaSCN in THF.

Conclusions

The combination of a structural tool such as IR spectrometry with a dynamic one such as microwave dielectric relaxation gives a more complete insight to the nature of the macrocycle electrolyte complex than is possible with either of the two separate methods. The infrared method, by detecting a vibrating entity or its change due to different environments, is somewhat faster than the microwave dielectric method which detects the rotation of the dipolar species in solution. This is indeed an advantage for the analysis of the rotating species, as they cannot escape detection by a parallel probing of their existence by infrared analysis, in a comparable concentration range.

The present study confirms these considerations, giving complementary and dramatic evidence of the effect of the addition of a macrocycle such as 18C6 to an electrolyte such as NaSCN in THF.

Extension of the above studies to solutions of lithium salts which are relevant to the construction of secondary lithium batteries is presently underway.

Acknowledgment. The authors are grateful to the Army Research Office, Research Triangle Park, NC, Grant DAAG-29-85-K0048, and to the National Science Foundation, Grant CHE-8513266, for generous financial support of various aspects of the present project.

Registry No. Na, 7440-23-5; NaSCN, 540-72-7; 18C6, 17455-13-9.

(9) Metz, D. J.; Glines, A. *J. Phys. Chem.* **1967**, *71*, 1158. Kuss, E. *Z. Angew. Phys.* **1965**, *7*, 376.

Reprinted from The Journal of Physical Chemistry, 1987, 91, 4628.

Temperature Dependence of Ionic Association and of Molecular Relaxation Dynamics of $LiAsF_6$ in 2-Methyltetrahydrofuran

Naoki Inoue,[†] Meizhen Xu,[‡] and Sergio Petrucci*

Department of Chemistry and Weber Research Institute, Polytechnic University, Farmingdale, New York 11735 *(Received: January 16, 1987)*

Electrical conductance data in the temperature range +25 to −35 °C, when analyzed by the Fuoss–Kraus triple-ion theory of conductance, reveal the presence of both ion pairs and triple ions. Formation constants K_p and K_T, at various temperatures for ion pairs and triple ions, respectively, have been determined. These figures are compared with values calculated by the Bjerrum theory of ion-pair formation and by the Delsignore–Bjerrum theory for formation of triple ions, respectively. Evidence of the presence of triple ions persists (with the formation constant K_T somewhat increased) by allowing for measured changes of solvent permittivity with concentration of electrolyte. An analysis of the data at t = 25 °C, by retaining the solution permittivities but excluding triple ions, has been attempted with fair results, if the values of K_p are allowed to change with concentration, namely, with permittivity. Ultrasonic relaxation spectra, in the concentration range 0.1–0.4 M of $LiAsF_6$ and in the frequency range 0.5–400 MHz at 15 and 5 °C in 2-methyltetrahydrofuran (2-MeTHF), are reported. The results, combined with previous data at 25 °C, are interpreted as due to ion-pair dimerization. The forward and reverse rate constants and activation parameters $\Delta H^{\ddagger}$ and $\Delta S^{\ddagger}$ are reported together with the values of the dimerization constants K_q at various T's. The figures for K_q are compared to the values calculated by the Maaser–Bjerrum dimerization theory of ion-pair formation, giving pair to pair approach distances suggesting solvent-separated dimers. Infrared spectra in the $\bar{\nu}_3$ band envelope of the AsF_6^- ion, in the concentration range 0.05–0.8 M, reveal the presence of three separate bands. The spectral envelope was deconvoluted by three Gaussian–Lorentzian product functions centered at ~716, ~702, and ~675 cm^{-1}. The band at ~702 cm^{-1} is interpreted as due to "spectroscopically free" AsF_6^-, namely, as due to solvent-separated ion pairs and/or solvent-separated dimers. The band at ~716 cm^{-1} is interpreted as due to contact ion pairs, based on collateral evidence in 1,2-dimethoxyethane (1,2-DME). The band at ~675 cm^{-1}, according to literature evaluations of the AsF_6^- Raman and infrared spectra, is due to combination bands.

Introduction

Knowledge of the extent of association of electrolyte solutions, and the type, structure, and lifetime of the complex species in solutions used in secondary Li battery construction, is relevant information for electrochemists. The information becomes of paramount importance, in order to ascertain causes of battery failure when these units are subjected to low temperature as in stratospheric or subarctic conditions. Theoretically, there is need of knowledge but scarcity of data with regard to the lifetime and to the structure of complexes in media of low permittivity. By changing temperature, the permittivity changes without concomitant large changes in donor number of solvent or other factors which occur in the usual isothermal studies in mixed solvents of various compositions. Therefore, in order to isolate electrostatic long-range effects in ionic association of various species (without obscuring large changes of other factors), it appears that changing the temperature is an alluring way to perform these studies.

$LiAsF_6$ in 2-MeTHF, already studied at room temperature,[1] has now been investigated by electrical conductance down to t = −35 °C. In order to ascertain and confirm the structure of the $LiAsF_6$ in 2-MeTHF, infrared spectra of the $\bar{\nu}_3$ band envelope of AsF_6^- are reported.

Experimental Section

The equipment and procedure for the conductance and ultrasonic work have been reported elsewhere.[1-3] Similarly, the equipment and procedure for the infrared work have been reported.[4] The only change is the computer assistance to the 983-G Perkin-Elmer spectrometer provided by a 3600 Perkin-Elmer data station that allows for spectra production, video monitoring, disk recording and retrieving, data digitization, and hard copy recording via computer. (The authors are indebted to the Perkin-Elmer staff of Norwalk, CT, for instruction of use of the 3600 data station.)

For the products, $LiAsF_6$ was from Agri-Chemical Co., Atlanta, GA. It was redried at 70 °C in vacuo for 36 h. 2-MeTHF (Aldrich) was distilled under reduced pressure over metallic sodium and benzophenone. Solutions were used within 1 h after preparation for the ultrasonic and infrared work, minimizing (10–30 s) contact with the open atmosphere.

Solutions for conductance work were prepared by weight in situ, directly in the conductance cell, by adding a stock solution in weighed portions, to the weighed solvent in the cell. The stock solution, kept in a desiccator, was used within 6–8 h from its preparation.

Results

Figure 1, A, B, and C, reports the equivalent conductances vs. concentration, in the form log Λ vs. log c, for $LiAsF_6$ in 2-methyltetrahydrofuran (2-MeTHF) at 5, −15, and −35 °C, respectively. Table I reports the experimental Λ's and c's for the various temperatures investigated.

Figure 2A,B reports representative plots of the excess sound absorption per wavelength $\mu = \alpha_{exc}\lambda = (\alpha - Bf^2)(u/f)$, where α is the attenuation coefficient (Np/cm) of sound at the frequency f. B is the background ratio, $B = (\alpha/f^2)_{f \gg f_r}$, for frequencies f's much larger than the relaxation frequency f_r, in accord with the Debye function valid for a single relaxation process:

$$\frac{\alpha}{f^2} = \frac{A}{1 + (f/f_r)^2} + B \qquad (I)$$

The solid lines in Figure 2A,B are, in fact, in accord with eq I, written in the form

$$\mu = 2\mu_m \frac{f/f_r}{1 + (f/f_r)^2} \qquad (II)$$

where $\mu_m = \mu$ (for $f = f_r$), namely, the maximum excess sound absorption per wavelength, and $A = (2\mu_m)/(uf_r)$; u is the sound velocity. Table II reports the calculated parameters f_r, μ_m, B, and the measured sound velocities u for all the solutions of $LiAsF_6$

[†] On leave from the Department of Physics, Ehime University, Matsuyama, Japan.

[‡] On leave from the Department of Chemistry, University of Peking, Peking, People's Republic of China.

(1) Delsignore, M.; Maaser, H. E.; Petrucci, S. *J. Phys. Chem.* **1984**, *88*, 2405.

(2) Petrucci, S.; Hemmes, P.; Battistini, M. *J. Am. Chem. Soc.* **1967**, *89*, 5582.

(3) Darbari, G. S.; Richelson, M.; Petrucci, S. *J. Chem. Phys.* **1970**, *53*, 859. Petrucci, S. *J. Phys. Chem.* **1967**, *71*, 1174. Onishi, S.; Farber, H.; Petrucci, S. *J. Phys. Chem.* **1980**, *84*, 2922.

(4) Saar, D.; Petrucci, S. *J. Phys. Chem.* **1986**, *90*, 3326.

0022-3654/87/2091-4628$01.50/0

TABLE I: Equivalent Conductance Λ (S cm²/mol) and Molar Concentration c (mol/dm³) at t = 25, 5, −15, and −35 °C for $LiAsF_6$ in 2-MeTHF

t = 25 °C[a]		t = 5 °C		t = −15 °C		t = −35 °C	
Λ	$c \times 10^4$	Λ	$c \times 10^4$	Λ	$c \times 10^4$	Λ	$c \times 10^4$
			1st Run				
1.037_1	6.6112	4.966_5	5.7974	4.255_5	5.2038	5.5235	5.5345
0.894_5	9.5847	3.431_6	13.949	2.6909	18.282	3.9513	13.358
0.498_4	38.470	2.680_5	28.308	2.0330	38.389	3.0785	27.699
0.416_5	62.710	2.070_0	67.019	1.3753	112.73	2.4651	55.844
0.372_1	89.505	1.738_9	141.95	1.0609	251.86	1.8774	130.17
0.332_1	140.42	1.538_1	397.93	0.9849_5	425.65	1.4546	274.37
0.315_8	215.55	1.577_4	723.66	1.0513	706.70	1.2912	498.81
0.338_6	353.00	1.654_9	924.71	1.2334	1132.1	1.2577	780.85
						1.3492	972.82
			2nd Run				
		1.551_9	583.3				
		1.654_3	832.8	1.4487	1628.3	1.5649	1318.6
		1.828_1	1180.0	1.8250	2592.6	1.9144	2611.8
		2.475_3	2493.1				

[a] Data from ref 1.

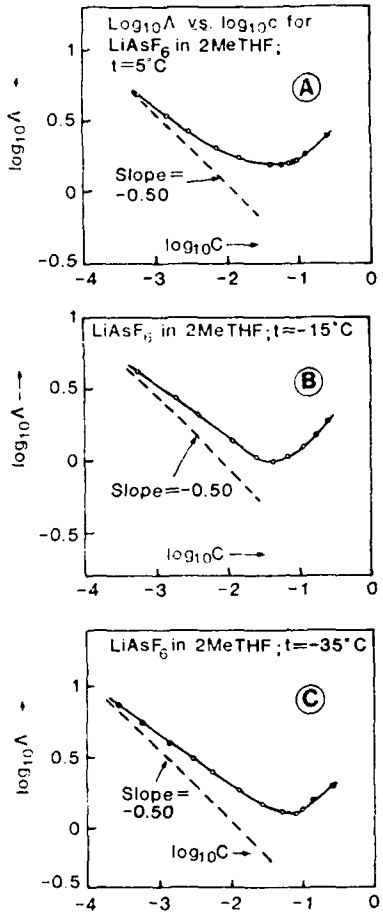

Figure 1. (A) log Λ vs. log c for $LiAsF_6$ in 2-MeTHF at t = 5 °C. (B) log Λ vs. log c for $LiAsF_6$ in 2-MeTHF at t = −15 °C. (C) log Λ vs. log c for $LiAsF_6$ in 2-MeTHF at t = −35 °C.

in 2-MeTHF investigated at 15 and 5 °C.

Figure 3A,B shows representative digitized infrared spectra of the $\bar{\nu}_3$ band envelope of the AsF_6^- ion. The solid lines have been drawn by fitting the digitized absorbances to the Gaussian–Lorentzian semiempirical product function[4]

$$A = \sum_{j=1}^{3} A_j^\circ \left\{ \exp\left[-\frac{(\bar{\nu} - \bar{\nu}_{0_j})^2}{2\sigma_j^2} \right] \right\} \left[1 + \frac{(\bar{\nu} - \bar{\nu}_{0_j})^2}{\sigma^2} \right]^{-1} \quad \text{(III)}$$

where $\exp(-(\bar{\nu} - \bar{\nu}_{0_j})/2\sigma_j^2)$ is the Gaussian and $[1 + (\bar{\nu} - \bar{\nu}_{0_j})^2/\sigma^2]^{-1}$ is the Lorentzian factor of (III). $\Delta\bar{\nu}_{1/2}$ represents the width of

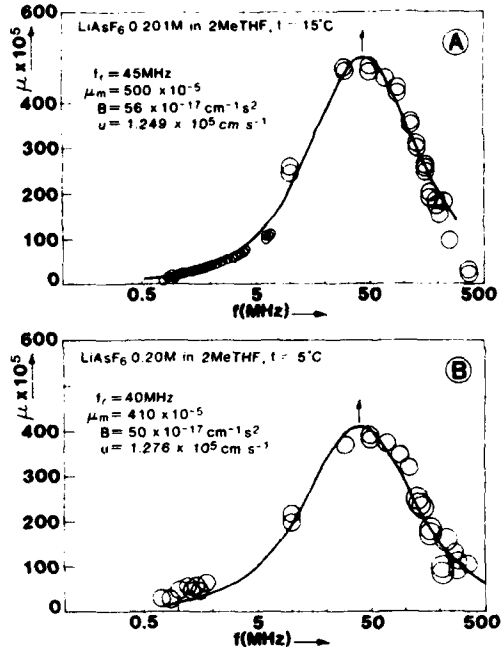

Figure 2. (A) Excess sound absorption per wavelength, μ, vs. frequency, f, for $LiAsF_6$ (0.20 M) in 2-MeTHF; t = 15 °C (M = mol/dm³). (B) μ vs. f for $LiAsF_6$ (0.20 M) in 2-MeTHF; t = 5 °C (M = mol/dm³).

TABLE II: Ultrasonic Relaxation Parameters f_r, μ_m, B, and Sound Velocities u for $LiAsF_6$ in 2-MeTHF at the Concentrations and Temperatures Investigated

c, mol/dm³	f_r, MHz	$\mu_m \times 10^5$	$B \times 10^{17}$, cm⁻¹ s²	$u \times 10^{-5}$, cm/s
		t = 15 °C		
0.40	70	570	62	1.249
0.30	65	530	52	1.245
0.20_1	45	500	56	1.259
0.10_5	50	350	55	1.258
		t = 5 °C		
0.40_6	60	670	50	1.296
0.30	40	600	50	1.300
0.20	40	410	50	1.276
0.10_6	30	270	46	1.285

each band at half-maximum absorbance, $A_j^\circ/2$. A_j° corresponds to the maximum absorbance for $\bar{\nu} = \bar{\nu}_{0_j}^\circ$ for each band. Notice that for a pure Gaussian function $A = A_j^\circ \exp[-(\bar{\nu} - \bar{\nu}_{0_j})^2/2\sigma_j^2]$ and $\sigma = \Delta\bar{\nu}_{1/2}/2.355$, whereas for a pure Lorentzian $A = A_j^\circ[1 + (\bar{\nu} - \bar{\nu}_{0_j})^2/2\sigma_j^2]^{-1}$ and $\sigma = \Delta\bar{\nu}_{1/2}/2.00$. The factors 2.355 and 2.00 relate the half-bandwidths of the respective functions to the

TABLE III: Calculated Infrared Parameters A_j^0, $\bar{\nu}_j$, and $\Delta\nu_{1/2}$ for the Concentrations Investigated of $LiAsF_6$ in 2-MeTHF

l_{cell}, cm	c, mol/dm^3	$\bar{\nu}_{717}$, cm^{-1}	A_0^{717}	$\bar{\nu}_{702}$, cm^{-1}	A_0^{702}	$\bar{\nu}_{675}$, cm^{-1}	A_0^{675}	$\Delta\nu_{1/2}$,[a] cm^{-1}
0.00259	0.803	717.5	1.35	702	1.15	676	0.50	13
0.00258	0.601	717.5	1.25	702	1.00	676	0.40	12
0.00270	0.502	717	1.32	702	1.05	676	0.36	12
0.00268	0.402	717	1.11	702	0.92	676	0.29	12
0.00270	0.302	717	0.83	702	0.78	675	0.22	12
0.00504	0.210	716	0.85	702	1.00	675	0.20	12
0.00496	0.106	717	0.55	702.5	0.50	676	0.17	12
0.00468	0.053	716	0.17_2	702.5	0.25_6	675	0.04	12

[a] $(\Delta\nu_{1/2})_{717} = (\Delta\nu_{1/2})_{702} = (\Delta\nu_{1/2})_{675}$.

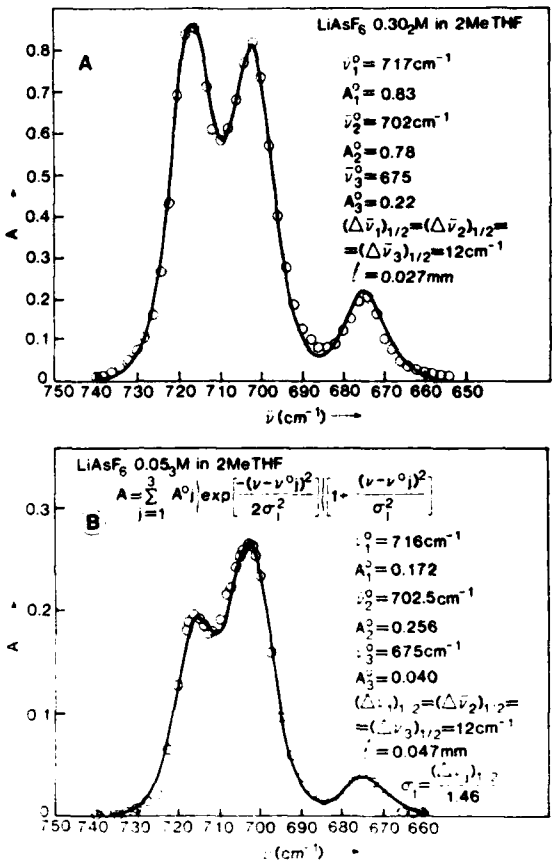

Figure 3. (A) Digitized infrared spectrum of the $\bar{\nu}_3$ spectral envelope of $LiAsF_6$ (0.30 M) in 2-MeTHF. (B) Digitized infrared spectrum of the $\bar{\nu}_3$ spectral envelope of $LiAsF_6$ (0.05 M) in 2-MeTHF.

standard error σ. For instance, for a pure Gaussian $A/A_0 = 0.50 = e^{-(\bar{\nu}-\bar{\nu}_0)^2/2\sigma^2} = \exp[-(\Delta\bar{\nu}_{1/2}^2/4)/2\sigma^2]$, giving $2.3548 = \Delta\bar{\nu}_{1/2}/\sigma$. As a pure Gaussian function is particularly appropriate for infrared spectrum of solids and a pure Lorentzian is appropriate for infrared spectra of gases, the product function (III) is an average function, attempting empirically, but quite successfully, to reproduce the line shape of infrared spectra in the liquid state. Table III reports the calculated parameters A_{0j}, $\bar{\nu}_j$, and $\Delta\bar{\nu}_{1/2}$ for the three Gaussian–Lorentzian product functions used to describe the $\bar{\nu}_3$ band envelope of $LiAsF_6$ in 2-MeTHF.

Calculations and Discussion

Electrical Conductivity. Traditionally, since the appearance of the Fuoss–Kraus theory,[5] the analysis of conductance data, in media of permittivity lower than 10, has been carried out, with inclusion of triple ions as contributing species to the total conductance. Recently, however, the existence of triple ions in solution has been subjected to question. The analysis of conductance data has been carried out without the inclusion of triple ions[6] even in media of low permittivity. Also, the increase in conductance with concentration (from the value predicted by the dissociation of simple ion pairs) has been suggested[7] to be due to the increase of the permittivity of the solution with electrolyte concentration. Indeed, if the electrolyte is present mainly in the form of dipolar ion pairs, the polarization of the solution, and hence its permittivity, is increased. At high electrolyte concentration this effect is overwhelming. In the past we have shown[8] that, by including the solution permittivities into the Fuoss–Kraus theory, it applicability was extended up to ~0.1 M for $LiClO_4$ in dimethyl carbonate at t = 25 °C.

The question of concern is whether at relatively low concentrations ($c \lesssim 10^{-2}$ M) the effect of the permittivity increase is relevant to the existence of triple ions and to their postulated contributions to the conductance of the solution. In order to probe into this question, the conductance of the solutions investigated in this work will be dealt with first in the conventional way by approximating the permittivity to the one of the solvent. The analysis will be repeated with the available solution permittivity data by retaining the triple ions. Finally, the analysis will be repeated with the solution permittivity data, eliminating the triple ions as postulated species contributing to the total conductance.

Delsignore et al.[1] reported conductance data for $LiAsF_6$ in 2-MeTHF at 25 °C. Some of their data have been reanalyzed by the Fuoss–Kraus triple-ion conductance theory[5]

$$\Lambda g(c)c^{1/2} = \frac{\Lambda_0}{K_p^{1/2}} + \frac{\Lambda_T^{\circ} K_T}{K_p^{1/2}}\left(1 - \frac{\Lambda}{\Lambda_0}\right)c \qquad \text{(IV)}$$

with

$$g(c) = \frac{\exp\left(-\frac{2.303}{\Lambda_0^{1/2}}\beta'(c\Lambda)^{1/2}\right)}{\left(1 - \frac{S}{\Lambda_0^{3/2}}(c\Lambda)^{1/2}\right)\left(1 - \frac{\Lambda}{\Lambda_0}\right)^{1/2}}$$

and

$$\beta' = \frac{1.8247 \times 10^6}{(\epsilon T)^{3/2}}$$

$$S = \alpha\Lambda_0 + \beta = \frac{0.8206 \times 10^6}{(\epsilon T)^{3/2}} + \frac{82.501}{\eta(\epsilon T)^{1/2}}$$

In the above, ϵ is the permittivity, η the viscosity, and T the absolute temperature. The values of ϵ = 6.24 and η = 0.0047 P have been taken from previous work.[1] The value Λ_0 = 22.53 S cm^2/mol at t = 25.00 °C, in propylene carbonate,[9] is judged particularly reliable. As η = 0.0253 P,[9] it gives $\Lambda_0\eta$ = 0.570 and, in 2-MeTHF, Λ_0 = 121 S cm^2/mol, lower than the value used previously,[1] and the very reason of reanalyzing the data in the conventional way.

Figure 4A reports the plot of $\Lambda g(c)c^{1/2}$ vs. $(1 - \Lambda/\Lambda_0)c$ for $LiAsF_6$ in 2-MeTHF. Linear regression gives r^2 = 0.997, intercept

(5) Fuoss, R. M.; Kraus, C. A. *J. Am. Chem. Soc.* **1933**, *55*, 2387. Fuoss, R. M.; Accascina, F. *Electrolytic Conductance*; Interscience: New York, 1959.

(6) Grigo, M. *J. Solution Chem.* **1982**, *11*, 529.
(7) Gestblom, B.; Svorstöl, I.; Songstad, J. *J. Phys. Chem.* **1986**, *90*, 4684.
(8) Delsignore, M.; Farber, H.; Petrucci, S. *J. Phys. Chem.* **1985**, *89*, 4968.
(9) Salomon, M.; Plichta, E. *J. Electrochim. Acta* **1984**, *29*, 731.

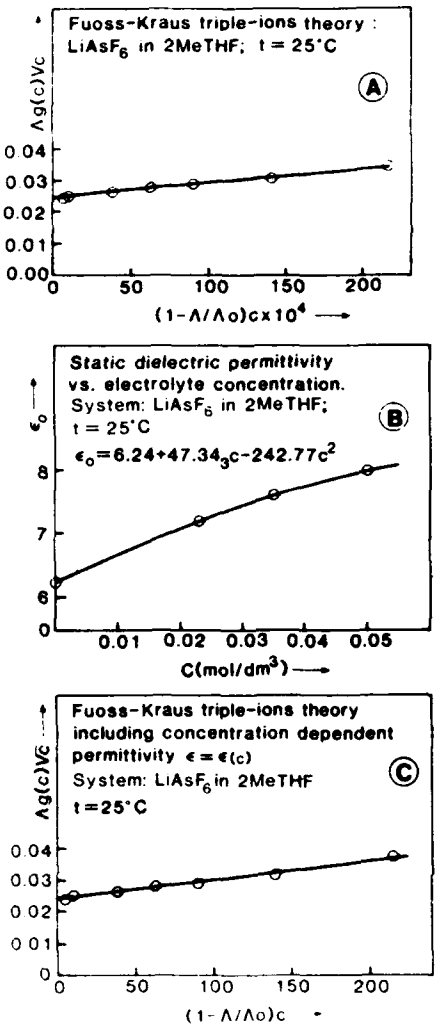

Figure 4. (A) $\Lambda c^{1/2}g(c)$ vs. c for $LiAsF_6$ in 2-MeTHF; t = 25 °C. (B) Dielectric permittivity, $\epsilon(c)$, vs. c for $LiAsF_6$ in 2-MeTHF; t = 25 °C. (C) $\Lambda c^{1/2}g(c)$ vs. c using $\epsilon = \epsilon(c)$ for $LiAsF_6$ in 2-MeTHF.

TABLE IV: Solvent Properties and Results of K_p and K_T by the Fuoss–Kraus Triple-Ion Conductance Equation for $LiAsF_6$ in 2-MeTHF at the Various Temperatures Investigated

t, °C	ϵ	η, P	Λ_0,[a] S cm²/mol	K_p, M^{-1}	K_T,[b] M^{-1}	c_{max} × 10⁴[c]
25	6.24	0.0047	121	2.5×10^7	29.4	215.5_5
5	6.77	0.0057	100	1.0×10^6	$20._3$	141.9_5
−15	7.38	0.0072_5	$78._6$	8.5×10^5	$9._8$	112.7_3
−35	8.10	0.0096_8	$58._9$	3.0×10^5	$1._3$	130.1_7

[a] Based on Walden's rule $\Lambda_0\eta = 0.570$. [b] Based on the arbitrary position $\Lambda_0^T = 2/3\Lambda_0$. [c] Maximum electrolyte concentration used in eq IV.

= −0.02447, and slope = 0.4793, from which one calculates K_p = $2.4_5 \times 10^7$ M^{-1} and K_T = 29.4 M^{-1} (M = mol/dm³) having retained the arbitrary condition $\Lambda_T^\circ = {}^2/_3\Lambda_0$, consistent with previous work.[1]

Table IV reports the results of the calculations by the Fuoss–Kraus conductance eq IV, at 5, −15, and −35 °C. For these calculations the permittivities ϵ and viscosities η have been calculated by the functions[10]

$$\epsilon = -1.14 + 2200/T$$

$$\log \eta = -3.635 + 386/T$$

Table IV also reports, for all the temperatures investigated, the maximum concentration used in eq IV. Figure 5A reports the

(10) Nicholls, D.; Sutphen, C.; Szwarc, M. *J. Phys. Chem.* **1968**, *72*, 1021.

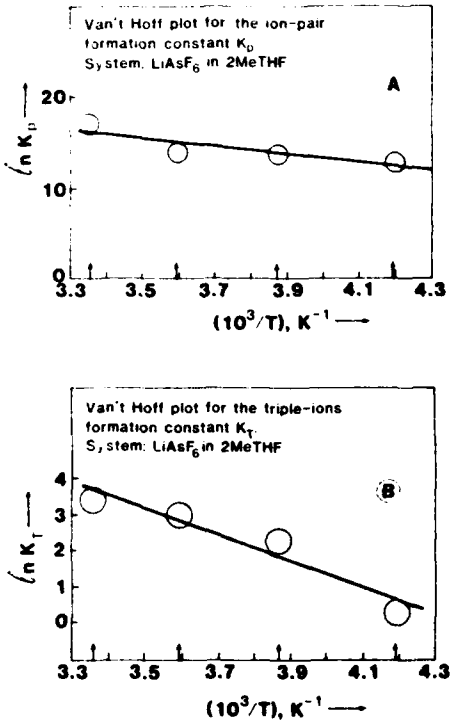

Figure 5. (A) van't Hoff plot of ln K_p vs. $1/T$ for $LiAsF_6$ in 2-MeTHF. (B) van't Hoff plot of ln K_T vs. $1/T$ for $LiAsF_6$ in 2-MeTHF.

van't Hoff plot of ln K_p vs. $1/T$ for $LiAsF_6$ in 2-MeTHF. Figure 5B reports the corresponding van't Hoff plot of ln K_T vs. $1/T$ for the same system.

The solid lines, calculated by linear regression, give from Figure 5A ΔS_p° = 63 cal/(K mol) and ΔH_p° = 7.28 kcal/mol. By equating K_p to the Bjerrum expression for ion-pair association[11]

$$K_{Bj} = \frac{4\pi L d^3}{1000}\beta^3 Q \qquad \text{(V)}$$

where

$$\beta = e^2/\epsilon dkT, \quad Q = \int_2^\beta \frac{e^Y}{Y^4}\,dY$$

one obtains the values of d, the ion-pair separation distance reported in Table V. The value at t = 25 °C is in good accord with the value $d_a = 4.6 \times 10^{-8}$ cm, calculated[1] from the Böttcher function[12] and dielectric permittivities. There appears to be a trend, d increasing with decreasing temperature. If true, this trend would suggest a tendency to form solvent-separated ion pairs by decreasing T (hence by increasing ϵ).

The triple-ion formation constants K_T have been compared to the Delsignore–Bjerrum[13] equilibrium constant

$$K_{BjT} = \frac{2\pi L a_T^3}{1000} b_T^{3/2} Q_T \qquad \text{(VI)}$$

with

$$b_T = \frac{e\mu}{\epsilon a_T^2 kT}; \quad Q = \sum_{n=\text{odd}} \left| \frac{Y^{(n-5/2)}}{(n-(5/2))n!} \right|_{Y=2}^{Y=b_T}$$

or

$$Q = -\frac{b_T^{-1.5}}{1.5} + \frac{b_T^{0.5}}{(0.5)3!} + \frac{b_T^{2.5}}{(2.5)5!} + \frac{b_T^{4.5}}{(4.5)7!} + \frac{b_T^{6.5}}{(6.5)9!} + \frac{b_T^{8.5}}{(8.5)11!} + \ldots - 0.2556$$

(11) Bjerrum, N. K. *Dan. Vidensk. Selsk. Mat-Fys. Medd.* **1926**, *7*, 9.
(12) Böttcher, C. F. J. *Theory of Electrical Polarization*; Elsevier: Amsterdam, 1973.
(13) Delsignore, M.; Farber, H.; Petrucci, S. *J. Phys. Chem.* **1986**, *90*, 66, 3294.

TABLE V: Calculated Ion-Pair Separation Distance d and Triple-Ion Separation Distance a_T, according to the Bjerrum and Delsignore–Bjerrum Theories, Respectively, for $LiAsF_6$ in 2-MeTHF at Various Temperatures

t, °C	K_p^{expti}, M^{-1}	$K_p^{calcd\,a}$, M^{-1}	K_T^{expti}, M^{-1}	$K_T^{calcd\,a}$, cm	$d \times 10^8$, cm	$a_T \times 10^8$, cm	$q_T \times 10^{8\,b}$
25	2.5×10^7	2.4×10^7	29.4	30.0	4.4_5	8.4	14.34
5	1.0×10^6	1.1×10^6	$20._3$	20.0	5.5	9.2	14.25
−15	8.5×10^5	9.0×10^5	$9._8$	$9._7$	5.5	11.0	14.27
−35	3.0×10^5	3.0×10^5	$1._3$	$1._3$	6.0	13.6	14.08

[a] The calculated K_p^{calcd} and K_T^{calcd} have been computed from eq V and VI, respectively, by changing d and a_T in steps of 0.1×10^{-8} cm. [b] Values of q_T represent the maximum distance of separation of an ion from the dipole pair in the triple ion.

using the experimental[1] $\mu = 22 \times 10^{-18}$ esu cm.

The results extending the series to $n = 15$ are reported in Table V. At $t = 25$ °C, $a_T = 8.4 \times 10^{-8}$ cm, namely, a_T larger than $1.5d$. (The axiom of three equal spheres at contact may suggest $a_T = 1.5d$.) The values of a_T seem, however, of reasonable magnitude, even at the lowest temperature, with the general condition $a_T \approx 2d$. In Table V the Delsignore–Bjerrum parameters[13] q_T are also reported, showing a_T approaching q_T (hence K_T approaching zero) as the temperature is lowered (hence, as ϵ is increased). In the above $q_T = [e\mu/(2\epsilon kT)]^{1/2}$, which corresponds to a ratio of 2 between the electrostatic ion dipole energy $e\mu/(\epsilon q_T^2)$ and kT.

Recently,[7] it has been inferred that because the permittivity of the electrolyte solution increases with concentration of electrolyte, the deviation of the slope of log Λ vs. log c from −0.50, namely, from the Ostwald mass law, may be due in part or all to changes in permittivity, thereby putting the very existence of triple ions under discussion. We agree that, at high concentrations, the permittivity effect becomes of paramount importance, as documented in a previous paper.[8] We were concerned, however, that even at low concentration ($c \leq 2 \times 10^{-2}$ M) the fact that $\epsilon(c)$ is larger than the solvent value may be significant.

We therefore took the Delsignore et al.[1] data of dielectric permittivity ϵ for $LiAsF_6$ in 2-MeTHF and fitted them by nonlinear regression to the equation at $t = 25$ °C

$$\epsilon = 6.24 + 47.34c - 242.77c^2$$

with determination coefficient $r^2 = 0.999\,999_7$ (Figure 4B). At each concentration used in the conductance work, ϵ was then calculated and eq IV applied (Figure 4C). Linear regression of $\Lambda g(c)c^{1/2}$ vs. $(1 - \Lambda/\Lambda_0)c$ gives $r^2 = 0.9965$, intercept = 0.024 30, and slope = 0.5874 from which $K_p = 2.48 \times 10^7$ M^{-1} and $K_T = 36._2$ M^{-1}, having used eq IV up to $c = 0.021\,55$ M. The change in K_p is insignificant, with respect to the calculation of K_p with $\epsilon = 6.24$, the solvent value. The change in K_T is about 20%, but using $\epsilon = \epsilon(c)$ does not cause K_T to become zero, as the allegation involving $\epsilon(c) > \epsilon_{solvent}$ may have implied. The condition $\Lambda_T^\circ = {}^2/_3\Lambda_0$ probably carries an incertitude at least as large as 20%.

There is, however, another way of analyzing the data by retaining $\epsilon = \epsilon(c)$ in the calculations of $g(c)$ (eq IV) but by assuming absence of triple ions. Equation IV then becomes

$$\Lambda g(c)c^{1/2} = \Lambda_0/K_p^{1/2} \qquad \text{(VII)}$$

The concentration dependence of the left side of the above equation may be absorbed by K_p, if one assumes that the increased permittivity of the solution causes K_p to decrease. Table VI reports the calculated K_p's according to eq VII. Also, in Table VI we report the calculated K_p using the Fuoss expression $K_F = K_0 e^\beta$ with $K_0 = (4\pi L\, d_F^3/3000)$ and $\beta = e^2/\epsilon d_F kT$ using the permittivity of the solutions and also using d_F as an adjustable parameter. From Table VI it is obvious that K_p decreases, as expected, but also that the K_F's reproduce the K_p's at the cost of decreasing d_F from 4.92×10^{-8} to $4.4_3 \times 10^{-8}$ cm. The fit is remarkable and suggests that, in principle, in the concentration range analyzed the change in permittivity of the solution may account for the increase in conductivity of the solution without the postulation of the presence of the triple ions. The trend in the d_F's, if real, may reflect the neglect of higher terms in the conductance equation, only the Onsager $S(c\Lambda/\Lambda_0)^{1/2}$ term having been retained. As for the presence of triple ions, it appears premature to draw conclusions before more extensive research is done with many solutions of known permittivities. There are at least two systems when the permittivity does not change appreciably with concentration but the conductance increases. Bu_3HNCl in toluene[14] at 35 °C showed only permittivity increases <1% in the concentration range 0 to 26.9×10^{-4} M, but the molar conductivities went through a minimum at $\sim 10^{-3}$ M. Further, for $LiBF_4$ in dimethoxymethane[13] at 25 °C, the solution permittivity does not change appreciably up to ~0.3 M but the molar conductivity increases with concentration. Evidently, for these systems the permittivity is not the factor to cause the increase of Λ. Further, there is spectroscopic evidence by IR of presence of triple ions as for the NaSCN in THF, showing a band[4,15] at ~2074 cm^{-1} which was attributed[15] to the Na^+SCNNa^+ species, the anion being a bidentate ligand.

TABLE VI: Calculated K_p's according to Eq VII and Calculated K_F's according to the Expression $K_F = (4\pi L d_F^3/3000)e^\beta$ with $\beta = e^2/\epsilon d_F kT$, Using $\epsilon = \epsilon(c)$ and d_F as an Adjustable Parameter (System $LiAsF_6$ in 2-MeTHF at $t = 25$ °C)

$c \times 10^4$, M	ϵ	$\Lambda g(c)c^{1/2} \times 10^2$	$K_p \times 10^{-7}$, M^{-1}	$K_F \times 10^{-7}$, M^{-1}	$d_F \times 10^8$, cm
0	6.24		2.48[b]	2.51	4.92
6.6112	6.27	2.4450	2.45	2.44	4.90
9.5847	6.29	2.5119	2.32	2.31	4.90
38.470	6.42	2.6765	2.04	2.04	4.82
62.710	6.53	2.7992	1.87	1.81	4.76
89.505	6.64	2.9389	1.70	1.68	4.69
140.42	6.86	3.2132	1.42	1.42	4.56
215.55	7.15	3.7189	1.06	1.04	4.43

[a] Value calculated from extrapolated data of $\Lambda g(c)c^{1/2}$ vs. $c(1 - (\Lambda/\Lambda_0))$.

TABLE VII: Values of the Rate Constants and Equilibrium Constants at Various Temperatures for the Dimerization of $LiAsF_6$ in 2-MeTHF[a]

t, °C	k_f, $M^{-1}\,s^{-1}$	k_r, s^{-1}	K_q, M^{-1}	$K_q^{calcd\,b}$, M^{-1}	$a_q \times 10^8$, cm
25	2.7×10^8[c]	1.5×10^8[c]	1.8[c]	1.80	9.4
15	2.0×10^8	1.4×10^8	1.4	1.36	9.7
5	1.4×10^8	1.2×10^8	1.2	1.19	9.8

[a] Calculated values of K_q and a_q according to the Maaser–Bjerrum theory of dimerization. [b] The calculated K_q^{calcd} have been computed from eq IX by changing a_q in steps of 0.1×10^{-8} cm. [c] Figure taken from ref 1.

Ultrasonic Relaxation Spectra. Delsignore et al.[1] interpreted the observed ultrasonic relaxation of $LiAsF_6$ in 2-MeTHF at $t = 25$ °C as due to a dimerization process according to the scheme

$$2LiAsF_6 \underset{k_r}{\overset{k_f}{\rightleftharpoons}} (LiAsF_6)_2$$

leading to the relation

$$\tau^{-1} = 2\pi f_r = 4k_f c_p + k_r \qquad \text{(VIII)}$$

with $K_q = k_f/k_r$. By approximating $c_p \simeq c$, namely, the ion-pair concentration to the total concentration, and by plotting τ^{-1} vs. c, we could calculate k_f, k_r, and hence K_q.

(14) Mead, D. J.; Fuoss, R. M. *J. Am. Chem. Soc.* **1942**, *64*, 277.
(15) Chabanel, M.; Wang, Z. *J. Phys. Chem.* **1984**, *88*, 1441.

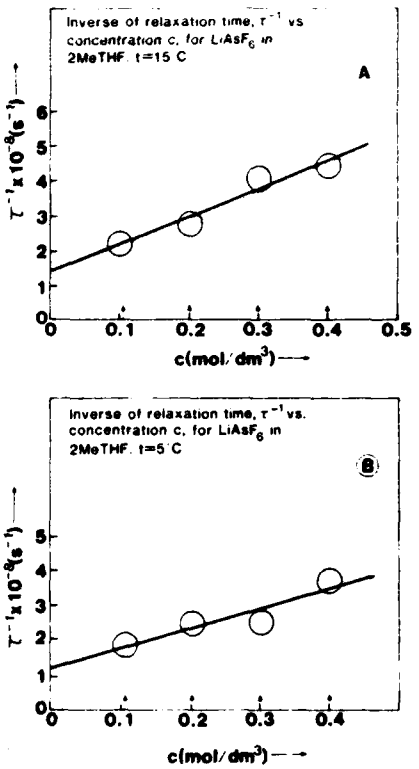

Figure 6. (A) τ^{-1} vs. c for $LiAsF_6$ in 2-MeTHF; t = 15 °C. (B) τ^{-1} vs. c for $LiAsF_6$ in 2-MeTHF; t = 5 °C.

Figure 6A,B reports such a plot. Specifically, at 15 °C, linear regression gives $r^2 = 0.96$, intercept = 1.38×10^8, and slope = $7.9_7 \times 10^8$. At 5 °C linear regression gives $r^2 = 0.85$, intercept = 1.22×10^8, and slope = $5.7_6 \times 10^8$.

In Table VII the values of k_f, k_r, and K_q at 25 °C, taken from previous work,[1] and at 15 and 5 °C, taken from the present data, are reported.

Figure 7, A and B, reports the Eyring plots of ln (k_f/T) and ln (k_r/T) vs. $1/T$, respectively. The solid lines have been calculated by linear regression. Specifically, one obtains from the data of Figure 7A

$$r^2 = 0.999, \quad \text{intercept} = 21.9, \quad \text{slope} = -2437$$

giving

$$\Delta H_f^\circ = 4.8_4 \text{ kcal/mol}, \quad \Delta S_f^\circ = -3.7_0 \text{ cal/(K mol)}$$

Also, one obtains from the data of Figure 7B

$$r^2 = 0.956, \quad \text{intercept} = 15.2_7, \quad \text{slope} = -637._4$$

giving

$$\Delta H_r^\circ = 1.2_7 \text{ kcal/mol}, \quad \Delta S_r^\circ = -16.8_7 \text{ cal/(K mol)}$$

Therefore

$$\Delta H_q^\circ = \Delta H_f^\circ - \Delta H_r^\circ = 3.6 \text{ kcal/mol}$$

and

$$\Delta S_q^\circ = \Delta S_f^\circ - \Delta S_r^\circ = 13._2 \text{ cal/(K mol)}$$

giving at T = 298.2 K

$$\Delta G_q^\circ = 3600 - 298\ (13.2) = -336._2 \text{ cal/mol}$$

and

$$K_q = \exp\left(\frac{336._2}{1.987 \times 298.2}\right) = 1.7_6 \text{ M}^{-1}$$

remarkably close to the value obtained before from the isothermal work at 25 °C. It was of interest, at this point, to compare the

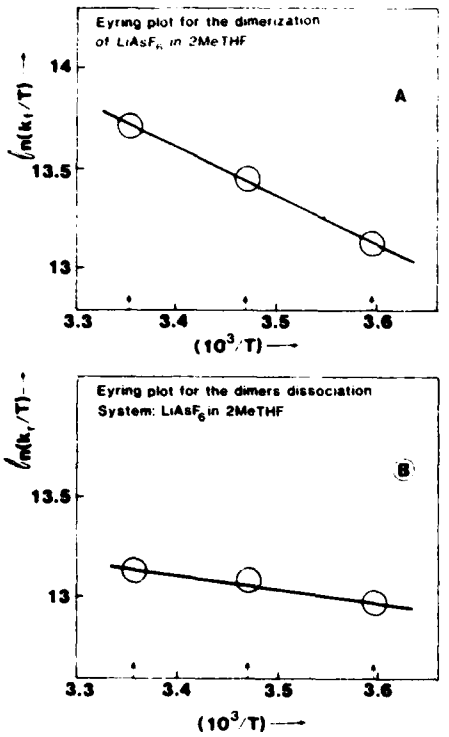

Figure 7. (A) Eyring plot of ln (k_f/T) vs. $1/T$ for $LiAsF_6$ in 2-MeTHF. (B) Eyring plot of ln (k_r/T) vs. $1/T$ for $LiAsF_6$ in 2-MeTHF.

experimental K_q from Table VI to theoretical values.

For this purpose we have used the Maaser–Bjerrum theory[16] which reads

$$K_{Bjq} = \frac{4\pi L a_q^3}{3000} b_q Q_q \qquad \text{(IX)}$$

with

$$b_q = \frac{\mu^2}{\epsilon a_q^3 kT}$$

and

$$Q_q = 0.6667 - \frac{1}{b_q} + \sum_{n_{odd}} \frac{1}{(n+2)!\ n}[b_q^n - (1.5)^n]$$

for all odd n's (n = 1, 3, 5, ...).

By extending the summation to n = 25, we have calculated K_{Bjq} by varying a_q in steps of 0.1 Å to match the experimental K_q's (1 Å = 1×10^{-8} cm).

Table VII reports the calculated K_q's and the corresponding a_q's. A small trend seems to exist; the a_q's slightly increasing by decreasing T (as noticed for the a_T's, above). Further, at t = 25 °C, $a_q = 9.4 \times 10^{-8}$ cm $\simeq 2d$ where $d = 4.6 \times 10^{-8}$ cm. This implies that the two dipoles are separated more from each other than the two ions in the pair, or presumably it implies a solvent-separated dimer.

Infrared Spectra. The Raman and infrared spectra of AsF_6^- in the solid state have been discussed in the literature.[17] The assignment of the fundamental vibrational frequencies has been done on the assumption of an octahedral O_h structure for AsF_6^-.

Three Raman-active fundamental vibrations, $\bar{\nu}_1(A_{1g}) \simeq 685$ cm^{-1}, $\bar{\nu}_2(E_g) \simeq 576$ cm^{-1} (doubly degenerate), and $\bar{\nu}_5(F_{2g}) \simeq 372$ cm^{-1}, were observed.[17] Two infrared-active vibrations, $\bar{\nu}_3(F_{1u}) \simeq 699$ cm^{-1} and $\bar{\nu}_4(F_{1u}) \simeq 392$ cm^{-1}, both triply degenerate, were also observed. The sixth vibration $\bar{\nu}_6$ was reported as inactive in both Raman and infrared spectra.[17] The vibrational mode of frequency $\bar{\nu}_6$, which is inactive in the O_h structure, was predicted

(16) Maaser, H. E.; Delsignore, M.; Newstein, M.; Petrucci, S. *J. Phys. Chem.* **1984**, *88*, 5100.
(17) Begun, G. M.; Rutenberg, A. C. *Inorg. Chem.* **1967**, *6*, 2212.

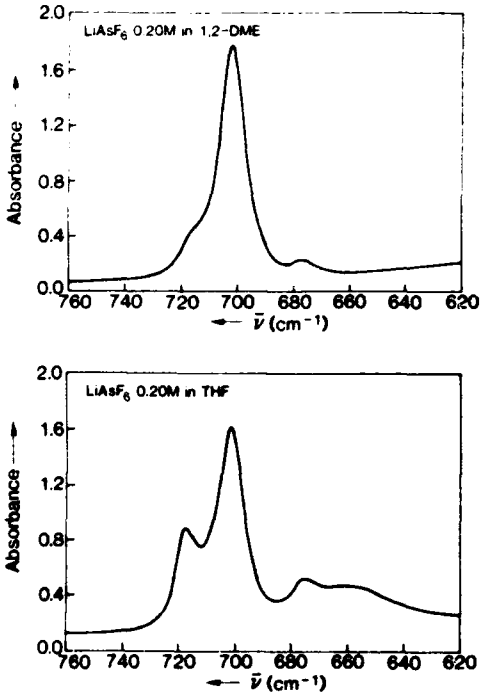

Figure 8. (A) Infrared spectrum of $LiAsF_6$ in 1,2-dimethoxyethane (DME) ($\bar{\nu}_3$ infrared envelope). (B) Infrared spectrum of $LiAsF_6$ in tetrahydrofuran (THF) ($\bar{\nu}_3$ infrared envelope). The shoulder at $\bar{\nu} \lesssim 660$ cm^{-1} is due to a solvent band.

to become infrared active in all the lower symmetries with expected frequencies in the 200–400-cm^{-1} range. In fact, the position of the ν_6 band was estimated[17] to be $\bar{\nu}_6 = 322$ cm^{-1} for AsF_6^-, a calculation based on force constant estimations. It is worth quoting[17] that the two combination bands ($\bar{\nu}_5 + \bar{\nu}_6$) and ($\bar{\nu}_2 + \bar{\nu}_6$) were expected to be active in the infrared band of these compounds. In fact, shoulders in the infrared spectra were observed[17] in the region of the $\bar{\nu}_3$ band. (Notice, in fact, that $\bar{\nu}_5 + \bar{\nu}_6 \sim 372 + 322 = 694$ cm^{-1} closely overlaps the $\bar{\nu}_3$ band, an observation to be quoted again below.)

We have chosen the $\bar{\nu}_3$ infrared band region for our study, as reported above in Table III. In view of the literature,[17] the band at 702 cm^{-1} can then be assigned to the "spectroscopically free" AsF_6^-, namely (in view of the conductance results, giving $K_p \cong 10^7$ M^{-1}), to a solvent-separated ion pair Li^+S,AsF_6^- and possibly to smaller amounts of solvent-separated dimers $(Li^+S,AsF_6^-)_2$, spectroscopically indistinguishable from Li^+S,AsF_6^-. The band at $\approx$717 cm^{-1} appears to change in maximum absorbance with the nature of the solvent. This is testified in the spectra reported in Figure 8A for $LiAsF_6$ in 1,2-DME of permittivity $\epsilon = 7.0$, and in Figure 8B for $LiAsF_6$ in THF of permittivity $\epsilon = 7.4$ (both ϵ's referring to $T = 298.2$ K). Further, in Figure 9B, $LiAsF_6$ in acetone shows that the band at 718 cm^{-1} is of minor relative maximum absorbance A_0 and is only necessary to describe the left "wing" of the $\bar{\nu}_3$ band of the AsF_6^- spectrum, which cannot be reproduced by a single Gaussian–Lorentzian band (Figure 9A). Acetone (dried over molecular sieves, distilled, and checked for absence of water bands at $\approx$3600 cm^{-1}) has a permittivity $\epsilon = 20.7$ at $T = 298.2$ K. Further, in 2-MeTHF, the value of A_0^{717} increases with respect to A_0^{702}, surpassing it at about $c = 0.3$ M (Table III). We assign this band at $\bar{\nu} \cong 717$ cm^{-1} to a contact species, which is favored either by decreasing the permittivity of the solvent or by increasing the electrolyte concentration (by mass law).

Previous ultrasonic work, for $LiAsF_6$ in 1,2-DME,[18] did not reveal the presence of dimers, but only the presence of an outer sphere to contact ion pair equilibrium

$$L^+S,AsF_6^- \rightleftharpoons LiAsF_6 + S$$

(18) Farber, H.; Petrucci, S. *J. Phys. Chem.* **1983**, *87*, 3515.

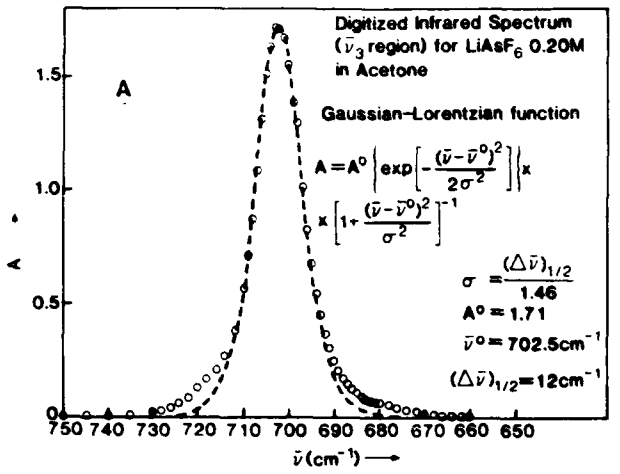

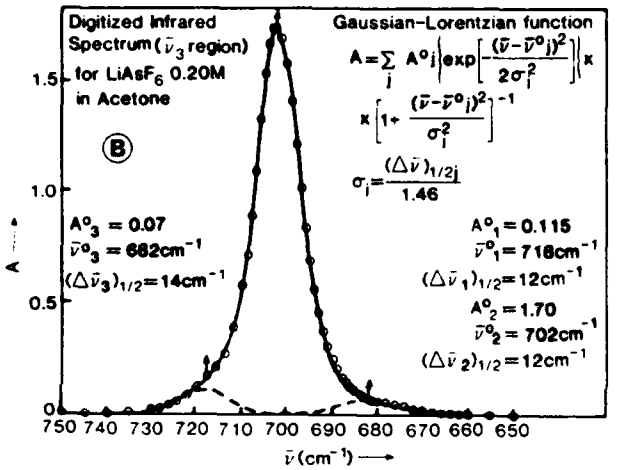

Figure 9. (A) Digitized infrared spectrum of $LiAsF_6$ (0.20 M) in acetone ($\bar{\nu}_3$ region). Dashed line represents a single Gaussian–Lorentzian band. (B) Digitized infrared spectrum of $LiAsF_6$ (0.20 M) in acetone. Solid line represents the sum of three Gaussian–Lorentzian bands.

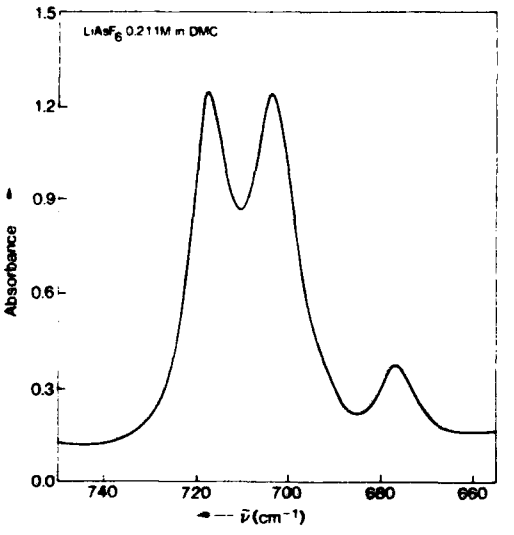

Figure 10. Infrared $\bar{\nu}_3$ band envelope of $LiAsF_6$ (0.20 M) in dimethyl carbonate.

strongly shifted toward the left. Raman spectra[18] confirmed this assignment, the $\bar{\nu}_1(A_{1g})$ band, at $\approx$680 cm^{-1}, being almost without either discernible band asymmetry or satellite bands present.

Similarity of the infrared bands positions in 1,2-DME at about 717, 702, and 677 cm^{-1} with the ones of $LiAsF_6$ in 2-MeTHF

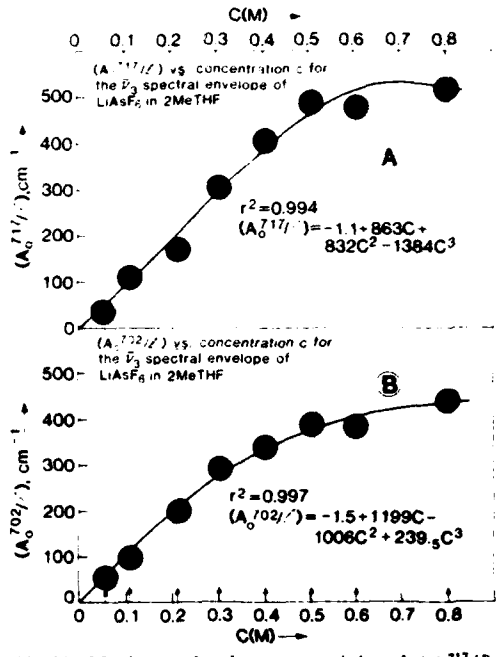

Figure 11. (A) Maximum absorbance per unit length (A_0^{717}/l) vs. concentration c of $LiAsF_6$ in 2-MeTHF. (B) Maximum absorbance per unit length (A_0^{707}/l) vs. concentration of electrolyte $LiAsF_6$ in 2-MeTHF.

suggests that the origin of these three bands is the same. This leads toward assignment of the 717-cm^{-1} band to contact ion pairs, $LiAsF_6$. Probably the contact ion pairs are in much larger relative concentration in 2-MeTHF with respect to 1,2-DME, judging from the relative band amplitudes at $\bar{\nu} \approx 717$ cm^{-1}. By the same argument, in acetone (Figure 9A,B), these contact species are almost absent. This is in accord with expectations due to the permittivities of the three solvents.

The interpretation of the band at ≈676 cm^{-1} can be achieved by assigning this band as due to a combination band[17] ($\nu_5 + \bar{\nu}_6$), $\bar{\nu}_6$ being present when the O_h symmetry is lowered because of the formation of contact species. Figure 10 shows the $\bar{\nu}_3$ region of the infrared spectrum of $LiAsF_6$ in dimethyl carbonate (DMC), a solvent of permittivity $\epsilon = 3.1$.[8] The spectrum looks qualitatively similar to the one in 2-MeTHF at similar concentrations. Notice that the band at 676 cm^{-1} is practically invisible for the spectrum of $LiAsF_6$ in acetone (Figure 9), where only a minuscule band contribution at $\bar{\nu} = 682$ cm^{-1} is needed in order to describe the lower "wing" of the spectrum. On the other hand, for $LiAsF_6$ in DMC, dimers were found to be present,[8] with an apparent formation constant $K_q \cong 50$ M^{-1}. One could then argue that lowering of the O_h symmetry of AsF_6^- is also due to some contact dimers, contributing to the band at $\bar{\nu} \cong 676$ cm^{-1}. This band appears to be present in different but increasing relative amplitudes in THF, 1,2-DME, 2-MeTHF, and DMC. In acetone the satellite bands at 718 and 682 cm^{-1} are almost absent. Energetically, dimers should not be stable configurations in acetone, the dipole–dipole energy being small with respect to kT, due to the permittivity $\epsilon = 20.7$ at $T = 298.2$ K.

Lack of visibility of the dimers in the infrared spectrum of $LiAsF_6$ in 2-MeTHF, despite their formation constants $K_q = 1.8$ M^{-1} at 25 °C, may be rationalized if they are in the majority of the outer-sphere or solvent-separated type. This was suggested by theoretical calculations above, indicating $a_q = 9.4 \times 10^{-8}$ cm $\cong 2d$, d being the ion-pair separation distance. Because of the likely contribution of both species LiS,AsF_6 and $(LiS,AsF_6)_2$ to the band at $\bar{\nu} = 702$ cm^{-1}, we believe that any attempt at calculating formation constants from the absorbances of the two visible bands at 702 and 717 cm^{-1} may lead to meaningless results.

In order to facilitate future calculations from the present data, as reported in Table III, we have expressed the absorbances per unit length, A_0^{717}/l, A_0^{702}/l, and A_0^{676}/l, by polynomials in the electrolyte concentration c (mol/dm^3). Specifically, nonlinear regression gives

$$A_0^{717}/l = -1.1 + 863c + 832c^2 - 1384c^3, \quad \text{with } r^2 = 0.994$$

$$A_0^{702}/l = -1.5 + 1199c - 1006c^2 + 239.5c^3, \quad \text{with } r^2 = 0.997$$

$$A_0^{676}/l = 0.062 + 2006.4c + 233.9c^2 - 241.5c^3, \text{ with } r^2 = 0.996$$

having given a 50% statistical weight to the origin.

Acknowledgment. This work was supported by the Army Office for Scientific Research, Durham, NC, under Grant No. DAAG-29-85-K0048. Thanks are expressed for their generous support.

Registry No. $LiAsF_6$, 29935-35-1.

Reprinted from The Journal of Physical Chemistry, 1987, 91, 3047.

Molecular Relaxation Dynamics and Structure of $LiClO_4$ Solutions in 2-Methyltetrahydrofuran

Heidrun Maaser,[†] Meizhen Xu, Paul Hemmes,[‡] and Sergio Petrucci*

Weber Research Institute and Department of Chemistry, Long Island Center, Polytechnic University, Farmingdale, New York 11735 *(Received: July 1, 1986; In Final Form: October 3, 1986)*

Electrical conductance data in the temperature range +25 to −43 °C are reported and interpreted by the Fuoss–Kraus triple-ion theory. Theoretical expressions for the thermodynamic parameters for triple ions ΔH°_T and ΔS°_T have been derived. Comparison is made between the experimental figures of ΔH° and ΔS° and the corresponding values calculated from the Bjerrum theory of ion pair formation. Comparison is also made between the experimental ΔH°_T and ΔS°_T and the values now calculated from theory. Both these tests give reasonable estimates of the ion pair separation distance d and of the ion to dipole separation distances a (in the triple ion.) Infrared spectra of the (infrared-active) ν_4 band of the perchlorate anion in the wavenumber band 550–700 cm^{-1} reveal a complex spectral envelope which can be deconvoluted into three Gaussian–Lorentzian bands. One of them, centered at ~625 cm^{-1}, is assigned to the "spectroscopically free" ClO_4^- ion (that is, to the solvent-separated Li^+S, ClO_4^- and/or to the solvent-separated dimer (Li^+S, ClO_4^-···Li^+S, ClO_4^-) where S is a solvent molecule), the perchlorate ion having T_d symmetry. The other bands centered at 639 and 654 cm^{-1} are presumed to be due to contact species, the ClO_4^- having lower symmetry. The maximum band absorbances have been correlated to the electrolyte concentration by polynomial functions. Ultrasonic relaxation spectra in the concentration range 0.05–0.4 M and frequency range 0.5–400 MHz are described by a single Debye relaxation function. Independence of the relaxation frequency on electrolyte concentration for $c > 0.1$ M and linearity of the maximum excess absorption coefficient of sound per wavelength μ_m on concentration identify the ultrasonic relaxation process as due to a first-order or pseudo-first-order process. The ultrasonic spectra are interpreted by the second step of the dimerization equilibrium $2M \rightleftarrows M\cdots M \rightleftarrows M_2$, namely, by the scheme $M\cdots M \rightleftarrows M_2$ ($k_{2,-2}$) where M is the monomeric ion pair, M···M a solvent-separated dimer or quadrupole, and M_2 a contact dimer. Temperature dependence of the ultrasonic relaxation spectra allows for estimation of activation and thermodynamic parameters of the observed equilibrium. Microwave dielectric relaxation spectra in the frequency range ~0.8–90 GHz and concentration range 0.05–0.3 M are interpreted by two Debye relaxation processes at 1.8 and 35 GHz, respectively. The one at lower frequency is attributed to the presence of the solute. Böttcher plots of the lower relaxation strength $\phi(\epsilon)$ vs. total concentration of electrolyte show a marked concave down curvature, revealing that not all of the electrolyte exists in dipolar form. Since $K_A \simeq 10^8$ M^{-1} and the concentration of triple ions is small, no appreciable extent of free ions exists in solution as to cause the curvature of the Böttcher plot. The observed phenomenon is interpreted as evidence of the presence of dimer ion pairs or quadrupoles. M···M, the solvent-separated dimers, are the predominant species in solution, and previous theoretical work predicts that the ion pair components can rotate independently of each other. In fact, by approximating $(M\cdots M) \simeq c/2$ and plotting the Böttcher relaxation strength function $\phi(\epsilon)$ vs. $c/2$, one observes an approximately linear correlation.

Introduction

Past work[1] with $LiAsF_6$ in 2-methyltetrahydrofuran (2MeTHF) has indicated a sizeable amount of dimerization of the electrolyte for this system (which is relevant to batteries construction). It has been observed[2] that, in ethereal solvents, $LiClO_4$ is a weaker electrolyte than $LiAsF_6$. Hence, one could infer that, in the multistep equilibria leading to contact dimers or quadrupoles, $LiClO_4$ is shifted toward formation of the latter species in larger amounts than $LiAsF_6$. The above was judged interesting enough that comparison between $LiAsF_6$ and $LiClO_4$ in 2MeTHF was thought to be desirable information. In the process we have

[†] Colgate Palmolive, Piscataway, NJ 08854.
[‡] Miles Laboratories, Elkhart, IN 46514.

(1) Delsignore, M.; Maaser, H. E.; Petrucci, S. *J. Phys. Chem.* **1984**, *88*, 2405.
(2) Farber, H.; Irish, D. E.; Petrucci, S. *J. Phys. Chem.* **1983**, *87*, 3515.

0022-3654/87/2091-3047$01.50/0

TABLE I: Equivalent Conductance Λ (Ω^{-1} cm^2 equiv^{-1}) and Concentration c (mol/dm^3) for $LiClO_4$ in 2MeTHF

$c \times 10^4$	Λ	$c \times 10^4$	Λ	$c \times 10^4$	Λ
		t = 25.00 °C			
2.1329	0.7462	56.573	0.1784	830.59	0.1952
4.9423	0.5113	101.64	0.1476	1097.3	0.2200
10.683	0.3582	179.08	0.1294	2591.1	0.3227
27.842	0.2357	257.16	0.1230		
		t = 5.00 °C			
7.9115	0.4620	134.81	0.1703	1177.74	0.1746
24.568	0.3006	285.96	0.1468		
60.889	0.2147	537.50	0.1433		
		t = −15 °C			
6.1472	0.7019	147.31	0.2103	1175.9	0.1802
13.818	0.5093	298.79	0.1763	1580.95	0.2079
56.736	0.2897	668.83	0.1604		
		t = −35 °C			
9.7009	0.7675	156.65	0.2519	1296.05	0.1825
24.149	0.5239	307.81	0.2059	1983.9	0.2226
54.723	0.3791	660.51	0.1678		
		t = −43 °C			
5.3754	0.9582	94.881	0.3274	799.14	0.1654
12.990	0.7124	211.08	0.2464	964.67	0.1655
36.006	0.4756	454.59	0.1871		

investigated the conductance of $LiClO_4$ in 2MeTHF down to −43 °C, namely, to temperatures comparable to subarctic or stratospheric conditions. This hopefully will give information relevant to the solution behavior of batteries subjected to the same conditions. Theoretically, we have used these data to evaluate the thermodynamic parameters for triple-ion formation which were compared with the corresponding theoretical quantities derived below.

We have also performed infrared spectra on $LiClO_4$ solutions in 2MeTHF, which have proven to be useful in giving structural information in a concentration range where conductance theory fails.

The above background has been useful in the subsequent work on the dynamics of the solute species in solution performed by ultrasonic relaxation kinetics and by microwave dielectric spectrometry.

Experimental Section

The equipment and procedure for the conductance,[3] IR spectra,[4] and ultrasonic[5] and microwave dielectric spectra[1] have been described before. $LiClO_4$ (Johnson Matthew Inc., Seabrook, NH) was redried at 70 °C in vacuo overnight. 2MeTHF (Aldrich) was distilled over metal sodium and benzophene under reduced pressure. Solutions were prepared by weight for the conductance work; with volumetric flasks for the IR and ultrasonic and dielectric work (adding solvent to weighed $LiClO_4$ predried directly in the same flasks), contact with the atmosphere of the solution in all cases was limited to 30–60 s, namely, to the time necessary to fill the IR and ultrasonic cells. For the conductance work at low temperatures, addition of the weighed portions of stock solution, from weighing burets, to the solution of the conductance cell was performed outside the thermostat, after the conductance cell had returned to room temperature. This was done in order to avoid condensation of atmospheric humidity because of temperature gradients.

Results and Calculations

Electrical Conductance. Figure 1 reports representative plots of the log of the equivalent conductivity Λ for $LiClO_4$ vs. the log of the concentration c, at various temperatures. Table I reports

TABLE II: Static Permittivity ε, Viscosity η of 2MeTHF, Calculated Limiting Equivalent Conductance Λ_0 (Walden's Rule), and Values of K_A and K_T for $LiClO_4$ in 2MeTHF at the Temperature Investigated

T, K	ε	η, P	Λ_0, Ω^{-1} cm^2 equiv^{-1}	K_A, M^{-1}	K_T, M^{-1}	$c_{max} \times 10^4$, M
298.15	6.24	0.0047	144	$1.8_2 \times 10^8$	33	179.08
278.15	6.77	0.0057	119	$3.5_5 \times 10^7$	$20._3$	285.96
258.15	7.38	0.0072_5	93	3.1×10^7	$10._9$	298.79
238.15	8.10	0.0096_8	70	$1.0_5 \times 10^7$	$11._4$	307.81
230.15	8.42	0.0110	61	7.2×10^6	$6._6$	211.08

TABLE III: Experimental Association Constants K_A, Calculated Values of K_F (Eq III) and K_{Bj} (Eq IV), and Corresponding Distance Parameters d_F and d_{Bj} for $LiClO_4$ in 2MeTHF at the Various Temperatures Investigated

T, K	K_A, M^{-1}	K_F, M^{-1}	$d_F \times 10^8$, cm	K_{Bj}, M^{-1}	$d_{Bj} \times 10^8$, cm
298.15	$1.8_2 \times 10^8$	1.82×10^8	4.36	1.86×10^8	3.95
278.15	$3.5_5 \times 10^7$	3.57×10^7	4.74	3.58×10^7	4.28
258.15	3.1×10^7	3.06×10^7	4.72	3.08×10^7	4.26
238.15	$1.0_5 \times 10^7$	1.03×10^7	5.00	1.04×10^7	4.50
230.15	7.2×10^6	7.26×10^6	5.10	7.17×10^6	4.59

the corresponding values of Λ and c at all the temperatures investigated. The data have been interpreted by the Fuoss–Kraus triple-ion theory[6] in the form

$$\Lambda g(c)c^{1/2} = \frac{\Lambda_0}{K_A^{1/2}} + \frac{\Lambda_0^T K_T}{K_A^{1/2}}\left\{1 - \frac{\Lambda}{\Lambda_0}\right\}c \qquad \text{(I)}$$

where

$$g(c) = \frac{\exp\left[-\frac{2.303}{\Lambda_0^{1/2}}\beta'(c\Lambda)^{1/2}\right]}{\left(1 - \frac{S}{\Lambda_0^{3/2}}(c\Lambda)^{1/2}\right)\left(1 - \frac{\Lambda}{\Lambda_0}\right)^{1/2}} \qquad \text{(II)}$$

is a term lumping all the interionic terms together.[6] In particular, $\beta' = 1.8247 \times 10^6/(\epsilon T)^{3/2}$ is the Debye–Hückel term of the activity coefficient $f = \exp[(-2.303/\Lambda_0^{3/2})\beta'(c\Lambda)^{1/2}]$ and $S = [0.8204 \times 10^6/(\epsilon T)^{3/2}]\Lambda_0 + 82.501/\eta(\epsilon T)^{1/2}$ is the Onsager coefficient of the conductance equation $\Lambda = \Lambda_0 - S(c\Lambda/\Lambda_0)^{1/2}$. In the above the values of the permittivity ε and of the viscosity coefficient η have been taken from the work of Szwarc et al.[7] both at T = 298 K and at the other temperatures. At T = 298.15 K the value of $\Lambda_0(LiClO_4)$ = 26.75 Ω^{-1} cm^2 equiv^{-1} in propylene carbonate[8] of viscosity η = 0.0253 P has been retained, giving $\Lambda_0\eta$ = 0.677. Then from assumed consistency of the Walden rule, one calculates Λ_0 = 144 Ω^{-1} cm^2 equiv^{-1} in 2MTHF of η = 0.0047 P. Figure 2 shows a plot of eq 1, namely, $\Lambda g(c)c^{1/2}$ vs. $(1 - \Lambda/\Lambda_0)c$ at t = 25 °C. The solid line calculated by linear regression up to $c = 179 \times 10^{-4}$ M gives r^2 = 0.993, intercept = 0.01068, and slope = 0.2353, from which one evaluates $K_A = 1.8_3 \times 10^8$ M^{-1} and K_T = 35 M^{-1} having arbitrarily retained the position $\Lambda_T^\circ = {}^2/_3\Lambda_0$ = 96 Ω^{-1} cm^2 equiv^{-1} as done before.[2] Table II reports the values of Λ_0 (from Walden's rule), ε, η, K_A, and K_T at all the temperatures investigated. Table II also reports the maximum concentration for each case used in applying eq I.

Thermodynamic Parameters. In this section we shall try to extract information of thermodynamic nature from the above data. We start by matching the values of K_A with the Fuoss association formation constant[9]

$$K_F = \frac{4\pi L d_F^3}{3000}e^b; \quad \beta = \frac{e^2}{\epsilon d_F kT} \qquad \text{(III)}$$

where L is Avogadro's number, d_F is the minimum distance in

(3) Petrucci, S.; Hemmes, P.; Battistini, M. *J. Am. Chem. Soc.* **1967**, *89*, 5552.
(4) Saar, D.; Petrucci, S. *J. Phys. Chem.* **1986**, *90*, 3326.
(5) Petrucci, S. *J. Phys. Chem.* **1967**, *71*, 1174. Petrucci, S.; Battistini, M. *J. Phys. Chem.* **1967**, *71*, 1181. Onishi, S.; Farber, H.; Petrucci, S. *J. Phys. Chem.* **1980**, *84*, 2922. Reference 1. Petrucci, S.; Adamic, R. J.; Eyring, E. M. *J. Phys. Chem.* **1986**, *90*, 1677.
(6) Fuoss, R. M.; Kraus, C. A. *J. Am. Chem. Soc.* **1933**, *55*, 476. Fuoss, R. M.; Accascina, F. *Electrolytic Conductance*; Interscience: New York, 1959.
(7) Nicolls, N.; Sutphan, C.; Szwarc, M. *J. Phys. Chem.* **1968**, *72*, 1021.
(8) Salomon, M.; Plichta, E. J. *Electrochim. Acta* **1984**, *29*, 731.
(9) Fuoss, R. M. *J. Am. Chem. Soc.* **1958**, *80*, 5059.

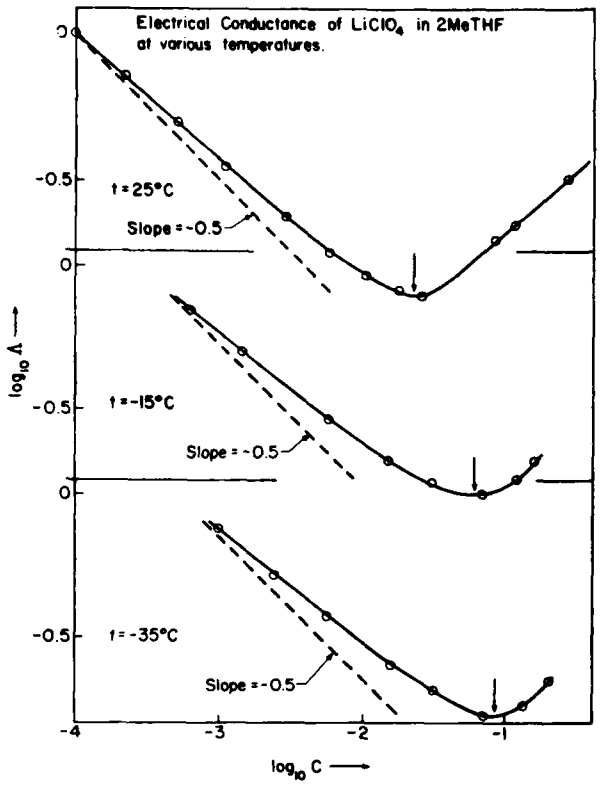

Figure 1. Representative plot of log Λ vs. log c at various temperatures for $LiClO_4$ in 2MeTHF. The arrow indicates the approximate position of the minimum in Λ.

the ion pair, and ϵ is the permittivity, with other symbols having their usual significance. Table III reports the calculated K_F, the experimental K_A, and the corresponding values of d_F used for the fit (within ±0.01 Å). The d_F's average to $\bar{d}_F = 4.78 \times 10^{-8}$ cm with a slight trend to increasing d by lowering the temperature or increasing the permittivity of the solvent. As $\bar{d}_F = 4.78$ Å is much larger than the sum of the bare radii of Li^+ and ClO_4^-, this trend might imply an increased solvation of the ions (assuming the trend not to be due to experimental fluctuations in the K_A's).

Notice also that, at these low permittivities, there is not much advantage in using the more accurate Bjerrum expression

$$K_{Bj} = \frac{4\pi L d_{Bj}^3}{1000}\beta^3 Q(\beta) \qquad \text{(IV)}$$

as the asymptotic expansion of $Q(\beta)$ leads to[10]

$$K_{Bj} \simeq \frac{4\pi L d_{Bj}^3}{1000}\frac{e^\beta}{\beta}$$

which for large β's identifies numerically with the Fuoss function K_F as $c^\beta/3 \approx e^\beta/\beta$, the e^β term being predominant. A check of the closeness of the two equations has been made by recalculating K_{Bj}, fitting it to the experimental data. For this calculation, the asymptotic expansion made by Fuoss and Kraus[10] has been retained for Q

$$\log Q(\beta) \simeq 0.4343\beta - 4\log\beta + \log(1+\delta)$$

with

$$\delta = \frac{4}{\beta} + \frac{4\times5}{\beta^2} + \frac{4\times5\times6}{\beta^3} + \ldots \qquad \text{(V)}$$

sufficiently valid for $\beta > 15$.[10] In the present case δ has been expanded up to the term in β^5. The results are collected in Table III together with the corresponding values of d_{Bj} used for the fit (within ± 0.01 Å). The $\bar{d}_{Bj}$'s average to $\bar{d}_{Bj} = 4.3_2 \times 10^{-8}$ cm with

(10) Harned, H.; Owen, B. B. *The Physical Chemistry of Electrolytic Solutions*, 3rd ed.; Reinhold: New York, 1958; pp 170–171.

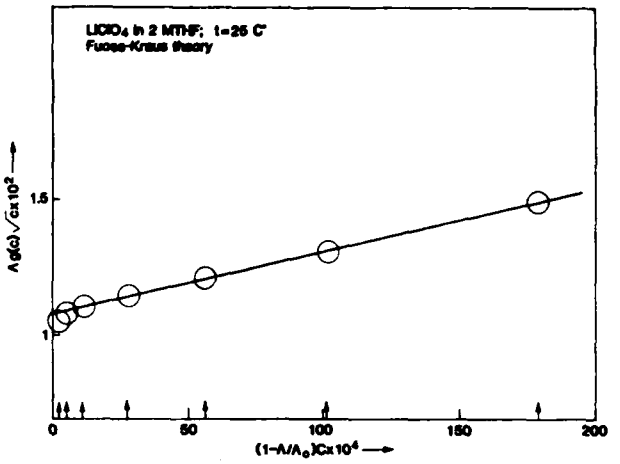

Figure 2. Fuoss–Kraus plot of $(\Lambda g(c)c^{1/2})$ vs. $(1 - \Lambda/\Lambda_0)c$ for $LiClO_4$ in 2MeTHF at $t = 25$ °C.

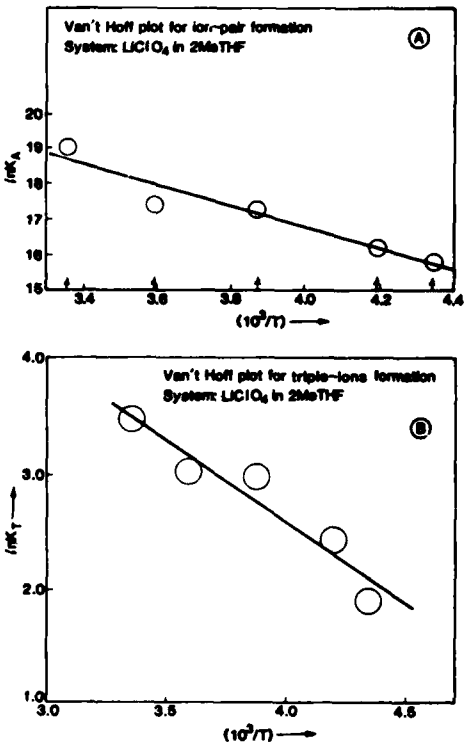

Figure 3. (A) van't Hoff plot of ln K_A vs. $1/T$ for $LiClO_4$ in 2MeTHF. (B) van't Hoff plot of ln K_T vs. $1/T$ for $LiClO_4$ in 2MeTHF.

a discernible trend to larger values by increasing permittivity and lowering temperature.

Figure 3A reports the van't Hoff plot of ln K_A vs. $1/T$. Linear regression gives $r^2 = 0.93$, intercept = 28.5_8, and slope = −2957, from which $\Delta H^\circ = 5867$ cal/mol and $\Delta S^\circ = 56.7$ cal/(K mol). In the past, some of us have calculated[11] the thermodynamic parameters associated with the Bjerrum functions IV, namely

$$\Delta G^\circ_{Bj} = -RT \ln K_{Bj}$$

$$\Delta S^\circ_{Bj} = R[\ln K_{Bj} - T\left[3 + \frac{e^\beta}{Q(\beta)\beta^3}\right]\left[\frac{1}{T} + \frac{d\ln\epsilon}{dT}\right] \qquad \text{(VI)}$$

$$\Delta H^\circ_{Bj} = -RT^2\left[3 + \frac{e^\beta}{Q(\beta)\beta^3}\right]\left[\frac{1}{T} + \frac{d\ln\epsilon}{dT}\right]$$

In 2MeTHF $d\ln\epsilon/dT = -4.705 \times 10^{-3}$ from the permittivity data

(11) Williams, J.; Petrucci, S. *J. Phys. Chem.* **1973**, *77*, 130.

TABLE IV: Experimental and Calculated (Eq VII) Values of the Triple-Ion Formation Constant and Value of the Ion–Dipole Distance a Calculated from the Delsignore–Bjerrum Theory (Eq VII)

T, K	K_T, M^{-1}	K_T (eq VII), M^{-1}	$a \times 10^8$, cm
298.15	33	33.17	5.95
278.15	$20._3$	20.62	6.40
258.15	$19._9$	19.68	6.40
238.15	$11._4$	11.31	7.20
230.15	6.6	6.58	8.30

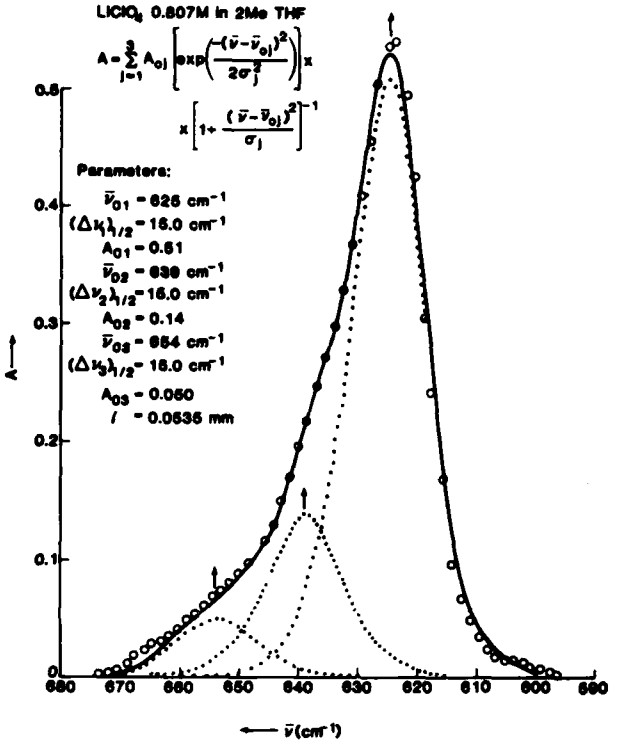

Figure 4. Digitized absorbance A vs. wavenumber $\bar{\nu}$ for the ν_4 region of the infrared spectrum of $LiClO_4$ (0.42 M) in 2MeTHF. The dashed lines correspond to the three Gaussian–Lorentzian component bands of the spectral envelope (solid line).

of the literature at various T's.[7]

Equations VI for $\Delta S°_{Bj}$ and $\Delta H°_{Bj}$ have been evaluated for various values of the ion pair minimum distance d (varing it in steps of 0.01 Å). The calculated values are $\Delta S°_{Bj} = 56.7_5$ cal/(K mol) for $d = 3.83 \times 10^{-8}$ cm and $\Delta H°_{Bj} = 5867$ cal/(K mol) for $d = 3.48 \times 10^{-8}$ cm. The figures for d are reasonable when compared to $d = 4.3_2 \times 10^{-8}$ cm, considering that they depend on $\Delta S°$, a quantity calculated by a long extrapolation, and $\Delta H°$, a quantity depending on the first derivative of ln K_A with respect to $1/T$. It appears therefore that $\bar{d} = (3.9 \pm 0.4) \times 10^{-8}$ cm, giving equal statistical weight to the three quantities.

We wish now to direct attention to the triple-ion formation constants. Recently,[12] we have proposed the Delsignore–Bjerrum expression for the triple-ion formation constant

$$K_T = \frac{2\pi La^3}{1000} b^{3/2} Q = K_0 b^{3/2}; \quad b = \frac{e\mu}{\epsilon a^2 kT} \qquad \text{(VII)}$$

with

$$Q = \int_2^b (\sinh \Psi / \Psi^{7/2})\, d\Psi$$

or or

$$Q = -\frac{b^{3/2}}{1.5} + \frac{b^{1/2}}{(1/2)3!} + \frac{b^{5/2}}{(5/2)5!} + \frac{b^{9/2}}{(9/2)7!} + \frac{b^{13/2}}{(13/2)9!}) + \ldots - 0.2556$$

$$Q = \sum_n \frac{b^{(n-(5/2))}}{(n-(5/2))n!}\Bigg|_2^b \qquad \text{(VIII)}$$

valid for all odd n's.

By extending n to $n = 15$, we have calculated the values of K_T according to eq VII varying the values of a, the ion to dipole minimum distance, within steps of ±0.05 Å. In the above the value $\mu_{LiClO_4} = 14.5 \times 10^{-8}$ esu cm found in THF by dielectric microwave spectrometry[13] has been retained in the present case, for the solvent 2MeTHF. The calculated values of K_T are reported in Table IV together with the used values of a. There is (as in the ion pair calculation) a definite trend for the a's to increase by increasing permittivity. The average values is $\bar{a} = 6.85 \times 10^{-8}$ cm, in reasonable accord with the axiom $1.5\bar{d} = \bar{a}$, leading to $\bar{d} = 4.57 \times 10^{-8}$ cm, reasonably close to the values of $\bar{d}_F$ and $\bar{d}_{Bj}$ reported above. Figure 3B reports the van't Hoff plot of ln K_T vs. $1/T$. Linear regression gives $r^2 = 0.91$, intercept = 8.33, and slope = −1436, from which $\Delta H°_T = 2.85$ kcal/mol and $\Delta S°_T = 16.6$ cal/(K mol).

It was of interest to compare these figures to corresponding theoretical parameters. To this end, we report the following derivation. From eq IV one writes

$$\Delta G°_T = -RT \ln K_T = -RT \ln K_0 - \tfrac{3}{2}RT \ln b - RT \ln Q \qquad \text{(IX)}$$

then

$$\Delta S°_T = -\left[\frac{\partial \Delta G°_T}{\partial T}\right] = R \ln K_0 + \tfrac{3}{2}R \ln b + \tfrac{3}{2}RT \frac{\partial \ln b}{\partial b}\frac{\partial b}{\partial T} + R \ln Q + RT \frac{\partial \ln Q}{\partial Q}\frac{\partial Q}{\partial b}\frac{\partial b}{\partial T}$$

$$\Delta S°_T = R \ln K_0 + R \ln Q + \tfrac{3}{2}R \ln b + RT\left[\frac{3}{2}\frac{1}{b} + \frac{1}{Q}\frac{\partial Q}{\partial b}\right]\frac{\partial b}{\partial T}$$

but

$$\frac{\partial b}{\partial T} = \frac{e\mu}{a^2 k}\left[\frac{1}{T}\frac{d\epsilon^{-1}}{d\epsilon}\frac{d\epsilon}{dT} + \frac{1}{\epsilon}\frac{dT^{-1}}{dT}\right] = -b\left[\frac{d \ln \epsilon}{dT} + \frac{1}{T}\right]$$

and

$$\frac{dQ}{db} = \frac{\sinh b}{b^{7/2}} = \frac{e^b - e^{-b}}{2b^{7/2}}$$

then

$$\Delta S°_T = R \ln K_0 + R \ln Q + \tfrac{3}{2}R \ln b - RT\left[\frac{3}{2} + \frac{1}{Q}\frac{e^b - e^{-b}}{2b^{5/2}}\right]\left[\frac{d \ln \epsilon}{dT} + \frac{1}{T}\right] \qquad \text{(X)}$$

and

$$\Delta H°_T = \Delta G°_T + T\Delta S°_T = -RT^2\left[\frac{3}{2} + \frac{1}{Q}\frac{e^b - e^{-b}}{2b^{5/2}}\right]\left[\frac{d \ln \epsilon}{dT} + \frac{1}{T}\right] \qquad \text{(XI)}$$

Values of $d \ln \epsilon/dT = -4.705 \times 10^{-3}$ were taken from literature results.[7] By varying a in steps of $\pm 0.1 \times 10^{-8}$ cm, it was calculated $\Delta H°_T = 2.92$ kcal/mol for $a = 4.50 \times 10^{-8}$ cm and $\Delta S°_T = 16.7$ cal/(K mol) for $a = 5.0 \times 10^{-8}$ cm. These figures for a are smaller than the one calculated from the K_T but still reasonable considering that the van't Hoff plot gives $\Delta H°_T$ from the derivative of ln K_T vs. $(1/T)$ and that $\Delta S°_T$ implies a long extrapolation.

Infrared Spectra. The perchlorate ion has tetrahedral symmetry, T_d, when spectroscopically free with nine normal modes of vibration. The free ion shows four fundamental vibrational bands,[14] of which two are Raman-active only and the others are

(12) Delsignore, M.; Farber, H.; Petrucci, S. *J. Phys. Chem.* **1986**, *90*, 66.

(13) Farber, H.; Petrucci, S. *J. Phys. Chem.* **1975**, *79*, 1221.

(14) Irish, D. E. In *Ionic Interactions*; Petrucci, S., Ed.; Academic: New York, 1971; Vol. II. Burger, K. *Coordination Chemistry*; Chemical Rubber Co.: Cleveland, OH, Chapter 3, and Butterworth: London, 1973. Translated edition of *Modern Koordinacios Kemiai Vizsgalo Modszerek*; Akademiai Kiado: Budapest, Hungary, 1967. Gans, P. *Vibrating Molecules*; Chapman and Hall: London, 1971; p 196.

TABLE V: Interpretation of the $\bar{\nu}_4$ Band Envelope of the Infrared Spectrum of $LiClO_4$ in 2MeTHF by Three Gaussian–Lorentzian Product Functions

$$A = \sum_{j=1}^{j=3} A_j^\circ \left[\exp\left(-\frac{(\bar{\nu} - \bar{\nu}_{0j})^2}{2\sigma_j^2} \right) \right] \left[1 + \frac{(\bar{\nu} - \bar{\nu}_{0j})^2}{\sigma_j^2} \right]^{-1}$$

C_{LiClO_4}, M	l_{cell}, mm	ν_{01}, cm^{-1}	$(\Delta\nu_1)_{1/2}$, cm^{-1}	A_1°	ν_{02}, cm^{-1}	$(\Delta\nu_2)_{1/2}$, cm^{-1}	A_2°	ν_{03}, cm^{-1}	$(\Delta\nu_3)_{1/2}$, cm^{-1}	A_3°
1.01	0.0527	625	15	0.64	639	15	0.15	654	15	0.080
0.80_7	0.0535	625	15	0.51	639	15	0.14	654	15	0.050
0.61	0.0537	624.5	14.5	0.41	639	14.5	0.12	654	14.5	0.044
0.42	0.0512	625	14	0.288	639	14	0.06	654	14	0.032
0.30	0.0504	625	14	0.22	639	14	0.035	654	14	0.028
0.21_5	0.0488	625	14	0.17	639	14	0.026	654	14	0.022
0.10_2[a]	0.0468	624	12	0.06_6						

[a] Satellite bands are no longer detectable at this concentration.

both Raman- and infrared-active. Specifically, the nondegenerate $\bar{\nu}_1 = 935$ cm^{-1} band, corresponding to symmetrical stretch, is only Raman-active. The doubly degenerate band at $\bar{\nu}_2 \simeq 462$ cm^{-1} (symmetrical bend) is also infrared-inactive. Of the other two bands, the triply degenerate $\bar{\nu}_3 \simeq 1102$ cm^{-1} (asymmetrical stretch) and the triply degenerate $\bar{\nu}_4 \simeq 628$ cm^{-1} (asymmetrical bend) are both Raman- and infrared-active.

We have chosen this last band as the spectral range of study because the solvent is transparent in this wavenumber region. Upon perturbation of the ClO_4^- ion through coordination or interaction involving a single oxygen atom Li–$OClO_3$, the symmetry is lowered to C_{3v}; there is a partial lifting of the degeneracy of the F_2 modes to give two lines (A and E species) respectively at 574 and 585 cm^{-1}.

Similarly, upon interaction of the ClO_4^- ion through two oxygen atoms as in the chelate

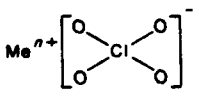

there is removal of the degeneracy because the symmetry is lowered to C_{2v} with possible appearance of three distinct lines, the A_1, B_1, and B_2 species with bands centered at 641, 610, and 571 cm^{-1}, respectively.[14]

In practice, at times these additional bands either are not visible or appear as shoulders, depending on the relative concentration of the species.

As shown below, for the spectra of this work, the majority of the ClO_4^- appears to remain in the T_d symmetry with a band at 625 cm^{-1}. A satellite band at 643 cm^{-1} appears, but no bands at 610 and at 571 cm^{-1} are visible. In addition, a band at 654 cm^{-1} appears, making the interpretation based on lowering of the symmetry from T_d to C_{2v} doubtful.

Figure 4 shows a representative digitized spectrum of $LiClO_4$ in 2MeTHF. The solid line has been calculated as the sum of three Gaussian–Lorentzian product functions of the type[15]

$$A = \sum_{j=1}^{j=3} A_j^\circ \left[\exp\left(-\frac{(\bar{\nu} - \bar{\nu}_{0j})^2}{2\sigma_j^2} \right) \right] \left[1 + \frac{(\bar{\nu} - \bar{\nu}_{0j})^2}{\sigma_j^2} \right]^{-1} \quad \text{(XII)}$$

where A is the absorbance, A_j° is the maximum absorbance of a given band centered at the wavenumber $\bar{\nu}_{0j}$, σ_j is the corresponding variance, $\sigma_j = (\Delta\bar{\nu}_j)_{1/2}/1.46$, where $(\Delta\bar{\nu}_j)_{1/2}$ is the width of each band at half the maximum absorbance, $A_j^\circ/2$.

Equation XII is a *semiempirical expression* trying to mediate, for each band, the fitting by a Gaussian factor, $\exp[-(\bar{\nu} - \bar{\nu}_0)^2/2\sigma^2]$ (which is particularly appropriate for solids),[16] and the fitting by a Lorentzian factor, $[1 + (\bar{\nu} - \bar{\nu}_0)^2/\sigma^2]^{-1}$ (which is particularly appropriate for gases),[16] to the case of a liquid as an intermediate state of aggregation between solid and gas.

In other words, eq XII tries to represent the shape of a single infrared band in a liquid as a 50% average of the functional shape of a solid and a gas. Equation XII was used by Irish et al. in liquids,[17] and it has also been utilized in this laboratory in the past, for electrolyte solutions.[4,18] Functionally, a pure Gaussian function with $\sigma_j = (\Delta\bar{\nu})_{1/2}/2.355$ causes A_j° to decrease too fast, by increasing $(\bar{\nu} - \bar{\nu}_{0j})$, to be able to account for the "wings" of a single band of an infrared spectrum in liquids. A pure Lorentzian function with $\sigma_j = (\Delta\bar{\nu}_j)_{1/2}/2.00$ causes A_j° to decrease more slowly by increasing $(\bar{\nu} - \bar{\nu}_{0j})$. By multiplying A_j° by both factors, as in eq XII, the "wings" of the infrared spectra are described more successfully. This is shown in Figure 4, in the wavenumber range 610–600 cm^{-1}, where influence from the satellite bands is negligible.

The overall fit of the spectral envelope, which is quite sensitive to variation of the parameters for each band, has been achieved by minimizing the quantity $|\sum_j A_{calcd} - A|$, where the summation is extended to the all digitized data. Table V reports the parameters $\bar{\nu}_{0j}$, $(\Delta\bar{\nu}_{1/2})_j$, and A_j used to deconvolute the infrared spectral envelopes at all the electrolyte concentrations investigated.

Previous attempts of fitting the spectra by two Gaussian–Lorentzian components were numerically rather successful at the cost of shifting the satellite band from $\bar{\nu}_{02} = 650$ cm^{-1} at $c = 0.215$ M to $\bar{\nu}_{02} = 643$ cm^{-1} at $c = 1.01$ M, broadening $\Delta\bar{\nu}_{1/2}$ from 25 to 30 cm^{-1} for the two above concentrations. Both these shifts were judged not acceptable, probably reflecting the computer attempt at describing the satellite shoulder by a single band.

From Figure 4 and Table V, it appears that the band at $\bar{\nu}_{01} \cong 625$ cm^{-1} corresponds to the spectroscopically free ClO_4^-. Given $K_A \approx 10^8$ M^{-1} from the conductance data, it is apparent that the major species in solution of $LiClO_4$ in 2MeTHF is either a solvent-separated ion pair (Li^+S, ClO_4^-) or a solvent-separated dimer (Li^+S, ClO_4^-, S_n, Li^+S, ClO_4^-), both species being spectroscopically indistinguishable by the IR spectra above. This is a relevant point in view of the results by ultrasonic relaxation given below. In other words, at the higher concentrations used in the infrared work (with respect to conductivity), it is not unconceivable that solvated dimers (solvent-separated ion pair dimers) exist. These species are not distinguishable from solvated monomer ion pairs, the only source of information being the ClO_4^- $\bar{\nu}_4$ vibration and its perturbation by "contact" with cationic species. The other two bands of much smaller amplitude at ~639 and ~654 cm^{-1} are tentatively attributed to contact species, although their molecular nature is not definite. In Figure 5, the maximum absorbances per unit length of cell (A_j°/l) are plotted vs. the total concentration of electrolyte. Nonlinear regression, giving 50% statistical weight to the origin,

(15) Saar, D.; Brauner, J.; Farber, H.; Petrucci, S. *J. Phys. Chem.* **1978**, *82*, 545.

(16) Donogadze, R. R.; Itskovitch, E. M.; Kuznetsov, A. M.; Vorotytsev, A. M. A. *J. Phys. Chem.* **1975**, *79*, 2827.

(17) Davis, A. R.; Irish, D. E.; Rodin, R. B.; Weerheim, A. J. *Appl. Spectrosc.* **1972**, *26*, 384.

(18) Saar, D.; Brauner, J.; Farber, H.; Petrucci, S. *J. Phys. Chem.* **1978**, *82*, 545. Irish, D. E.; Tang, S. Y.; Talts, H.; Petrucci, S. In *Techniques and Applications of Fast Reactions in Solution*; Gettings, W. J., Wynn Jones, E., Eds.; R. Reidel: Dordrecht, 1979; p 333.

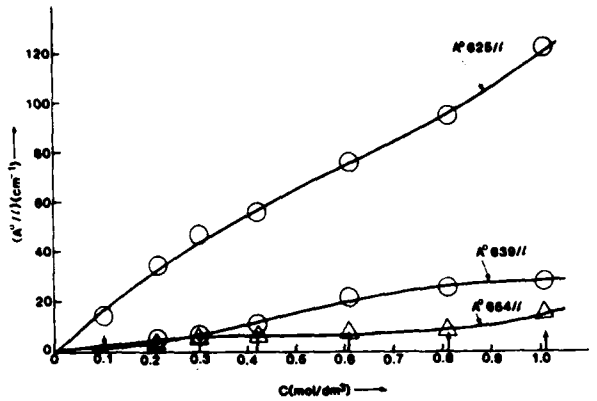

Figure 5. Infrared maximum absorbances per unit length of the three Gaussian–Lorentzian bands of the deconvoluted ν_4 envelope vs. concentration for $LiClO_4$ in 2MeTHF.

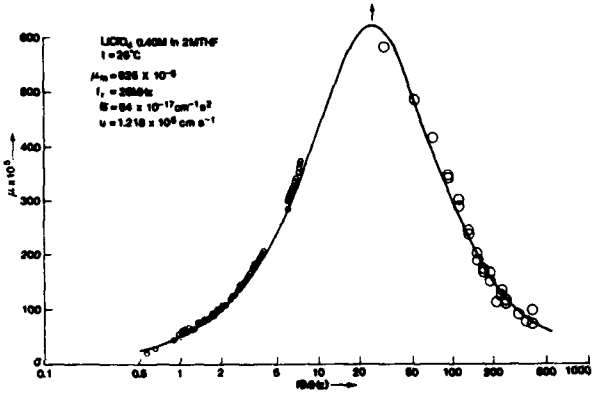

Figure 6. Representative ultrasonic relaxation spectrum expressed as excess sound absorption per wavelength $\mu = \alpha_{exc}\lambda$ vs. frequency f for $LiClO_4$ in 2MeTHF.

fits a cubic polynomial to the data for the three bands according to the calculated functions:

$$A^\circ_{625/l} = -0.1627 + 180.78c - 141.55c^2 + 80.71c^3; \quad r^2 = 0.999$$

$$A^\circ_{639/l} = 0.01505 + 5.404c + 84.71c^2 - 61.76c^3; \quad r^2 = 0.996$$

$$A^\circ_{654/l} = -0.0089 + 31.109c - 52.75c^2 + 36.34c^3; \quad r^2 = 0.998$$

The solid lines in Figure 5 depict the three functions above.

Ultrasonic Relaxation. With the structural information outlined above, from the conductance and infrared results, we wish now to discuss the dynamics of $LiClO_4$ complexes in 2MeTHF studied by ultrasonic relaxation techniques.

In Figure 6 a representative plot of the excess sound absorption coefficient per wavelength $\mu = (\alpha - Bf^2)(u/f)$ is shown plotted vs. frequency f. The solid line is the fitted function according to a single Debye relaxation function:

$$\mu = 2\mu_{max}\frac{f/f_r}{1 + (f/f_r)^2} \qquad \text{(XIII)}$$

In the above, α is the attenuation coefficient (Np/cm), B is the background absorption $(\alpha/f^2)_{f \gg f_r}$ at frequencies much higher than the relaxation frequency f_r; also, $\mu = \mu_{max}$ at $f = f_r$. Table VI reports all the calculated ultrasonic parameters and the sound velocity u. Figure 7 shows μ_{max} vs. $c \times 10^{-3}$ (mol/cm^3). The solid line has been calculated by linear regression, giving $r^2 = 0.98$, intercept $= 19.6 \times 10^{-5}$, and slope $= 15.99$ (giving 50% of weight to the origin). The fact that μ_m is approximately linear with c and that (Table VI) f_r is independent of concentration for $c > 0.1$ M suggest that the observed ultrasonic relaxation corresponds to first-order or a pseudo-first-order process.

TABLE VI: Calculated Ultrasonic Parameters μ_m, f_r, B, and Sound Velocity u for $LiClO_4$ in 2MeTHF at the Concentrations and Temperatures Investigated

t, °C	c, M	$\mu_m \times 10^5$	f_r, MHz	$B \times 10^{17}$, cm^{-1} s^2	$\mu \times 10^5$, cm/s
25	0.40	625	25	54	1.218
25	0.29	480	25	52	1.222
25	0.20	370	25	47	1.214
25	0.11	250	22	50	1.208
25	0.05	150	20	46.5	1.207
15	0.30	450	22	47	1.275
5	0.30	380	18	44	1.305
−5	0.30	334	15.5	40	1.351

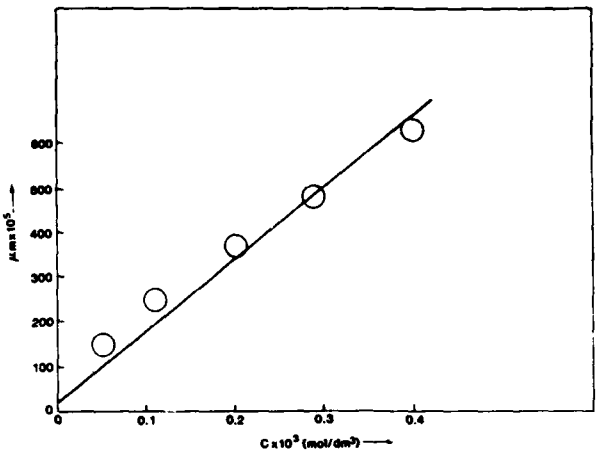

Figure 7. Excess maximum sound absorption per wavelength μ_m vs. concentration c, for $LiClO_4$ in 2MeTHF at $t = 25$ °C.

Maaser,[19] in her Doctoral dissertation, investigated $LiClO_4$ in a 50% mixture of 2MeTHF–THF by the ultrasonic pulse technique. She reported two relaxation processes which were interpreted as related to the two-step dimerization process

$$2M \underset{k_{-1}}{\overset{k_1}{\rightleftharpoons}} M,M \underset{k_{-2}}{\overset{k_2}{\rightleftharpoons}} M_2 \qquad \text{(XIV)}$$

with M the monomer ion pair, M,M the solvent-separated dimer $(LiClO_4 \cdots LiClO_4)$, and M_2 the contact dimer $(LiClO_4)_2$. By going to pure 2MeTHF, the above process may have shifted to the right enough that the scheme

$$M,M \underset{k_{-2}}{\overset{k_2}{\rightleftharpoons}} M_2 \qquad \text{(XV)}$$

may remain (at $c > 0.1$ M) the relevant process that can be observed by ultrasonic relaxation. For the "slow" process associated with scheme XIV one writes

$$\mu_{II} = \frac{\pi}{2\beta_s}\frac{\Delta V_{II}^2}{RT}\Gamma_{II}^{-1} \qquad \text{(XVI)}$$

with[12]

$$\Delta V_{II} = \Delta V_2 + \frac{1/4(M)}{1/4(M) + (M,M)}\Delta V_1 \simeq \Delta V_2 \qquad \text{(XVII)}$$

for $(M) \ll (M, M)$

$$\Gamma_{II}^{-1} = \left[\frac{1}{1/4(M) + (M,M)} + \frac{1}{(M_2)}\right]^{-1} \simeq \left[\frac{1}{(M,M)} + \frac{1}{(M_2)}\right]^{-1}$$

$$\Gamma_{II}^{-1} = \frac{(M_2)(M,M)}{(M_2) + (M,M)} = \frac{K_2(M,M)}{1 + K_2} = \frac{K_2}{(1 + K_2)^2}[(M,M) + (M_2)] \qquad \text{(XVIII)}$$

(19) Maaser, H. E. Doctoral Dissertation, Rutgers University, 1982.

with

$$K_1 = \frac{k_1}{k_{-1}} = \frac{(M,M)}{(M)^2} \qquad K_2 = \frac{k_2}{k_{-2}} = \frac{(M_2)}{(M,M)}$$

Then

$$\mu_{II} = \frac{\pi}{2\beta_s}\frac{\Delta V_2^2}{RT}\frac{K_2}{(1+K_2)^2}[(M,M) + (M_2)] \quad (XIX)$$

and since

$$c = 2(M_2) + 2(M,M) + (M) \simeq 2(M_2) + 2(M,M)$$

$$\mu_{II} \simeq \frac{\pi}{4\beta_s}\frac{\Delta V_2^2}{RT}\frac{K_2}{(1+K_2)^2}c \quad (XX)$$

predicting an approximate linearity between μ_{II} and c, as observed (Figure 7). For $c > 0.1$ M, where presumably $(M) \ll (M,M)$, (M_2) (as shown by the constancy of f_r in Table VI), scheme XV predicts also that

$$\tau^{-1} = 2\pi f_r = k_2 + k_{-2} \quad (XXI)$$

where τ is the relaxation time of the observed process. The infrared spectra, above, seem to indicate, however, that solvent-separated species are preponderant. This would imply that the equilibrium constant

$$K_2 = \frac{(M_2)}{(M,M)} = \frac{k_2}{k_{-2}} < 1$$

and that

$$\tau^{-1} \cong k_{-2} = \frac{kT}{h}e^{\Delta S_{-2}^{\circ}/R}e^{-\Delta H_{-2}^{\circ}/RT} \quad (XXII)$$

where the symbols have their usual significance. Equation XXII leads to

$$\frac{d \ln (\tau^{-1}/T)}{d(1/T)} = -\frac{\Delta H_{-2}^{\circ}}{R} \quad (XXIII)$$

Linear regression of $\ln (\tau^{-1}/T)$ vs. $1/T$ gives $r^2 = 0.978$, intercept $= 16.27$, and slope $= -930._3$, from which one calculates $\Delta S_{-2}^{\circ} = -14.9$ cal/(K mol) and $\Delta H_{-2}^{\circ} = 1.85$ kcal/mol. Also for scheme XV

$$\mu_m = \frac{\pi}{4\beta_s}\frac{\Delta V_{II}^2}{RT}\frac{K_2}{(1+K_2)^2}c \quad (XXIV)$$

(having set $c \cong 2(M,M) + 2(M_2)$). In the above β_s is the adiabatic compressibility, $\beta_s = (\rho u^2)^{-1}$, and ρ is the density of the liquid (approximated to the solvent density). ΔV_{II} is the adiabatic volume change;[12] $\Delta V_{II} \simeq \Delta V_2$ for $(M) \ll (M,M)$. Equation XXIV leads to (for $K_2 < 1$)

$$\frac{d \ln (\mu_m T/u^2)}{d(1/T)} \cong \frac{d \ln K_2}{d(1/T)} = -\frac{\Delta H_2}{R} \quad (XXV)$$

neglecting the temperature dependence of ρ. From the data of Table VI, linear regression of the quantity $\ln (\mu_m T/u^2)$ vs. $1/T$ gives $r^2 = 0.999$, intercept $= -16.98_9$, and slope $= -1810$, from which $\Delta H_2 = 3.60$ kcal/mol and $\Delta H_2^{\circ} = \Delta H_2 + \Delta H_{-2}^{\circ} = 5.4_5$ kcal/mol. All the kinetic and thermodynamic parameters for $LiClO_4$ in 2MeTHF are collected in Table VII.

Microwave Dielectric Relaxation. Figure 8 reports the coefficients of the real part ϵ' and of the imaginary part ϵ_d'' of the complex permittivity $\epsilon^* = \epsilon' - J\epsilon_d''$ of $LiClO_4$ (0.1 M) in 2MeTHF. In the above ϵ_d'' is the coefficient of the imaginary part of the permittivity ϵ'' corrected by the conductance contribution to the loss $\epsilon_\chi'' = 1.8 \times 10^{12}\,\chi/f$, namely, $\epsilon_d'' = \epsilon'' - \epsilon_\chi''$. The solid lines in Figure 8 are the sum of two Debye contributions centered at 1.8 and 35 GHz, respectively. The one at 35 GHz is attributed to the dielectric relaxation of the solvent, whereas the one at 1.8 GHz is due to the presence of the solute. Table VIII reports the parameters ϵ_0, $\epsilon_{\infty 1}$ $\epsilon_{\infty 2}$, f_1, and f_2 according to the functions

$$\epsilon' = (\epsilon_0 - \epsilon_{\infty 1})\frac{1}{1+(f/f_1)^2} + (\epsilon_{\infty 1} - \epsilon_{\infty 2})\frac{1}{1+(f/f_2)^2} + \epsilon_{\infty 2}$$

$$\epsilon'' = (\epsilon_{01} - \epsilon_{\infty 1})\frac{f/f_1}{1+(f/f_1)^2} + (\epsilon_{\infty 1} - \epsilon_{\infty 2})\frac{f/f_2}{1+(f/f_2)^2} \quad (XXVI)$$

Figure 9 reports the Böttcher plot of the function

$$\phi(\epsilon) = (\epsilon_0 - \epsilon_{\infty 1})\frac{2\epsilon_0 + 1}{3\epsilon_0} = \frac{4\pi Lc \times 10^{-3}}{(1-\alpha f)^2}\frac{\mu^2}{3kT} \quad (XXVII)$$

vs. the total concentration c of electrolyte. In the above, where

TABLE VII: Collected Kinetic and Thermodynamic Parameters for the Observed Equilibrium in Solutions of $LiClO_4$ in 2MeTHF

$k_{-2} \simeq \tau^{-1} = 1.5 \times 10^8\ s^{-1}$	$\Delta H_2 = 3.60$ kcal/mol
$\Delta S_{-2}^{\circ} = -14.9$ cal/(K mol)	$\Delta H_2^{\circ} = 5.45$ kcal/mol
$\Delta H_{-2}^{\circ} = 1.85$ kcal/mol	

TABLE VIII: Dielectric Relaxation Parameters ϵ_0, $\epsilon_{\infty 1}$, $\epsilon_{\infty 2}$, f_1, f_2, and Experimental Electrical Conductivity χ for $LiClO_4$ in 2MeTHF at $t = 25$ °C

C, M	ϵ_0	$\epsilon_{\infty 1}$	$\epsilon_{\infty 2}$	f_1, GHz	f_2, GHz	χ, Ω^{-1} cm^{-1}
0.30	9.8	6.1	2.5	1.8	35	2.23×10^{-4}
0.207	8.9	6.2	2.5	1.8	35	1.29×10^{-4}
0.106	7.8	6.2	2.5	1.8	35	3.59×10^{-5}
0.0468	7.2	6.2	2.5	1.8	35	1.03×10^{-5}

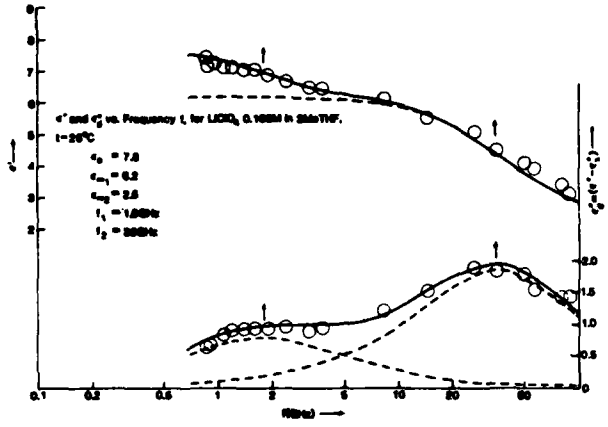

Figure 8. ϵ', the coefficient of the real part of the complex permittivity, and ϵ_d'', the dipolar component of the coefficient of the imaginary part, of the complex permittivity $\epsilon^* = \epsilon' - J\epsilon_d''$, with $\epsilon_d'' = \epsilon'' - 1.8 \times 10^{12}\,\chi/f$, plotted vs. the frequency f. System: $LiClO_4$ (0.1 M) in 2MeTHF at $t = 25$ °C.

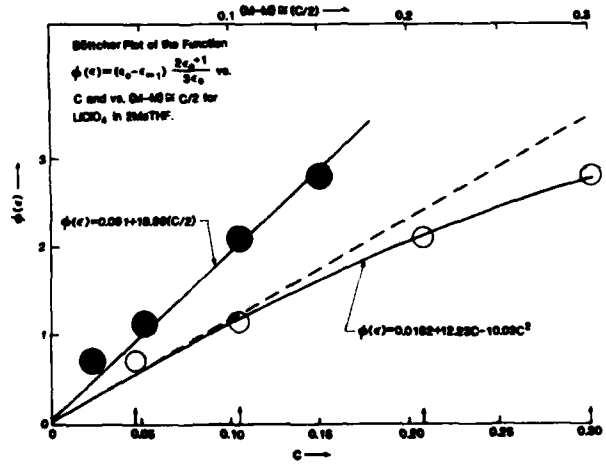

Figure 9. Böttcher plot of the function $\phi(\epsilon)$ vs. the total concentration c and $c/2$ for $LiClO_4$ in 2MeTHF.

α is the polarizability and f the internal field factor term, the expression $(1 - \alpha f)^2$ has been approximated to unity, as done before.[1]

A definitive curvature of the plot is visible. In fact, a quadratic function can interpret satisfactorily the function $\phi(\epsilon) = 0.0182 + 12.23c - 10.02c^2$ with a determination coefficient $r^2 = 0.997$, having given 50% statistical weight to the origin. As $K_A \simeq 10^8$ M^{-1} and the extent of triple-ion concentration is quite small, the inability of the total concentration to correlate linearly with $\phi(\epsilon)$ cannot be attributed to free ions, yet it means that not all of the electrolyte exists as dipolar species. The above could be taken to reinforce the evidence given above by ultrasonic relaxation of the presence of contact dimer ion pairs M_2 which are presumably antiparallel apolar species. The ultrasonic work, however, indicates that the monomeric pairs (M) $\ll$ (M···M), namely, that they are in minor concentration, the solvent-separated dimers (M···M) being the major species present. Theoretically, work expressed by the Maaser–Bjerrum theory[20] assumes successfully that the dipolar component ion pairs of M···M are free to rotate independently of each other. The mass conservation law states that

$$c = (M) + 2(M\cdots M) + 2(M_2)$$

as (M···M) is the predominant species, one may (as a zeroth approximation) equate $c \simeq 2(M\cdots M)$. Therefore, $\phi(\epsilon)$ ought to be approximately linear to $c/2$. Figure 9 shows this approximate linearity. The solid line corresponds to

$$\phi(\epsilon) = 0.061 + 18.96(c/2)$$

with $r^2 = 0.991$ having given 50% statistical weight to the origin. It is also suggestive that by equating 18.96 to the slope of the Böttcher function $(4\pi L \times 10^{-3} \mu^2)/3kT$, it results $\mu = 17.6 \times 10^{-18}$ esu cm, namely, $d = 3.7 \times 10^{-8}$ cm (having taken $\mu = de$), which is comparable to $\bar{d} = (3.9 \pm 0.4) \times 10^{-8}$ cm found by conductance above. Similarly, from the Debye relation

$$\tau = (4\pi d^3/kT)\eta$$

with $\eta = 0.0047$ P,[1] equating the microscopical relaxation time τ to the time decay of the polarization due to the solute $\tau \approx (2\pi f_1)^{-1} = 88.4 \times 10^{-12}$ s, one calculates $d = 3.95 \times 10^{-8}$ cm, again a comparable quantity (for the charge separation of the rotating dipoles) to the figures given above.

Conclusions

In dilute solutions electrical conductivity data, coupled with the Bjerrum theory and the Delsignore–Bjerrum theory for ion pairs and triple ions, respectively, give equilibrium constants, thermodynamic parameters, and reasonable estimates of d and a (the minimum distance for the two species).

At higher concentrations, infrared spectra reveal the presence of three types of complexes, solvent-separated entities (probably Li–ClO_4 and (Li–ClO_4–Li–ClO_4)) and two other species, possibly contact species. The solvent-separated species are in preponderance over the other species. Ultrasonic relaxation, in a concentration range comparable with the infrared study, reveals the presence of a first-order equilibrium between two species. The equilibrium is interpreted as due to solvent-separated vs. contact dimer ion pairs. Kinetic and thermodynamic parameters are extracted from the data. Comparing $LiClO_4$ and $LiAsF_6$ in 2MeTHF from a previous work,[1] it appears that for the latter electrolyte the equilibrium

$$2M \rightleftarrows M\cdots M \rightleftarrows M_2$$

was shifted toward the left, the overall $K_q \simeq 1._1$ M^{-1} where $K_q = K_1(1 + K_2)$. For $LiClO_4$ the equilibrium appears shifted toward the right. This implies (M) $\ll$ (M···M), and because we have estimated (M_2) < (M···M), the solvent-separated dimers appear to be the preponderant species in solutions of $LiClO_4$ in 2MeTHF in the concentration range ~0.2–1 M. The analysis by dielectric spectra reinforces the evidence of the presence of dimer ion pairs. The Böttcher function $\phi(\epsilon)$ is approximately proportional to $c/2$, which is roughly equal to the concentration of the solvent-separated dimers (M···M).

TABLE IX: Calculation of K_A (Eq XXVIII) and of K_F (Eq III) Using $\epsilon = \epsilon(c)$ and d_F's as Variable Parameters for $LiClO_4$ in 2-MeTHF; t = 25 °C

$c \times 10^4$, M	$\Lambda g(c)c^{1/2} \times 10^3$	$K_A \times 10^8$, M^{-1}	$K_F \times 10^6$, M^{-1}	$d_F \times 10^8$, cm
0	(10.698)	1.81	1.82	4.36
2.1329	10.489	1.89	1.87	4.32
4.9423	10.817	1.77	1.77	4.33
10.683	11.075	1.69	1.68	4.33
27.842	11.471	1.58	1.59	4.32
56.573	12.153	1.40	1.42	4.30
101.63_9	13.217	1.19	1.20	4.28
179.07_8	15.023	0.91_9	0.92_3	4.23

Acknowledgment. The authors express their gratitude to the Army Office for Scientific Research, Durham, NC, for generous support through Grant No. DAAG-29-85-K0048.

Addendum

One referee questioned the qualification of the nature of the satellite bands for the ν_4 infrared spectrum of $LiClO_4$ in 2MeTHF. It may be useful to draw comparison with a current effort in this laboratory for $LiClO_4$ in 1,3-dioxolane. In this solvent the ν_4 envelope can be deconvoluted in only two bands centered at 625 and 639 cm^{-1}, the band at 654 cm^{-1} being absent. Onishi et al. (Onishi, S.; Farber, H.; Petrucci, S. *J. Phys. Chem.* **1980**, *84*, 2922) could not find an ultrasonic relaxation for $LiClO_4$ in 1,3-dioxolane, at variance with the finding of the present work in 2MeTHF, where the relaxation is interpreted as due to dimerization. Hence, by comparison of the above results, one could argue that the band at 654 cm^{-1} is due to dimers, probably of the contact type. (Solvent-separated dimers would be indistinguishable from solvent-separated ion pairs at 625 cm^{-1}.) Similarly, addition of 18C6 crown ether in molar ratio 1:1 to $LiClO_4$ in 1,3-dioxolane causes the disappearance of the 639-cm^{-1} band, only the one at 625 cm^{-1} remaining. One could argue that the crown ether causes separation of Li^+ from the anion. The band at 639 cm^{-1} could then be qualified as a contact species. It is unfortunate that addition of 18C6 to $LiClO_4$ in 2MeTHF causes precipitation of the electrolyte. Details of the work in 1,3-dioxolane with crown ethers, by several parallel methods, will be published at a later time.

Note Added in Proof. In analyzing the above conductance data, one could argue that the slope of the log Λ vs. log c plot, being different from −0.5, and the appearance of a minimum are due to an increase of the permittivity with concentration of the electrolyte (Table VIII). The very existence of the triple ions might be questioned on this basis.[21] We believe that the increase of the permittivity has an overwhelming importance *at high concentrations* ($c > 0.1$ M). In order to see whether the increase in the static permittivity is relevant also in the concentration range where conductance calculations have been performed, the static permittivities of the solutions of $LiClO_4$ in 2-MeTHF at t = 25 °C have been fitted to the cubic polynomial $\epsilon_0 = 6.27_5 + 20.174c - 57.063c^2 + 96.903c^3$. At each concentration of electrolyte, the quantity $g(c)$ (eq II) has been recalculated by using the solution permittivities (instead of the solvent permittivity).

By eliminating the contribution of the triple ions from the total conductance, the Fuoss–Kraus expression (eq I) reads

$$\Lambda g(c)c^{1/2} = \frac{\Lambda_0}{K_A^{1/2}} \qquad \text{(XXVIII)}$$

The concentration dependence of the left part of the equation could

(20) Maaser, H. E.; Delsignore, M.; Newstein, M.; Petrucci, S. *J. Phys. Chem.* **1984**, *88*, 5100.

(21) Songstad, Jon. University of Bergen, Norway, private communication.

be rationalized by changes in K_A, due to the increases of the permittivity of the solutions with electrolyte concentration. Table IX reports the calculated K_A's and the corresponding K_F's (eq III) using the permittivity of the solutions and the d_F's (the latter as adjustable parameters). The fit is remarkable and this approach opens an intriguing alternative (namely the changes in ϵ) to the presence of triple ions to account for conductance data even in diluted solutions.

Registry No. $LiClO_4$, 7791-03-9; 2MeTHF, 96-47-9.

END

DATE

FILMED

8-88

DTIC